National Library of Canada

Acquisitions and Bibliographic Services Branch

395 Wellington Street
Ottawa, Ontario
K1A 0N4

Bibliothèque nationale du Canada

Direction des acquisitions et des services bibliographiques

395, rue Wellington
Ottawa (Ontario)
K1A 0N4

Your file Votre référence

Our file Notre référence

NOTICE

The quality of this microform is heavily dependent upon the quality of the original thesis submitted for microfilming. Every effort has been made to ensure the highest quality of reproduction possible.

If pages are missing, contact the university which granted the degree.

Some pages may have indistinct print especially if the original pages were typed with a poor typewriter ribbon or if the university sent us an inferior photocopy.

AVIS

La qualité de cette microforme dépend grandement de la qualité de la thèse soumise au microfilmage. Nous avons tout fait pour assurer une qualité supérieure de reproduction.

S'il manque des pages, veuillez communiquer avec l'université qui a conféré le grade.

La qualité d'impression de certaines pages peut laisser à désirer, surtout si les pages originales ont été dactylographiées à l'aide d'un ruban usé ou si l'université nous a fait parvenir une photocopie de qualité inférieure.

Canada

Multidimensional Wavelets and Applications

A Ph.D. Thesis

By

Abderrazek KAROUI

submitted to the School of Graduate Studies and Research

in partial fulfillment of the requirements for

the degree of Doctor of Philosophy in Mathematics*

University of Ottawa
Ottawa, Ontario
Canada

* The Ph.D. Program is a joint program with
Carleton University, administred by the Ottawa-Carleton
Institute of Mathematics and Statistics

ISBN 0-612-11564-X

Canada

UNIVERSITÉ D'OTTAWA
UNIVERSITY OF OTTAWA

To the memory of my father

Abstract

In this thesis, one- as well as multi-dimensional biorthogonal wavelet filters are designed and used for the construction of compactly supported wavelet bases. In particular, an adaptation of the McClellan transformation is used to design nonseparable 2-D biorthogonal wavelet bases. Some examples of 2-D biorthogonal wavelet filters are given in the case of the quincunx sampling lattice. Some theoretical and technical results known in the one-dimensional case have been generalized to the n-dimensional case. This generalization leads to a better understanding of the theory and design of multidimensional biorthogonal wavelets. An important part of the thesis is devoted to the design of fast discrete wavelet transforms. The main ingredient of the algorithms is the use of a one-point quadrature formula for approximating the finest coefficients of the signals together with a suitable design and implementation of symmetric biorthogonal filters. Special attention is given to the case where the signals have sharp transition points. In this case, a smoothing process has been used to obtain an accurate reconstruction of the signal.

Acknowledgements

Grateful thanks are due to Dr. Rémi Vaillancourt for his suggestions, guidance, and very constructive criticism during the course of my research.

Grateful thanks are also due to the CIDA (Canadian International Development Agency), the University of Ottawa, the Mathematics Department and the Ontario Gouvernment for providing me with financial suport during my Ph.D. Program.

A very special thank is due to my family; I am specially grateful to my loving mother, Khadija, for all the care and love she gave me.

My deapest appreciations go to my fiancée, Aida, for her patient and her continuous support.

Contents

List of Tables

List of Figures

Chapter 1

Introduction

Wavelets are functions generated by translations and dilations of one basic function. They can represent a wide range of functions and operators without redundancy. Moreover, they provide an easy way of analysing functions whose Fourier analysis is complicated or even practically impossible.

A one dimensional (1-D) orthonormal wavelet basis for $L^2(\mathbb{R})$ is a family of functions

$$\psi_{j,k}(x) = 2^{-j/2}\psi(2^{-j}x - k), \qquad x \in \mathbb{R}, \qquad j,\ k \in \mathbb{Z}, \tag{1.1}$$

obtained by dilations and translations of a single (mother) wavelet $\psi \in L^2(\mathbb{R})$. Thus, any function f in $L^2(\mathbb{R})$ can be expressed in terms of the wavelets $\psi_{j,k}$:

$$f(x) = \sum_{j\in\mathbb{Z}} \sum_{k\in\mathbb{Z}} < f, \psi_{jk} > \psi_{jk}(x), \tag{1.2}$$

where the equality holds in the L^2-sense. The wavelet coefficients are given by the scalar products

$$< f, \psi_{jk} >= \int_{-\infty}^{\infty} f(x)\, \overline{\psi_{jk}(x)}\, dx. \tag{1.3}$$

We note that the dilation factor 2 appearing in (1.1) can be replaced by any integer $N \geq 2$. In this case, $N-1$ elementary wavelets $\psi^i(x)$, $\quad i = 1, \cdots, N-1$, are needed

to generate a wavelet basis of $L^2(\mathbb{R})$. Consequently, any function f in $L^2(\mathbb{R})$ can be expanded in the wavelet series:

$$f(x) = \sum_{i=1}^{N-1} \sum_{j \in \mathbf{Z}} \sum_{k \in \mathbf{Z}} < f, \psi^i_{jk} > \psi^i_{jk}(x), \tag{1.4}$$

An n-dimensional (n-D) family of orthonormal wavelets is an unconditional basis of $L^2(\mathbb{R}^n)$ given by a two-parameter family of functions

$$\Psi^i_{j,\boldsymbol{k}}(\boldsymbol{x}) = |\det \boldsymbol{D}|^{-j/2} \Psi^i(\boldsymbol{D}^{-j}\, \boldsymbol{x} - \boldsymbol{k}); j \in \mathbf{Z}, \boldsymbol{k} \in \mathbf{Z}^n, i = 1, \ldots, d-1. \tag{1.5}$$

Here, $\boldsymbol{x} \in \mathbb{R}^n$, $\boldsymbol{D}$ is a dilation matrix [40], satisfying $|\det \boldsymbol{D}| = d$. In this case, for a given function $f(\boldsymbol{x}) \in L^2(\mathbb{R}^n)$, $f(\ \boldsymbol{x})$ is written in the form

$$f(\boldsymbol{x}) = \sum_{i=1}^{d-1} \sum_{j \in \mathbf{Z}} \sum_{k \in \mathbf{Z}} < f, \Psi^i_{j,\boldsymbol{k}} > \Psi^i_{j,\boldsymbol{k}}(\boldsymbol{x}). \tag{1.6}$$

Wavelets have a great ability of representing signals or functions in both the spatial and frequency domains. Consequently, they have found many applications in different fields, ranging from pure and applied mathematics to engineering.

In pure mathematics, wavelets are used to characterize some functional spaces, such as $L^p(\mathbb{R}^n)$ for $0 < p < \infty$, Hölder and Hardy spaces, etc. (see [51]). A proof by means of wavelets of the famous $T(1)$ theorem of David and Journé [19] on the L^2-continuity of a class of linear singular integral operators is found in [52], pp. 267–278.

In numerical analysis, wavelets are used as an efficient tool for the rapid numerical application of certain types of linear operators to arbitrary vector-valued functions [5], [4]. They are also used in the numerical solution of different types of differential equations [35], [70], [23]. They are widely and efficiently applied in engineering, for example in sound analysis [43], image processing [3], [20], [25], to cite but a few.

Note that the theory of wavelets has been developed only recently by A. Grossman and J. Morlet [30], Y. Meyer [51], S. Mallat [46], I. Daubechies [14] and others. However, the historical origins of wavelets go to the beginning of the 20th century. The first known wavelets are due to Haar [31]; they are denoted by $h_{jk}(x)$ with integer

indices j, k and they are defined by

$$h_{jk}(x) = \begin{cases} 2^{-j/2} & \text{if } 2^j(k-1) < x < 2^j(k-\frac{1}{2}), \\ -2^{-j/2} & \text{if } 2^j(k-\frac{1}{2}) \leq x < 2^j k, \\ 0 & \text{otherwise.} \end{cases}$$

A breakthrough in the development of wavelets is the well known Calderón identity. This identity ([51], page 16) is defined as follows:

If $\Psi(\boldsymbol{x}) \in L^1(\mathbb{R}^n)$ whose integral over $\mathbb{R}^n$ is zero and whose Fourier transform $\widehat{\Psi}(\boldsymbol{\xi})$, $\boldsymbol{\xi} \in \mathbb{R}^n$, satisfies the following condition:

$$\int_0^\infty \left|\widehat{\Psi}(t\boldsymbol{\xi})\right|^2 \frac{dt}{t} = 1, \quad \forall \boldsymbol{\xi} \neq 0, \tag{1.7}$$

and if we define $\Psi_t(\boldsymbol{x}) = t^{-n}\Psi(\frac{\boldsymbol{x}}{t})$ and Q_t denotes the operator on $L^2(\mathbb{R}^n)$ defined by $Q_t(f) = f * \Psi_t$, then

$$I = \int_0^\infty Q_t Q_t^* \frac{dt}{t}. \tag{1.8}$$

A. Grossman and J. Morlet [30] have used the above identity in deriving the continuous wavelet transform of a function $f(\boldsymbol{x})$ given by

$$f(\boldsymbol{x}) = \int_0^\infty \int_{\mathbb{R}^n} W(a,b)\Psi_{a,b}(\boldsymbol{x}) db \frac{da}{a^{n+1}},$$

where

$$W(a,b) = < f, \Psi_{a,b} > = \int f(\boldsymbol{x}) a^{-n/2} \Psi\left(\frac{\boldsymbol{x}-b}{a}\right) d\boldsymbol{x}, \; a > 0, \quad b \in \mathbb{R}^n.$$

A major achievement in the development of wavelets is due to the multiresolution analysis concept, introduced in 1986 by Y. Meyer [53] and S. Mallat [46]. Multiresolution analysis provides a natural framework for better understanding and designing wavelets. In 1987, I. Daubechies [14] has constructed for the first time some families of orthonormal and compactly supported wavelets.

It is well known that it is impossible to design symmetric and compactly supported 1-D orthonormal wavelets. Moreover, the design of nonseparable multidimensional and orthonormal wavelet bases faces many technical difficuties. Due to the

above limitations, we are essentially concerned with the design of 1-D as well as n-D biorthogonal wavelet bases, which are symmetric and compactly supported. As it will be seen in the following chapters, the construction of these wavelets is made possible by developing new design techniques and generalizing some results known in the 1-D case.

We should mention that this thesis is essentially based on published and submitted joint papers. The reader will realize that most of the chapters start by an introduction in which we refer to the problem to be studied. The aim of these introductions is to state what is done and what is to be done and also integrate the papers' work in the thesis. The chronological order of the thesis reflects that of the papers. In fact, it starts by the study of the 1-D biorthogonal wavelet bases, followed by the design of 2-D and multidimensional wavelets and finally, the improvement and implementation of fast wavelet transforms.

This work is organized as follows. In Chapter 2, we provide some design techniques for the construction of 1-D biorthogonal wavelet bases with compact support. In Chapter 3, we construct nonseparable bidimensional biorthogonal wavelet bases by using appropriate McClellan transformation. Chapter 4 is devoted to the generalization to the n-D case of some theoretical and technical results that will play important roles in the design and implementation of multidimensional wavelets. The development of fast 1-D and 2-D biorthogonal wavelet transform algorithm is done in Chapter 5. Chapter 6 is devoted to the design of a fast wavelet transform algorithm that is able to process signals with sharp transitions points. Finally, chapter 7 contains some concluding remarks.

Chapter 2

Design of Parametric Biorthogonal Wavelet Bases

It is known (see [15], pp. 252–253) that, in general, a single family of real orthonormal wavelets cannot be both compactly supported and symmetric. On the other hand, biorthogonal wavelets can be compactly supported and symmetric (see [15], p. 269, and [67]).

Biorthogonal wavelets with dilation factor 2, is a pair of families of dual wavelets, $\psi_{jk}(x)$ and $\tilde{\psi}_{jk}(x)$, derived from two mother wavelets, $\psi(x)$ and $\tilde{\psi}(x)$, respectively. They satisfy the conditions

$$\psi_{jk}(x) = 2^{-j/2}\psi(2^{-j}x - k), \quad \tilde{\psi}_{jk}(x) = 2^{-j/2}\tilde{\psi}(2^{-j}x - k). \tag{2.1}$$

If f is any function in $L^2(R)$, then f can be written in the forms:

$$f(x) = \sum_{j\in Z}\sum_{k\in Z} < f, \psi_{jk} > \tilde{\psi}_{jk}(x) = \sum_{j\in Z}\sum_{k\in Z} < f, \tilde{\psi}_{jk} > \psi_{jk}(x). \tag{2.2}$$

Hence, f is decomposed by one family and reconstructed by the other. From the signal processing point of view, dual wavelets correspond to different analysis and synthesis filters (see [61], [66], [67]). More generally, in [27] a signal is analysed and synthesized by means of different finite impulse response filters (FIR filters) of an M-channel filter bank.

Ph. Tchamitchian [63] constructed the first family of biorthogonal wavelets. In [24], sufficient conditions on the dual filters are provided to ensure the biorthogonality of the associated wavelets. In [11], it is shown that it is possible to construct symmetric biorthogonal wavelet bases with arbitrary high preassigned regularity.

Perfect reconstruction quadrature mirror filters (PR-QMF) in parametric form have been developed [6]. A partial generalization to the biorthogonal case was given in [67], where one of the filters is given in parametric form. In the present work, we provide some techniques for designing pairs of parametric biorthogonal wavelet filters. By a proper choice of the values of the parameters, the symmetric filters achieve optimal regularity or, equivalently, optimal number of vanishing moments.

2.1 Biorthogonal Wavelet Bases

In this section, we review the construction of wavelet bases. The first step consists in defining a simple, and a double, multiresolution analysis. As a consequence, we obtain 2π-periodic functions which generate families of filters. In the second step, wavelets are constructed by imposing some conditions on the filters.

2.1.1 Multiresolution analysis

In general, a smooth orthonormal wavelet basis is directly related to a multiresolution analysis [46], [47] which is defined as follows.

Definition 1 (Mallat) *A simple multiresolution analysis, $M1$, is a decreasing sequence of closed linear subspaces of $L^2(R)$,*

$$\{0\} \rightarrow \cdots \subset V_2 \subset V_1 \subset V_0 \subset V_{-1} \subset V_{-2} \cdots \rightarrow \subset L^2(R), \tag{2.3}$$

with the following properties:

$(P1)$ $\forall\, j \in Z, \quad f(x) \in V_{j+1} \Longleftrightarrow f(2x) \in V_j;$

(*P2*) $\exists\, \phi \in V_0 \subset L^2(R)$ *such that* $\phi_{0n}(x) = \phi(x-n)$ *is an orthonormal basis of* V_0.

It is easily seen from (P1) and (P2) that, for fixed $j \in Z$, the family

$$\phi_{jk}(x) = 2^{-j/2}\phi(2^{-j}x - k), \qquad k \in Z \tag{2.4}$$

is an orthonormal basis of V_j.

Definition 2 *For a given simple multiresolution analysis* $M1$, *the functions* ϕ_{jk}, $j,k \in Z$, *are called the scaling functions generated from the (father) scaling function* $\phi(x)$.

For fixed $j \in Z$, let W_j denote the orthogonal complement of V_j in V_{j-1}. The subspace W_j can be characterized in a simple way by the subspace W_0, and the latter can be recovered as follows.

Since $V_1 \subset V_0$, there exists a sequence, $\{\alpha_n\}_{n\in Z}$, of complex numbers such that

$$\frac{1}{2}\phi\left(\frac{x}{2}\right) = \sum_{n\in Z}\alpha_n\phi(x-n), \qquad \alpha_n = \frac{1}{2}\int_{-\infty}^{\infty}\phi\left(\frac{x}{2}\right)\overline{\phi(x-n)}\,dx, \tag{2.5}$$

(see [13]). The Fourier transform of the first expression in (2.5) is

$$\widehat{\phi}(2\xi) = \left[\sum_{n\in Z}\alpha_n e^{in\xi}\right]\widehat{\phi}(\xi) =: h_0(\xi)\widehat{\phi}(\xi). \tag{2.6}$$

A necessary condition to obtain a continuous $L^2(R)$ scaling function is that the function $h_0(\xi)$ satisfies the following conditions:

$$h_0(0) = 1, \qquad h_0(\pi) = 0. \tag{2.7}$$

It is proved in [51], pp. 71–73, that if a function ψ is defined by the series

$$\psi(x) = 2\sum_{n\in Z}(-1)^n\overline{\alpha_{1-n}}\phi(2x-n), \tag{2.8}$$

then $\psi_{0n}(x) = \psi(x-n)$ is an orthonormal basis of W_0. Finally, for fixed $j \in Z$, the sequence $\{\psi_{jk}\}_{k\in Z}$, where the notation in (2.1) is used, is an orthonormal basis of W_j.

We shall use the following terminology.

Definition 3 *For a given simple multiresolution analysis $M1$,*

(a) *the functions ψ_{jk}, $j,k \in Z$, are the orthonormal wavelets generated from the mother wavelet $\psi(x)$,*

(b) *$\mathcal{F}_0(\xi) = \sqrt{2}\sum_{n\in Z}\alpha_n e^{in\xi}$ is the frequency response of the filter associated with the multiresolution analysis $M1$, where the α_n are given by* (2.5).

Since $M1$ is restricted to unsymmetric orthonormal wavelet bases, we shall use a double version of (2.3) (see [11], [8]) denoted by $M2$, as our main tool in the construction of biorthogonal wavelet bases.

Definition 4 (Cohen et al.) *A double multiresolution analysis, $M2$, is defined as a pair of families, $\{V_j\}_{j\in Z}$ and $\{\tilde{V}_j\}_{j\in Z}$, of linear subspaces of $L^2(R)$, each of which satisfying* (2.3) *and properties* ($P1$) *of Definition 1. Moreover, the two families are related to each other by the following biorthogonality conditions:*

$$\widetilde{W}_j \perp V_j, \qquad W_j \perp \tilde{V}_j, \tag{2.9}$$

where W_j and $\widetilde{W}_j$ are the (non-orthogonal) complements of V_j and $\tilde{V}_j$ in V_{j-1} and $\tilde{V}_{j-1}$, respectively.

We now define dual scaling functions (see [7]), p. 151.

Definition 5 (Chui) *Two scaling functions ϕ and $\tilde{\phi}$, generating possibly different multiresolution analyses of $L^2(R)$, are said to be dual scaling functions if their scalar product satisfies the following conditions:*

$$< \phi(\cdot - j), \tilde{\phi}(\cdot - k) >:= \int_{-\infty}^{\infty} \phi(x-j)\overline{\tilde{\phi}(x-k)}\,dx = \delta_{j,k}, \quad j,\, k \in Z. \tag{2.10}$$

Given scaling functions, ϕ_{jk} and $\tilde{\phi}_{jk}$, and corresponding wavelets, ψ_{jk} and $\tilde{\psi}_{jk}$, then any $f \in L^2(R)$ can be written in the forms

$$\begin{aligned} f(x) &= \sum_{k\in Z} < f, \phi_{jk} > \tilde{\phi}_{jk}(x) + \sum_{\substack{n\in Z \\ n<j}} \sum_{k\in Z} < f, \psi_{nk} > \tilde{\psi}_{nk}(x) \\ &= \sum_{k\in Z} < f, \tilde{\phi}_{jk} > \phi_{jk}(x) + \sum_{\substack{n\in Z \\ n<j}} \sum_{k\in Z} < f, \tilde{\psi}_{nk} > \psi_{nk}(x). \end{aligned} \tag{2.11}$$

To characterize the spaces W_0 and $\widetilde{W}_0$ and construct the elementary dual wavelets ψ and $\tilde{\psi}$, we use a general method which is valid for a dilation factor $N \geq 2$ and which, for given dual scaling functions $\phi(x)$ and $\tilde{\phi}(x)$, constructs the $N-1$ elementary dual wavelets $\psi^i(x)$ and $\tilde{\psi}^i(x)$. This method is given in the following subsection.

A. A method for the construction of biorthogonal wavelets

Given dual scaling functions ψ^0, $\tilde{\psi}^0$ and a dilation factor N, we construct the dual wavelets ψ^i and $\tilde{\psi}^i$, for $i = 1, \ldots, N-1$, as follows.

Since V_0, $W_0 \subset V_{-1}$ and $\tilde{V}_0$, $\widetilde{W}_0 \subset \tilde{V}_{-1}$, then for all $i = 0, \ldots, N-1$, we have

$$\psi^i(x) = \sum_{n \in Z} \alpha_n^i \psi^0(Nx - n), \qquad \tilde{\psi}^i(x) = \sum_{n \in Z} \tilde{\alpha}_n^i \tilde{\psi}^0(Nx - n). \tag{2.12}$$

In terms of Fourier transforms, these conditions become

$$\widehat{\psi^i}(N\xi) = h_i(\xi)\widehat{\psi^0}(\xi), \qquad \widehat{\tilde{\psi}^i}(N\xi) = \tilde{h}_i(\xi)\widehat{\tilde{\psi}^0}(\xi),$$

for some $2\pi Z$-periodic functions $h_i(\xi)$ and $\tilde{h}_i(\xi)$. Now, for $k \in Z$,

$$\begin{aligned} \left\langle \psi^0(\cdot), \tilde{\psi}^0(\cdot - k) \right\rangle \delta_{0,k} &= \left\langle \widehat{\psi^0}(\cdot), \widehat{\tilde{\psi}^0}(\cdot)\, e^{-ik\cdot(\cdot)} \right\rangle \\ &= \int_0^{2\pi} e^{ik\xi} \left[\sum_{l \in Z} \overline{\widehat{\psi^0}(\xi + 2\pi l)} \widehat{\tilde{\psi}^0}(\xi + 2\pi l) \right] d\xi. \end{aligned}$$

Since $Z = NZ + \{0, 1, \cdots, N-1\}$, then

$$\sum_{i=0}^{N-1} \sum_{l \in Z} \overline{\widehat{\psi^0}(N\xi + 2\pi(Nl + i))} \widehat{\tilde{\psi}^0}(N\xi + 2\pi(Nl + i)) = 1.$$

Thus, the dual lowpass wavelet filters associated with $h_0(\xi)$ and $\tilde{h}_0(\xi)$ satisfy a relation given by

$$\sum_{k=0}^{N-1} \overline{h_0\left(\xi + \frac{2\pi k}{N}\right)} \tilde{h}_0\left(\xi + \frac{2\pi k}{N}\right) = 1. \tag{2.13}$$

By the same manipulations on the wavelets ψ^i and $\tilde{\psi}^i$, one can easily prove that the $N-1$ highpass wavelet filters associated with $h_i(\xi)$, $\tilde{h}_i(\xi)$ satisfy a relation given by

$$\sum_{k=0}^{N-1} \overline{h_i\left(\xi + \frac{2\pi k}{N}\right)} \tilde{h}_j\left(\xi + \frac{2\pi k}{N}\right) = \delta_{i,j}. \tag{2.14}$$

Now, if we define $\eta_k = 2\pi k/N$, then conditions (2.13), (2.14) can be stated in terms of two matrices U, V whose respective entries are

$$h_{i,j}(\xi) = h_j(\xi + \eta_i), \quad \tilde{h}_{i,j}(\xi) = \tilde{h}_j(\xi + \eta_i), \qquad i, j = 1, \ldots, N-1.$$

Hence, conditions (2.13), (2.14) are equivalent to

$$\overline{V}^t U = I_N, \tag{2.15}$$

where I_N is the $N \times N$ identity matrix. In other terms, the following equality holds

$$\begin{bmatrix} \overline{\tilde{h}_0(\xi)} & \overline{\tilde{h}_0(\xi+\eta_1)} & \cdots & \overline{\tilde{h}_0(\xi+\eta_{N-1})} \\ \overline{\tilde{h}_1(\xi)} & \overline{\tilde{h}_1(\xi+\eta_1)} & \cdots & \overline{\tilde{h}_1(\xi+\eta_{N-1})} \\ \vdots & \vdots & & \vdots \\ \overline{\tilde{h}_{N-1}(\xi)} & \overline{\tilde{h}_{N-1}(\xi+\eta_1)} & \cdots & \overline{\tilde{h}_{N-1}(\xi+\eta_{N-1})} \end{bmatrix}$$

$$\times \begin{bmatrix} h_0(\xi) & h_1(\xi) & \cdots & h_{d-1}(\xi) \\ h_0(\xi+\eta_1) & h_1(\xi+\eta_1) & \cdots & h_{d-1}(\xi+\eta_1) \\ \vdots & \vdots & & \vdots \\ h_0(\xi+\eta_{N-1}) & h_1(\xi+\eta_{N-1}) & \cdots & h_{N-1}(\xi+\eta_{N-1}) \end{bmatrix} = I_N.$$

Remark 1 For $N = 2$, the previous relation reduces to

$$\begin{bmatrix} \overline{\tilde{h}_0(\xi)} & \overline{\tilde{h}_0(\xi+\pi)} \\ \overline{\tilde{h}_1(\xi)} & \overline{\tilde{h}_1(\xi+\pi)} \end{bmatrix} \begin{bmatrix} h_0(\xi) & h_1(\xi) \\ h_0(\xi+\pi) & h_1(\xi+\pi) \end{bmatrix} = I_2.$$

Hence, a choice for the lowpass filters $h_1(\xi)$ and $\tilde{h}_1(\xi)$ is given by

$$h_1(\xi) = e^{i\xi}\tilde{h}_0(\xi+\pi), \quad \tilde{h}_1(\xi) = e^{i\xi}h_0(\xi+\pi).$$

Consequently, the dual wavelets are given by

$$\begin{aligned} \psi(x) &= \sum_{n\in Z}(-1)^n \tilde{\alpha}_{1-n}\phi(2x-n), \\ \tilde{\psi}(x) &= \sum_{n\in Z}(-1)^n \alpha_{1-n}\tilde{\phi}(2x-n). \end{aligned} \tag{2.16}$$

Relation (2.16) has been derived differently in [51]. □

Since the designed biorthogonal wavelets depend on the choice of the dual trigonometric polynomials $h_0(\xi)$ and $\tilde{h}_0(\xi)$, one may raise the following important question: under what conditions on h_0 and $\tilde{h}_0$ can one have a pair of smooth dual scaling functions and consequently a biorthogonal wavelet basis? Some answers, given in [11], [24] and [9], are briefly summarized in the following section.

2.2 Numerical Techniques for the Construction of Biorthogonal Wavelets

2.2.1 Necessary and sufficient conditions for the existence of smooth biorthogonal wavelet bases

From now on, we assume that the coefficients, α_n and $\tilde{\alpha}_n$, of h_0 and $\tilde{h}_0$, respectively, as defined in (2.12), are real, satisfy the symmetry relations $\alpha_{-n} = \alpha_n$ and $\tilde{\alpha}_{-n} = \tilde{\alpha}_n$, and are finite in number. This last assumption is equivalent to the compact support property of the constructed wavelets, (see [11]).

The biorthogonal version of the multiresolution analysis is used to construct a pair of dual scaling functions leading to a biorthogonal family of wavelets. This method (see [11]), essentially based on (2.6), implies that

$$\hat{\phi}(\xi) = \prod_{j=1}^{\infty} h_0(2^{-j}\xi), \qquad \hat{\tilde{\phi}}(\xi) = \prod_{j=1}^{\infty} \tilde{h}_0(2^{-j}\xi). \tag{2.17}$$

In [11] and [24], a set of conditions is provided on the dual 2π-periodic functions $h_0(\xi)$ and $\tilde{h}_0(\xi)$ so that the corresponding filters generate biorthogonal wavelet bases.

Conditions which ensure that the biorthogonal wavelet bases have preassigned regularities are stated in the following proposition.

Proposition 1 *Assume that both $h_0(\xi)$ and $\tilde{h}_0(\xi)$ can be factored in the form:*

$$h_0(\xi) = \left(\frac{1+e^{-i\xi}}{2}\right)^L f(\xi), \qquad \tilde{h}_0(\xi) = \left(\frac{1+e^{-i\xi}}{2}\right)^{\tilde{L}} \tilde{f}(\xi), \tag{2.18}$$

and suppose, that for some k, $\tilde{k} > 0$,

$$B_k := \sup_{\xi} |f(\xi)f(2\xi)\cdots f(2^{k-1}\xi)|^{1/k} < 2^{L-1/2}, \tag{2.19}$$

$$\tilde{B}_{\tilde{k}} := \sup_{\xi} |\tilde{f}(\xi)\tilde{f}(2\xi)\cdots \tilde{f}(2^{\tilde{k}-1}\xi)|^{1/\tilde{k}} < 2^{\tilde{L}-1/2}. \tag{2.20}$$

Then ϕ, $\tilde{\phi} \in L^2(R)$ *and*

$$\int_{-\infty}^{\infty} \phi(x)\overline{\tilde{\phi}(x-n)}\,dx = \delta_{0n}.$$

PROOF. See [11]. □

It then follows (see [11] and [24]) that if (2.19) and (2.20) are satisfied then there exist two positive numbers, ϵ, $\tilde{\epsilon} > 0$, and a positive constant c such that

$$|\widehat{\phi}(\xi)| < c(1+|\xi|)^{-L+\log(B_k)/\log(2)-\epsilon}, \tag{2.21}$$

$$|\widehat{\tilde{\phi}}(\xi)| < c(1+|\xi|)^{-\tilde{L}+\log(\tilde{B}_{\tilde{k}})/\log(2)-\tilde{\epsilon}}. \tag{2.22}$$

Now, by Theorem 3.8 in [11], if (2.21) and (2.22) are satisfied, then the dual wavelets constructed from the scaling functions $\phi(x)$ and $\tilde{\phi}(x)$ generate a pair of biorthogonal wavelet bases.

Remark 2 If there exists a constant $c > 0$ such that (2.21) and (2.22) are satisfied, then ϕ and $\tilde{\phi}$ belong to the Hölder spaces $C^{\epsilon}(R)$ and $C^{\tilde{\epsilon}}(R)$, for all $\epsilon < L - 1 - \log(B_k)/\log(2)$ and $\tilde{\epsilon} < \tilde{L} - 1 - \log(B_{\tilde{k}})/\log(2)$, respectively. □

It is proved in [9] that under some weaker conditions on the dual filters, it is possible to verify the global stability and the biorthogonality of the associated wavelets by using the transition operators, T_0 and $\tilde{T}_0$, associated with the biorthogonal wavelet filters, defined respectively by

$$T_0 f(\xi) = \left|h_0\left(\frac{\xi}{2}\right)\right|^2 f\left(\frac{\xi}{2}\right) + \left|h_0\left(\frac{\xi}{2}+\pi\right)\right|^2 f\left(\frac{\xi}{2}+\pi\right),$$

$$\tilde{T}_0 f(\xi) = \left|\tilde{h}_0\left(\frac{\xi}{2}\right)\right|^2 f\left(\frac{\xi}{2}\right) + \left|\tilde{h}_0\left(\frac{\xi}{2}+\pi\right)\right|^2 f\left(\frac{\xi}{2}+\pi\right),$$

where f is a 2π-periodic function. Now if we let

$$F_N = \left\{ \sum_{-N}^{N} c_k \, e^{ik\xi};\ \sum_{-N}^{N} c_k = 0 \right\}, \qquad \tilde{F}_{\tilde{N}} = \left\{ \sum_{-\tilde{N}}^{\tilde{N}} \tilde{c}_k \, e^{ik\xi};\ \sum_{-\tilde{N}}^{\tilde{N}} \tilde{c}_k = 0 \right\},$$

then the pair $\{h_0(\xi), \tilde{h}_0(\xi)\}$ generates biorthogonal Riesz bases (this fact is equivalent to the global stability of ψ_{jk} and $\tilde{\psi}_{jk}$) if and only if the spectral radii, $\rho(T_0)$ and $\rho(\tilde{T}_0)$, of the associated transition operators, T_0 and $\tilde{T}_0$, restricted to F_N and $\tilde{F}_{\tilde{N}}$, respectively, satisfy the inequalities

$$\rho(T_0) < 1, \qquad \rho(\tilde{T}_0) < 1. \tag{2.23}$$

Morevoer, if $|\lambda| < 1$, where λ is the eigenvalue of T_0 of largest modulus, then the scaling function ϕ associated with $h_0(\xi)$ belongs to the Besov spaces $B_2^{s,\infty}(R)$ for all $s < -\log(|\lambda|)/(2\log 2)$.

Different methods have been used to estimate the smoothness of the solutions of the dilation equations in general and of the constructed wavelets in particular. The description of these methods is beyond the scope of this thesis and the reader is referred to [56], [57], [22], [17] and [18].

In the previous subsections, we have seen the basic theoretical steps for the construction of biorthogonal wavelet bases; however, the actual construction relies on special numerical techniques described in the next subsection.

2.2.2 Construction of biorthogonal wavelets

The aim of this subsection is to derive the numerical techniques used in the construction of biorthogonal wavelet bases. In particular, we shall prove that it is possible to construct pairs of dual filters, the coefficients of which are given in parametric form. We shall first construct a 2π-periodic function, $h_0(\xi)$, which satisfies the conditions of subsection 2.1.1 and 2.2.1. Then, a dual 2π-periodic function, $\tilde{h}_0(\xi)$, will be determined in a straightforward way.

The construction of $h_0(\xi)$

Consider a 2π-periodic function

$$h_0(\xi) = \sum_{n=-N}^{N} \alpha_n e^{in\xi}. \tag{2.24}$$

We note that the symmetry of $h_0(\xi)$, that is $h_0(-\xi) = h_0(\xi)$, implies the symmetry of the associated wavelet. To have a mother wavelet which is symmetric around $x = 1/2$, we require that the coefficients α_n satisfy the following relations:

$$\alpha_n = \alpha_{-n}, \qquad 1 \le n \le N. \tag{2.25}$$

From conditions (2.7) and (2.25) we derive the following pair of linear equations:

$$\alpha_0 + 2\sum_{n=1}^{N} \alpha_n = 1, \qquad \alpha_0 + 2\sum_{n=1}^{N} (-1)^n \alpha_n = 0, \tag{2.26}$$

in the $N+1$ unknowns α_j, $j = 0, 1, \ldots, N$. This system has a parametric solution for all $N > 1$. The parameters have to be fixed so that the function f of (2.18) satisfies the inequality (2.19).

Note that, in general, the verification of (2.19) is not easy and cannot be done explicitly. Hence, one resorts to numerical methods to find a good approximation to the upper bound of B_k.

The problem in hand simplifies considerably if, instead of estimating B_k, we estimate the maximum of the absolute value of a piecewise polynomial approximation to $|f(\xi)f(2\xi)\cdots f(2^{k-1}\xi)|$. This method, which turns out to be very efficient in our case, is based on the following theorem.

Theorem 1 *Consider a 2π-periodic function*

$$h_0(\xi) = \sum_{n=-N}^{N} \alpha_n e^{in\xi}, \qquad \alpha_n \in R, \quad \alpha_n = \alpha_{-n}, \quad 1 \le n \le N. \tag{2.27}$$

Suppose that $h_0(0) = 1$ and that $h_0(\xi)$ can be factored in the form

$$h_0(\xi) = \left(\frac{1 + e^{i\xi}}{2}\right)^L f(\xi). \tag{2.28}$$

If we write

$$F_k(\xi) = f(\xi)f(2\xi)\cdots f(2^{k-1}\xi), \tag{2.29}$$

then, for all $\epsilon > 0$ *and* $k > 0$, *there exist a positive integer* r *and a finite partition of* $[0, 2\pi]$, *say* $(I_i)_{i\in I}$, *such that*

$$\left|\sup_{\xi}|F_k(\xi)|^{1/k} - \sup_{\xi}|P_{F_k}(\xi)|^{1/k}\right| < \epsilon, \tag{2.30}$$

where, for each i, *the function* $P_{F_k}(\xi)$ *is equal to a polynomial of degree* r *if* $\xi \in I_i$, *and* 0 *otherwise. Moreover, there exists a piecewise constant function* $P_{F_k}(\xi)$ *satisfying*

$$\left|sup_{\xi}|F_k(\xi)|^{1/k} - sup_{\xi}|P_{F_k}(\xi)|^{1/k}\right| \leq const\left\{\left[1 + \frac{h}{\sup_{\xi}|F_k(\xi)|}\sum_{j=-KN}^{KN}|\beta_j|\right]^{1/k} - 1\right\},$$

where h *is the size of the partition and the* β_j *depends on* $F_k(\xi)$.

Proof: The proof is in three parts.

(a) If

$$Q_n(\cos\xi) = a_0 + a_1\cos\xi + \cdots + a_n\cos n\xi, \qquad a_\nu \in R, \quad 0 \leq \nu \leq n,$$

we obtain an estimate for the upper bound of $\sup_\xi |Q_n(\cos\xi)|$. For $\nu = 1, 2, \ldots, n$, expand $\cos\nu\xi$ in a Taylor series around a point ξ_ν to be fixed later. Thus we have

$$\cos\nu\xi = \sum_{j=0}^{r}(-1)^j\frac{[\nu(\xi-\xi_\nu)]^j}{j!}\cos^{(j)}\xi_\nu + R_{r+1}(\xi),$$

where

$$|R_{r+1}(\xi)| \leq \nu^{r+1}\frac{|\xi-\xi_\nu|^{r+1}}{(r+1)!}.$$

Since $Q_n(\cos\xi)$ is 2π-periodic, it suffices to find the supremum over $[0, 2\pi]$:

$$\sup_{\xi\in[0,2\pi]}|Q_n(\cos\xi)|.$$

Because

$$[0, 2\pi] \subset \bigcup_{m=1}^{([2\pi n]+1)/2} I_m, \qquad I_m = \left[\frac{2m-2}{n}, \frac{2m}{n}\right],$$

where $[r]$ denotes the integer part of the real number r, it follows that

$$\sup_{\xi\in[0,2\pi]} |Q_n(\cos\xi)| = \max_m \left\{ \sup_{\xi\in I_m} |Q_n(\cos\xi)| \right\}.$$

Now, for fixed m, $1 \le m \le ([2\pi n]+1)/2$, let $\xi_m = (2m-1)/n$. Then, for $\xi \in I_m$, a Taylor expansion of order r of $Q_n(\cos\xi)$ around ξ_m gives

$$\begin{aligned} Q_n(\cos\xi) &= a_0 + \sum_{\nu=1}^{n} a_\nu \left(\sum_{j=1}^{r} \frac{[\nu(\xi-\xi_m)]^j}{j!} \cos^{(j)}\xi_m + R_{r+1}(\xi) \right) \\ &= P_{Q_n}^m(\xi) + R(\xi). \end{aligned} \tag{2.31}$$

(b) If $P_{Q_n}(\xi)$ is a function whose restriction on each I_m is a polynomial $P_{Q_n}^m(\xi)$ and 0 outside, then it is clear that

$$\sup_{\xi\in[0,2\pi]} |Q_n(\cos\xi) - P_{Q_n}(\xi)| \le \sum_{\nu=1}^{n} \frac{|a_\nu|}{(r+1)!}. \tag{2.32}$$

Since, $h_0(\xi) = \left(\frac{1+e^{i\xi}}{2}\right)^L f(\xi)$ given by (2.28) is symmetric and 2π-periodic, then necessarily

$$e^{iL\xi/2} f(\xi) = \sum_{n=0}^{N} \left(\delta_{-n}\, e^{-in\xi/2} + \delta_n\, e^{in\xi/2} \right)$$

is symmetric in $e^{i\xi/2}$, that is $\delta_{-n} = \delta_n$. Also, it is clear that

$$\sup_\xi |f(\xi)| = \sup_\xi \left| e^{iL\xi/2} f(\xi) \right| = \sup_\xi \left| e^{iL\xi} f(2\xi) \right|,$$

where, now, $e^{iL\xi} f(2\xi)$ is real since it is symmetric in $e^{i\xi}$. By part (a) of the proof, if

$$e^{iL\xi} f(2\xi) = \sum_{j=-N}^{N} \gamma_j e^{ic_j\xi}, \qquad c_{-j} = -c_j,\ \gamma_{-j} = \gamma_j,\ 1 \le j \le N,$$

then there exists a function $P_f(x)$, associated with a finite partition, $(I_n)_n$, of $[0, 2\pi]$, such that

$$\sup_\xi |f(\xi) - P_f(\xi)| \le \sum_{j=-N}^{N} \frac{|\gamma_j|}{(r+1)!}.$$

(c) Finally, we prove the general case. For any positive integer k, $k \ge 1$, and $F_k(\xi)$ defined by (2.29), the reader can easily check that if $K = (1+2^{k-1})2^{k-2}$, then the

function

$$e^{iK\xi}F_k(2\xi) = \sum_{j=-KN}^{KN} \beta_j e^{id_j\xi}, \qquad d_{-j} = -d_j,\ \beta_{-j} = \beta_j,\ 1 \le j \le KN,$$

is symmetric in $e^{i\xi}$. By choosing the partition

$$[0, 2\pi] = \bigcup_{l=1}^{([2KN\pi]+1)/2} I_l, \qquad I_l = \left[\frac{2l-2}{KN}, \frac{2l}{KN}\right],$$

and using the techniques employed in part (a) of the proof, we construct a function P_{F_k}, whose restriction on each interval I_l is a polynomial of degree r, and which is equal to zero outside $[0, 2\pi]$. Moreover, $P_{F_k}(\xi)$ satisfies

$$\sup_{\xi\in[0,2\pi]} |F_k(\xi) - P_{F_k}(\xi)| \le \sum_{j=-KN}^{KN} \frac{|\beta_j|}{(r+1)!}.$$

This implies the following inequalities:

$$\begin{aligned} \sup_\xi |P_{F_k}(\xi)| &\le \sup_\xi |F_k(\xi)| + \sum_{j=-KN}^{KN} \frac{|\beta_j|}{(r+1)!} \\ &\le \sup_\xi |F_k(\xi)| \left[1 + \frac{1}{\sup_\xi |F_k(\xi)|} \sum_{j=-KN}^{KN} \frac{|\beta_j|}{(r+1)!}\right] \end{aligned} \tag{2.33}$$

and

$$\begin{aligned} &\left| \left[\sup_\xi |P_{F_k}(\xi)|\right]^{1/k} - \left[\sup_\xi |F_k(\xi)|\right]^{1/k} \right| \\ &\le \sup_\xi |F_k(\xi)|^{1/k} \left\{ \left[1 + \frac{1}{\sup_\xi |F_k(\xi)|} \sum_{j=-KN}^{KN} \frac{|\beta_j|}{(r+1)!}\right]^{1/k} - 1 \right\} \\ &\le \text{const} \left\{ \left[1 + \frac{1}{\sup_\xi |F_k(\xi)|} \sum_{j=-KN}^{KN} \frac{|\beta_j|}{(r+1)!}\right]^{1/k} - 1 \right\}. \end{aligned} \tag{2.34}$$

Finally, since $h_0(0) = 1$ implies that $\sup_\xi |F_k(\xi)| \ge 1$, then the right-hand side of (2.34) can be made arbitrarily small by choosing r sufficiently big. Now, if for a given finite partition, $(I_i)_i$, of $[0, 2\pi]$, the restriction of $P_{F_k}(\xi)$ on I_i is approximated by the constant value $F_k(\xi_i)$, where ξ_i is the midpoint of the interval I_i, then the error made in approximating $\sup_\xi |F_k(\xi)|^{1/k}$ is bounded by

$$\text{const} \left\{ \left[1 + \frac{h}{\sup_\xi |F_k(\xi)|} \sum_{j=-KN}^{KN} |\beta_j|\right]^{1/k} - 1 \right\}, \tag{2.35}$$

where h is the size of the partition. This completes the proof. □

Remark 3 The numerical method described in the above Remark can be applied to the more general case where the function $h_0(\xi)$ in Theorem 1 needs not be symmetric. In fact, if $h_0(\xi) = \sum_{-n_0}^{N} \alpha_n e^{in\xi}$, then $f(\xi) = \sum_{-n_0}^{N-L} \beta_n e^{in\xi}$, and

$$|f(\xi)\overline{f(\xi)}| = \sum_{-n_0}^{N-L} \beta_n^2 + 2 \sum_{\substack{-n_0 \le i,j \le N-L \\ i \neq j}} \beta_i \beta_j \cos(i-j)\xi.$$

Hence, if a good approximation to the maximum of $|f(\xi)|^2$ can be obtained by using the above numerical methods, the same is true for $F_k(\xi)$.

The construction of $\tilde{h}_0(\xi)$

Once $h_0(\xi)$ is given in parametric form, the construction of its dual, $\tilde{h}_0(\xi)$, is straightforward. We use the fact that these two functions need to satisfy the following identity:

$$h_0(\xi)\overline{\tilde{h}_0(\xi)} + h_0(\xi+\pi)\overline{\tilde{h}_0(\xi+\pi)} = 1, \qquad \forall\, \xi \in [0,\pi]. \tag{2.36}$$

Moreover, since $h_0(0) = 1$ and $h_0(\pi) = 0$, then necessarily

$$\tilde{h}_0(0) = 1. \tag{2.37}$$

If we require some regularity (at least continuity) on the wavelet $\tilde{\psi}(x)$, then by an argument given in [14], $\tilde{h}_0(\xi)$ also has to satisfy the condition:

$$\tilde{h}_0(\pi) = 0. \tag{2.38}$$

It is trivial to see that if the two functions

$$h_{n_0}(\xi) = \sum_{n=-n_0}^{n_0} \alpha_n\, e^{in\xi} \tag{2.39}$$

and

$$\tilde{h}_{N_0}(\xi) = \sum_{n=-N_0}^{N_0} \beta_n\, e^{in\xi}, \tag{2.40}$$

satisfy (2.36), then the number $n_0 + N_0$ has to be an odd integer, with $\beta_{N_0} \neq 0$.

W.L.O.G. we may assume that $N_0 > n_0$, if $h_{n_0}(\xi)$ is given in terms of $n_0 - 1$ parameters, then by choosing a symmetric 2π-periodic dual function $\tilde{h}_{N_0}(\xi)$ of the form (2.40) for some integer k, and applying conditions (2.36) and (2.38), one obtains the following system of linear equations in β_j:

$$\begin{aligned} \sum_{i+j=2n} \alpha_i \beta_j &= \delta_{0n}, \qquad 0 \leq n \leq \frac{n_0 + N_0 - 1}{2}, \\ \beta_0 + 2\sum_{j=1}^{N_0} (-1)^j \beta_j &= 0. \end{aligned} \tag{2.41}$$

The solution of (2.41) gives us the coefficients of $\tilde{h}_{n_0}(\xi)$ which obviously depend on the parameters α_j. Once the parameters in $\tilde{h}_{N_0}(\xi)$ are fixed, the piecewise constant approximation described in Theorem 1 is used to decide whether or not the dual 2π-periodic functions, $h_{n_0}(\xi)$ and $\tilde{h}_{N_0}(\xi)$, generate a biorthogonal wavelet basis.

It is an interesting feature of the above general method that any pair of symmetric biorthogonal wavelet filters can be easily obtained from it as shown by the following theorem.

Theorem 2 *Any continuous symmetric biorthogonal wavelet basis generated by filters with real coefficients is a special case of the above construction method.*

Proof: Without loss of generality, we may assume that the coefficients of the filters are symmetric around $j = 0$. Thus we let

$$h_{n_0}(\xi) = \sum_{-n_0}^{n_0} \alpha_j e^{ij\xi}, \qquad \tilde{h}_{N_0}(\xi) = \sum_{-N_0}^{N_0} \beta_j e^{ij\xi}, \quad \alpha_j, \beta_j \in R,$$

be the symmetric 2π-periodic functions that generate the biorthogonal wavelet bases. Hence the spectral radii of the transition operators, T_0 and $\tilde{T}_0$, satisfy the inequalities (2.23).

We obtain $h_{n_0}(\xi)$ and $\tilde{h}_{N_0}(\xi)$ by solving the linear systems (2.26) and (2.41). Since system (2.26) corresponds to the minimal conditions on any candidate filter

for generating a biorthogonal wavelet basis, then, by fixing the values of the free parameters in the coefficients $\{\alpha_j\}_{0\le j\le n_0}$, one gets $h_{n_0}(\xi)$. Since $h_{n_0}(\xi)$ and $\tilde{h}_{n_0}(\xi)$ generate continuous biorthogonal wavelet bases, then the coefficients $\{\beta_j\}_{0\le j\le N_0}$ of $\tilde{h}_{n_0}(\xi)$ have to satisfy (2.41).

Consider the matrix A associated with system (2.41) in the unknowns β_j. There are two cases to consider depending upon the rank, rank$A$, of A. In the first case, rank$A = N_0 + 1$. Thus the solution of (2.41) is unique and obviously corresponds to the coefficients of $\tilde{h}_{n_0}(\xi)$.

In the more interesting, second, case, rank$A = r < N_0 + 1$. Thus the general solution of (2.41) contains $N_0 + 1 - r$ parameters, say $\nu_1, \nu_2, \ldots, \nu_{N_0+1-r}$, and it is of the following form:

$$\tilde{h}^{\nu}_{n_0} = \sum_{j=-N_0}^{N_0} \beta_j(\nu_1, \ldots, \nu_{N_0+1-r}) e^{ij\xi}, \tag{2.42}$$

where each $\beta_j(\nu_1, \ldots, \nu_{N_0+1-r})$ is linear in $\nu_1, \ldots, \nu_{N_0+1-r}$. It is clear that there exist numbers $\nu^0_1, \ldots, \nu^0_{N_0+1-r}$ such that the original $\tilde{h}_{n_0}(\xi)$ can be written in the form

$$\tilde{h}_{n_0} = \sum_{j=-N_0}^{N_0} \beta_j(\nu^0_1, \ldots, \nu^0_{N_0+1-r}) e^{ij\xi}.$$

This completes the proof of the theorem. □

If $h_{n_0}(\xi)$ and $\tilde{h}_{n_0}(\xi)$ are defined as in the proof of the previous theorem and if rank$A = r < N_0 + 1$, then we have the following corollary.

Corollary 1 *Under the conditions of the above theorem, for a fixed filter of length* $2n_0+1$ *and whose frequency response is given by* $\sqrt{2}\, h_{n_0}(\xi)$, *there exist infinitely many dual filters of length* $2N_0 + 1$ *with frequency responses given by* $\sqrt{2}\, \tilde{h}^{\nu}_{n_0}(\xi)$.

Proof: Suppose the spectral radii the transition operators, T_0 and $\tilde{T}_0$, satisfy (2.23). Then the inequality $\rho(\tilde{T}_0) < 1$ implies that there exists $\epsilon > 0$ such that $\rho(\tilde{T}_0) < 1 - \epsilon$. Let $\tilde{h}^{\nu}_{n_0}$ be given by (2.42). Thus there exist $\delta_1 > 0, \ldots, \delta_{N_0+1-r} > 0$ such that, if $\tilde{T}^{\nu}_0$

is the transition operator associated with $\tilde{h}^{\nu}_{n_0}$, then

$$\rho(\tilde{T}^{\nu}_0) < 1, \qquad \forall\, \nu = (\nu_1, \ldots, \nu_{N_0+1-r}),$$

where $\nu_i \in (\nu_i^0 - \delta_i, \nu_i^0 + \delta_i)$. $\square$

Finally, note that even if (2.41) has a unique solution, then it is possible to extend this solution in such a way as to generate an infinite family of dual filters. This is given by the following theorem

Theorem 3 *Consider a 2π-periodic function,*

$$h_{n_0}(\xi) = \sum_{j=-n_0}^{n_0} \alpha_j\, e^{ij\xi}, \qquad \alpha_j \in \mathbb{R}, \quad \alpha_j = \alpha_{-j}, \quad 1 \le j \le n_0.$$

Assume that, for some $N_0 > n_0$, there exists a real dual trigonometric function

$$\tilde{h}_{n_0}(\xi) = \sum_{j=-N_0}^{N_0} \beta_j\, e^{ij\xi}, \qquad \beta_j \in \mathbb{R}, \quad \beta_j = \beta_{-j}, \quad 1 \le j \le N_0,$$

such that $h_{n_0}(\xi)$ and $\tilde{h}_{n_0}(\xi)$ satisfy condition (2.13) and $\tilde{h}_{n_0}(\xi)$ factors in the form

$$\tilde{h}_{n_0}(\xi) = \left(\frac{1+e^{i\xi}}{2}\right)^2 \tilde{f}(\xi),$$

where $\tilde{f}(\xi)$ is a trigonometric function satisfying

$$\sup_{\xi} \left|\tilde{f}(\xi)\, \tilde{f}(2\xi) \cdots \tilde{f}(2^{k-1}\xi)\right|^{1/k} \le 2^{3/2-\epsilon},$$

for some positive integer $k \ge 1$ and $\epsilon > 0$. Then, for all $N = N_0 + 2l$, l a positive integer, there exists a set S of trigonometric functions of length $2N+1$, dual to $h_{n_0}(\xi)$ and having parametric coefficients.

Proof: To prove, for a fixed positive integer l, that there exists an infinite set of dual trigonometric functions of length $N_0 + 2l$, it is enough to prove the result for $N = N_0 + 2$. Hence, if we let

$$\tilde{h}_N(\xi) = \sum_{j=-N_0-2}^{N_0+2} \gamma_j\, e^{ij\xi},$$

where

$$\gamma_j = \begin{cases} \beta_j + \delta_j, & \text{if } -N_0 \le j \le N_0, \\ \delta_j, & \text{if } N_0 + 1 \le |j| \le N_0 + 2, \end{cases}$$

then

$$\tilde{h}_N(\xi) = \tilde{h}_{n_0}(\xi) + \tilde{h}^1_{N_0}(\xi),$$

where

$$\tilde{h}^1_{N_0}(\xi) = \sum_{j=-N_0-2}^{N_0+2} \delta_j \, e^{ij\xi}$$

and $\delta_j = \delta_{-j}$. Since $\tilde{h}_N(\xi)$ has to satisfy the identity

$$h_{n_0}(\xi)\,\tilde{h}_N(\xi) + h_{n_0}(\xi+\pi)\,\tilde{h}_N(\xi+\pi) = 1,$$

then the coefficients of $\tilde{h}^1_{N_0}(\xi)$ have to satisfy the following homogeneous system of $(n_0 + N_0 + 3)/2$ linear equations in δ_j:

$$\delta_0 + 2 \sum_{j=1}^{N_0+2} (-1)^j \delta_j = 0, \tag{2.43}$$

$$\sum_{i+j=2n} \alpha_i \delta_j = 0, \qquad 0 \le n \le \frac{n_0 + N_0 + 1}{2}, \tag{2.44}$$

in the $N_0 + 3$ unknowns δ_j, $j = 0, 1, \ldots, N_0 + 2$. Since $N_0 > n_0$, this system has a parametric solution of the form:

$$\delta_j(\delta_{N_0+2}) = \tau_j \, \delta_{N_0+2}, \qquad 0 \le j \le N_0 + 1.$$

Hence

$$\tilde{h}_N(\xi) = \tilde{h}_{n_0}(\xi) + \sum_{j=-N_0-2}^{N_0+2} \tau_j \, \delta_{N_0+2} \, e^{ij\xi}$$

and $h_{n_0}(\xi)$ satisfies equation (2.13).

To prove that, under some conditions on the τ_j, we obtain dual filters that lead to the construction of an infinite family of biorthogonal wavelet bases, we consider the matrix, A, associated with the linear system (2.41) in the unknowns β_j. Since the elements of A are bounded, then for all j, $0 \le j \le N_0 + 2$, we have $|\tau_j| \le C$ for some

constant C. Moreover, because $\tilde{h}^1_{N_0}(\xi)$ is symmetric and $\tilde{h}^1_{N_0}(\pi) = 0$, this function can be factored in the form

$$\tilde{h}^1_{N_0}(\xi) = \left(\frac{1+e^{i\xi}}{2}\right)^2 \tilde{f}^1(\xi).$$

This implies that

$$\tilde{h}_N(\xi) = \tilde{h}_{n_0}(\xi) + \tilde{h}^1_{N_0}(\xi) = \left(\frac{1+e^{i\xi}}{2}\right)^2 \left[\tilde{f}(\xi) + \tilde{f}^1(\xi)\right].$$

Since, $|\tau_j| \leq C$, then there exist two real numbers, $l_{N_0+2} < L_{N_0+2}$, such that for all $\delta_{N_0+2} \in [l_{N_0+2}, L_{N_0+2}]$, we have

$$\sup_{\xi} |\tilde{f}^1(\xi)| < 2^{3/2}(2^{-\epsilon/2} - 2^{-\epsilon}).$$

If we write $\tilde{F}(\xi) := \tilde{f}(\xi) + \tilde{f}^1(\xi)$, then it is clear that

$$\sup_{\xi} |\tilde{F}(\xi)\tilde{F}(2\xi)\cdots\tilde{F}(2^{k-1}\xi)|^{1/k} < 2^{3/2} \times 2^{-\epsilon/2}.$$

Consequently, for all $\delta_{N_0+2} \in [l_{N_0+2}, L_{N_0+2}]$, there exists a dual trigonometric function of length $N_0 + 2$.

By repeating the above technique as many times as required, one easily proves that there exist two real numbers, $l_N < L_N$, such that for all $\delta_N \in [l_N, L_N]$, there exists a dual trigonometric function $\tilde{h}_{\delta_N}(\xi)$ of length $2N+1$, the coefficients of which depend linearly on the parameter δ_N. Furthermore, $h_{n_0}(\xi)$ and $\tilde{h}_{\delta_N}(\xi)$ generate a biorthogonal wavelet basis.

2.3 Numerical Results

The techniques of the previous section have been used to construct filters of length seven and nine, respectively. The coefficients of the dual of each filter are given in parametric form. Let $h_N(\xi)$ and $\tilde{h}_N(\xi)$ denote the dual trigonometric polynomials that generate a set of biorthogonal wavelet bases. Here the integer N stands for the number of vanishing moments [5] of the corresponding wavelets. Since, the coefficients

of $\bar{h}_N(\xi)$ are given in parametric form, we have used the numerical techniques of the previous section to obtain an approximation to the range, $[l_N, L_N]$, of the parameter μ, for which condition (2.20) is satisfied by $\bar{h}_N(\xi)$.

To obtain the filters associated with $h_N(\xi)$ and $\bar{h}_N(\xi)$, it suffices to multiply their coefficients by $\sqrt{2}$.

The decay associated with the Fourier transform of a scaling function $\phi(x)$ is defined as the largest positive real number ϵ such that, for some constant C, the following inequality holds:

$$\int_{-\infty}^{\infty} |\hat{\phi}(\xi)|(1+|\xi|)^{\epsilon}\, d\xi < C.$$

By a classical result from Fourier analysis, one concludes that the scaling function $\phi(x)$ and the corresponding wavelet $\psi(x)$ are at least of class $C^{\epsilon-1}$.

In Table 2.1 [37], we list the coefficients α_n of $h_N(\xi)$ and β_n of $\bar{h}_N(\xi)$, for $N = 2,\ 4$ and 6.

In Table 2.2, we give the range $[l_N, L_N]$ of the parameter μ appearing in $\bar{h}_N(\xi)$ of Table 2.1, and list an estimate of the decays ϵ_N, $\bar{\epsilon}_N$ associated with ϕ_N and $\bar{\phi}_N$ respectively, where the parameter μ is set at 1.0, 1.25 and 2.5, respectively.

Eight iterations of the constructive cascade algorithm given in [15], pp. 202–205, produce a good approximation to the graphs of the scaling functions and the corresponding wavelets.

In Figs. 2.1 to 2.3, we present six sets of graphs of $\phi_N(x)$, $\bar{\phi}_N(x)$, $\psi_N(x)$ and $\bar{\psi}_N(x)$, corresponding to $N = 2$, 4 and 6, respectively. In these figures, the parameter μ was set at 1.0, 1.25 and 2.5, respectively. In Fig. 2.4, the decays, $\bar{\epsilon}_N(\mu)$, associated with the Fourier transforms, $\hat{\bar{\phi}}_N(\xi)$, of the parametric scaling functions, are graphed against the parameter μ, for $N = 2$, 4 and 6, respectively.

Table 2.1: The coefficients α_n of $h_N(\xi)$ and β_n of $\tilde{h}_N(\xi)$.

N	n	α_n	β_n
2	0	0.550	$0.569\,105\,691\,0 + 0.060\,975\,609\,8\,\mu$
	±1	0.250	$0.365\,650\,406\,5 - 0.067\,073\,170\,7\,\mu$
	±2	-0.025	$-0.083\,333\,333\,3$
	±3	0.000	$-0.120\,528\,455\,3 + 0.070\,121\,951\,2\,\mu$
	±4	0.000	$0.048\,780\,487\,7 - 0.030\,487\,880\,4\,\mu$
	±5	0.000	$0.004\,878\,048\,7 - 0.003\,048\,788\,0\,\mu$
4	0	0.593 750 0	$0.520\,023\,738\,6 + 0.011\,332\,417\,4\,\mu$
	±1	0.304 687 5	$0.295\,215\,790\,9 - 0.009\,043\,040\,2\,\mu$
	±2	$-0.046\,875\,0$	$-0.043\,576\,845\,4 - 0.003\,434\,065\,9\,\mu$
	±3	$-0.054\,687\,5$	$-0.066\,317\,288\,8 + 0.014\,079\,670\,3\,\mu$
	±4	0.000 000 0	$0.044\,939\,760\,7 - 0.005\,265\,567\,7\,\mu$
	±5	0.000 000 0	$0.022\,701\,399\,3 - 0.005\,380\,036\,6\,\mu$
	±6	0.000 000 0	$-0.013\,241\,336\,3 + 0.003\,434\,065\,9\,\mu$
	±7	0.000 000 0	$-0.001\,599\,901\,5 + 0.003\,434\,065\,9\,\mu$
	±8	0.000 000 0	$0.001\,866\,551\,8 - 0.000\,400\,641\,0\,\mu$
6	0	0.480 468 750	$0.652\,550\,142\,8 + 0.002\,034\,171\,4\,\mu$
	±1	0.301 562 500	$0.311\,632\,251\,0 - 0.001\,218\,971\,7\,\mu$
	±2	0.026 562 500	$-0.147\,006\,292\,1 - 0.000\,888\,136\,7\,\mu$
	±3	$-0.051\,562\,500$	$-0.094\,861\,784\,2 + 0.002\,128\,062\,5\,\mu$
	±4	-0.016796875	$0.102\,878\,181\,4 - 0.000\,728\,562\,3\,\mu$
	±5	0.000 000 000	$0.037\,606\,500\,2 - 0.001\,058\,792\,7\,\mu$
	±6	0.000 000 000	$-0.043\,722\,261\,0 + 0.000\,861\,540\,9\,\mu$
	±7	0.000 000 000	$-0.003\,013\,442\,6 + 0.000\,101\,345\,9\,\mu$
	±8	0.000 000 000	$0.013\,307\,065\,2 - 0.000\,288\,523\,5\,\mu$
	±9	0.000 000 000	$-0.001\,927\,659\,8 + 0.000\,057\,019\,6\,\mu$
	±10	0.000 000 000	$-0.001\,731\,765\,3 + 0.000\,026\,595\,7\,\mu$
	±11	0.000 000 000	$0.000\,564\,135\,6 - 0.000\,008\,663\,7\,\mu$

Table 2.2: The range $[l_N, L_N]$, for $N = 4$ and 6, of the parameter μ appearing in $\widetilde{h}_N(\xi)$ of Table 2.1 and the optimum lower bounds, ϵ_N and $\bar{\epsilon}_N$, associated to $\widehat{\phi}_N(\xi)$ and $\widehat{\bar{\phi}}_N(\xi)$, respectively.

N	$[l_N, L_N]$	ϵ_N	$\bar{\epsilon}_N$
2	$[-0.13, 2.21]$	1.609 2	1.452 9
4	$[-9.50, 8.70]$	2.111 5	2.916 6
6	$[-39.5, 41.5]$	4.021 7	2.544 3

Table 2.3: The coefficients α_n, $-6 \leq n \leq 6$, of $h_8(\xi)$ and β_n, $-13 \leq n \leq 13$, of $\widetilde{h}_8(\xi)$.

n	α_n	β_n	n	β_n
0	0.546 875 000	0.575 488 869 8	± 7	$-0.000\,271\,925\,9$
± 1	0.332 031 250	0.273 034 506 0	± 8	0.008 072 258 8
± 2	$-0.003\,906\,250$	$-0.095\,275\,997\,9$	± 9	$-0.001\,197\,803\,0$
± 3	$-0.091\,796\,875$	$-0.037\,299\,560\,3$	± 10	$-0.001\,556\,962\,9$
± 4	$-0.023\,437\,500$	0.079 048 638 3	± 11	0.000 396 316 4
± 5	0.009 765 625	0.015 396 951 3	± 12	0.000 134 711 4
± 6	0.003 906 250	$-0.028\,167\,086\,0$	± 13	$-0.000\,058\,486\,8$

Lastly, we have constructed a pair of biorthogonal wavelet filters given by means of the functions $h_8(\xi)$ and $\widetilde{h}_8(\xi)$. The associated dual wavelets ψ_8 and $\widetilde{\psi}_8$ have eight vanishing moments. The coefficients α_j, $-6 \leq j \leq 6$, and β_j, $-13 \leq j \leq 13$, of $h_8(\xi)$ and $\widetilde{h}_8(\xi)$ are listed in Table 2.3. By using the same numerical approximation as before, the decays associated with the Fourier transform of ϕ_8 and $\widetilde{\phi}_8$ are, approximately, $\alpha \approx 4.0774$ and $\bar{\alpha} \approx 2.6090$, respectively. Six iterations of the constructive cascade algorithm have been used to construct a good approximation to the graphs of the scaling functions, ϕ_8 and $\widetilde{\phi}_8$, and their respective wavelets, ψ_8 and $\widetilde{\psi}_8$. These graphs are shown in Fig. 2.5, respectively.

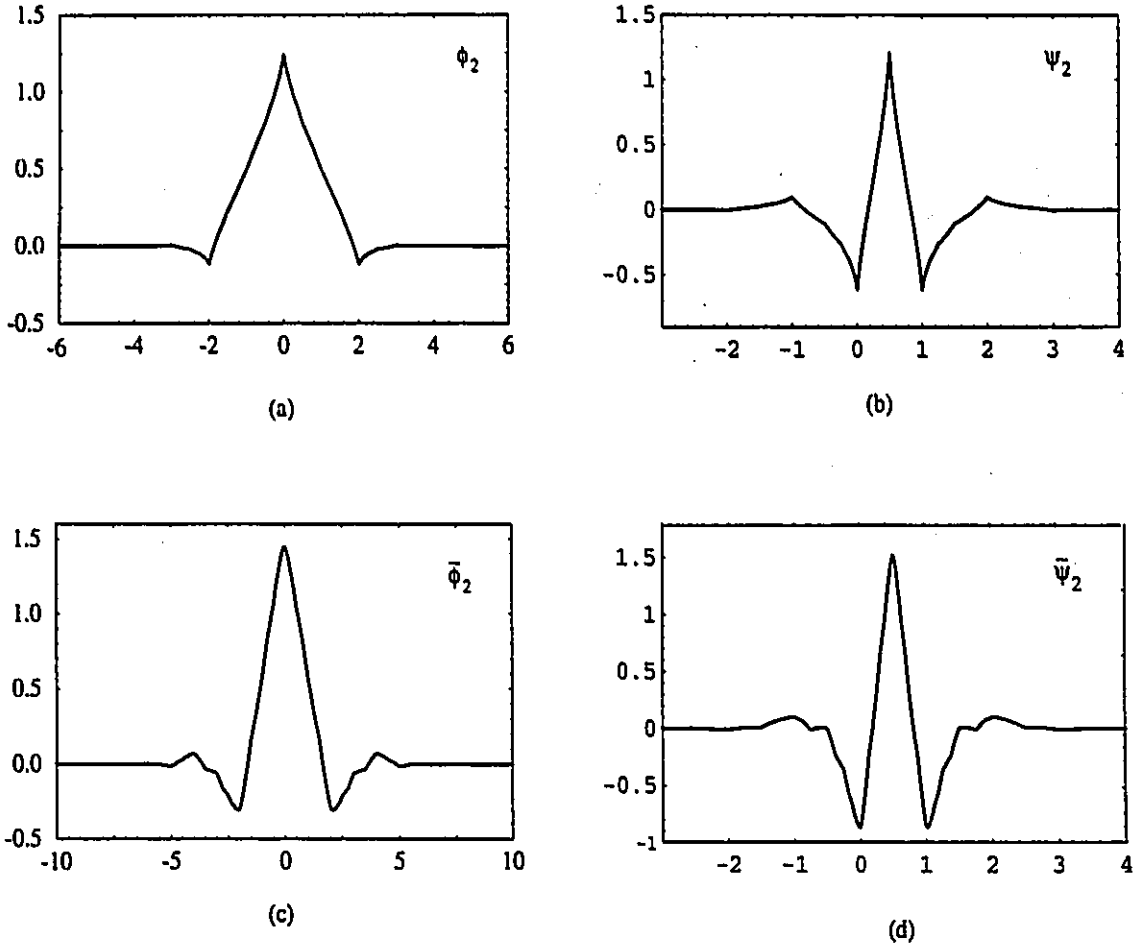

Figure 2.1: Graphs of (a) scaling function $\phi_2(x)$, (b) wavelet $\psi_2(x)$, (c) scaling function $\tilde{\phi}_2(x)$ and (d) wavelet $\tilde{\psi}_2(x)$, for $\mu = 1.0$.

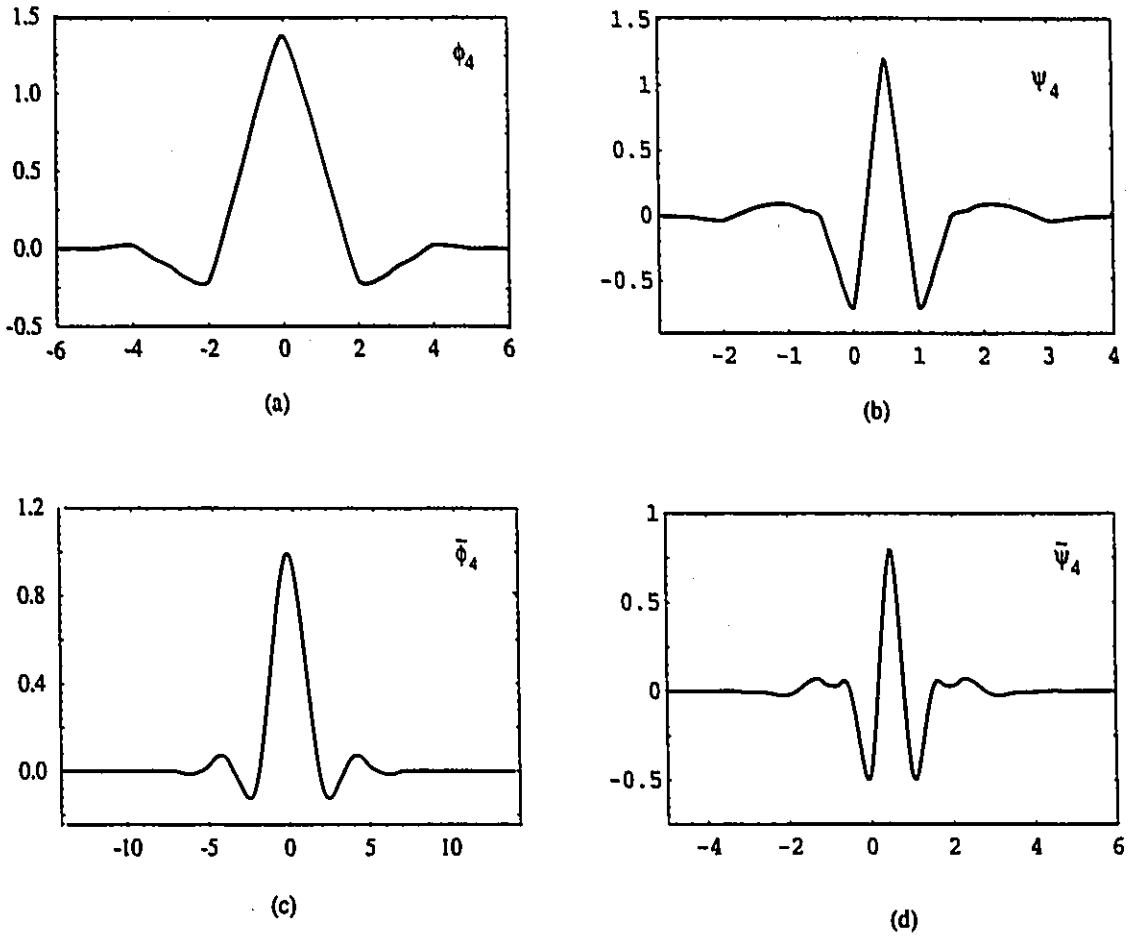

Figure 2.2: Graphs of (a) scaling function $\phi_4(x)$, (b) wavelet $\psi_4(x)$, (c) scaling function $\tilde{\phi}_4(x)$ and (d) wavelet $\tilde{\psi}_4(x)$, for $\mu = 1.25$.

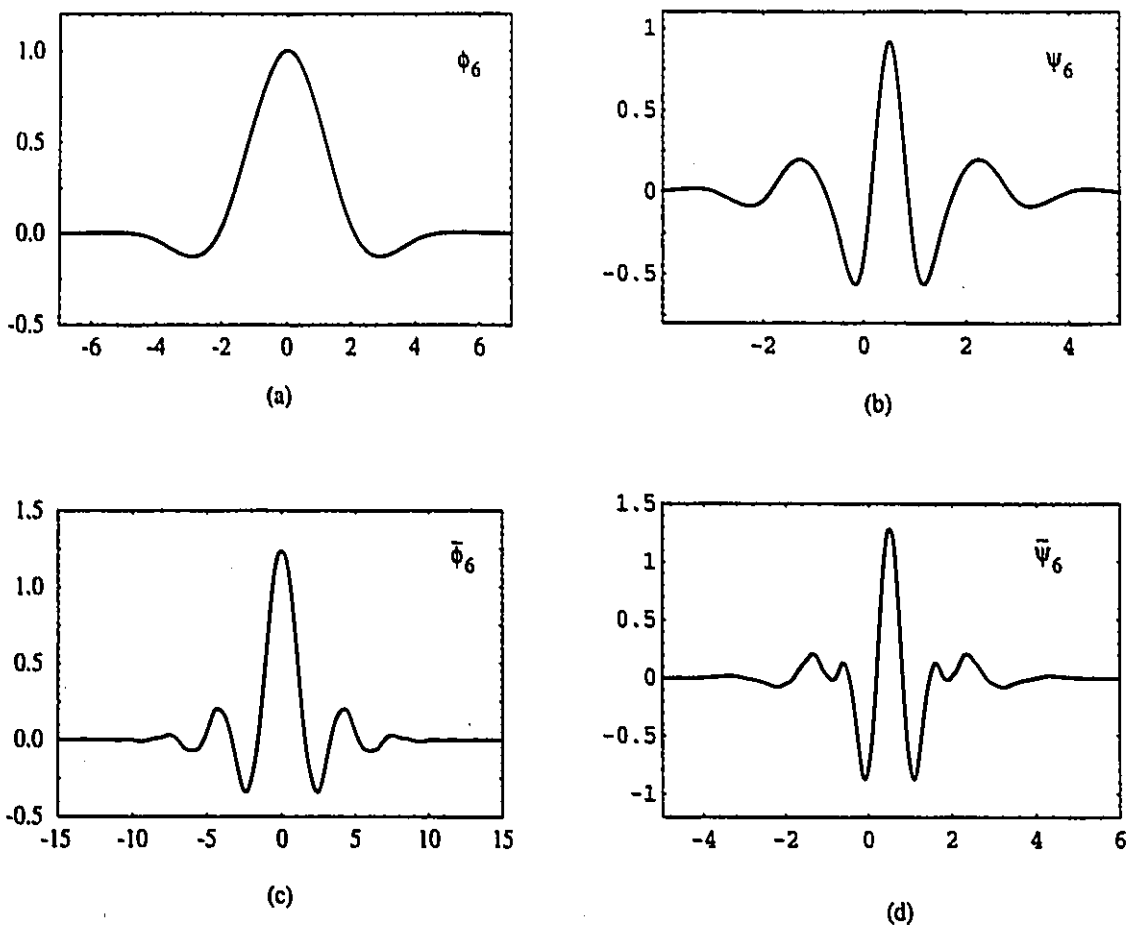

Figure 2.3: Graphs of (a) scaling function $\phi_6(x)$, (b) wavelet $\psi_6(x)$, (c) scaling function $\tilde{\phi}_6(x)$ and (d) wavelet $\tilde{\psi}_6(x)$, for $\mu = 2.5$.

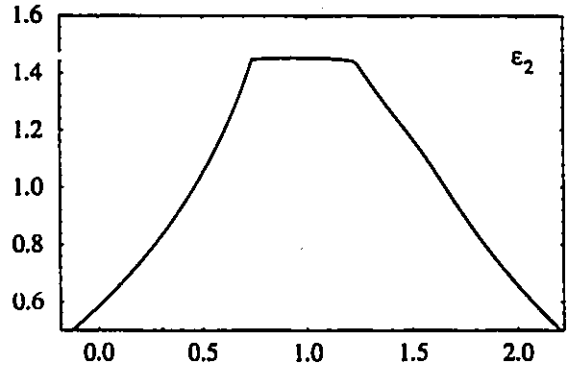

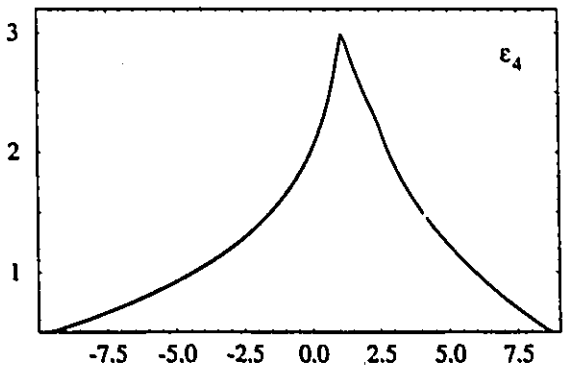

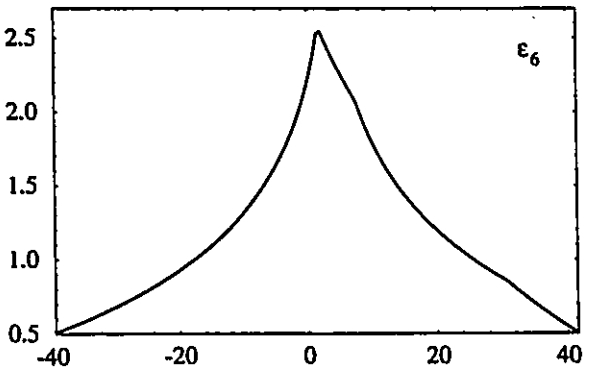

Figure 2.4: Graphs of decay function, $\tilde{\epsilon}_N(\mu)$, of $\hat{\tilde{\phi}}_N(\xi)$ for $N = 2$, 4 and 6, respectively.

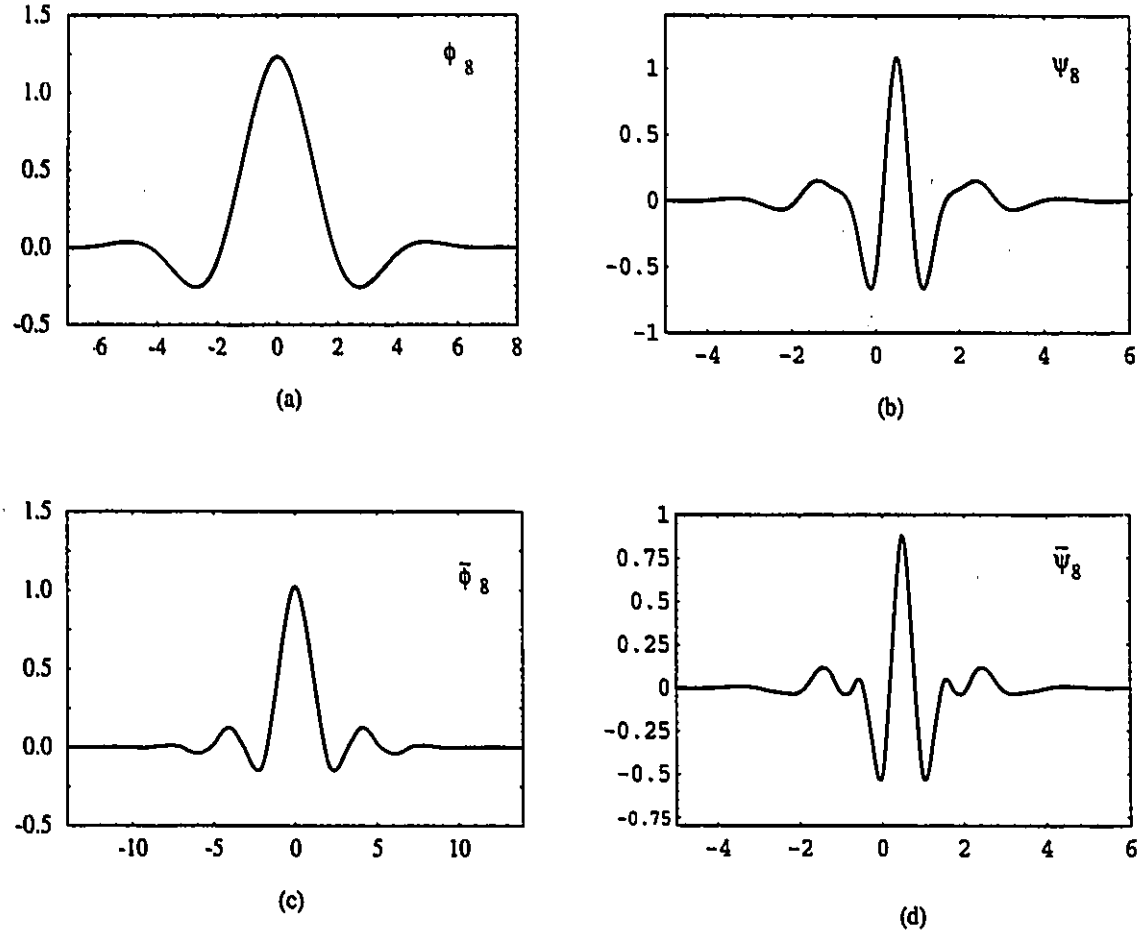

Figure 2.5: Graphs of (a) scaling function $\phi_8(x)$, (b) wavelet $\psi_8(x)$, (c) scaling function $\tilde{\phi}_8(x)$ and (d) wavelet $\tilde{\psi}_8(x)$.

Chapter 3

McClellan Transformation and the Construction of Biorthogonal Wavelet Bases of $L^2(\mathbb{R}^2)$

In recent years, the interest in two-dimensional (2-D) digital signal processing has prompted intensive research in the design of 2-D finite inpulse response (FIR) and infinite inpulse response (IIR) filter banks (see, [44], [59] and [68]). Wavelets, due to their close connection with filter banks, have made possible the implementation of new efficient algorithms for many signal processing applications. Although extensive work has been done in the design of one-dimensional (1-D) wavelets, (see [14], [51], [11], [60]), only a few papers, (see [10], [54], [29]), have dealt with nonseparable 2-D wavelets. Consequently, the design of 2-D wavelets is still essentially done by tensor product of a 1-D wavelet basis. Such wavelets have separable variables; thus details of a 2-D signal in arbitrary directions are not as well represented as in the horizontal and vertical directions. Hence, it is desirable to design nonseparable bidimensional wavelets. Unfortunately, as in filter bank theory, the design of multidimensional wavelets is complicated because many techniques and results from 1-D do not generalize to higher dimensions. Moreover, the design of bidimensional wavelets depends critically on the given dilation matrix $\boldsymbol{D}$, its eigenvalues, λ_1 and λ_2, the norm $\| \boldsymbol{D}^{-1}\|_2$ of its inverse and the absolute value $|\det \boldsymbol{D}|$ of its determinant.

The McClellan transformation (see [21] pp. 137–148) is an efficient tool for generating and implementing multidimensional FIR filters from a 1-D zero-phase FIR filter bank (see [48], [49], [50]). In this chapter, we show how to adapt this transformation in order to construct nonseparable wavelet bases of $L^2(\mathbb{R}^2)$. Note that due to the zero-phase restriction, the McClellan transformation can be applied only on a symmetric biorthogonal wavelet filter of finite length; consequently it generates only biorthogonal 2-D wavelets. Our technique not only allows the use of a large number of transfer functions, $F(\omega_1, \omega_2)$, but also preserves the number of vanishing moments.

The following letters will be used: $\boldsymbol{D} \in \mathbb{Z}^{2\times 2}$ is a 2×2 matrix with integer elements, $\boldsymbol{x} = (x_1, x_2)^t$, $\boldsymbol{\omega} = (\omega_1, \omega_2)^t$, are two-vectors, with real components, and $\boldsymbol{k} = (k_1, k_2)^t$, $\boldsymbol{n} = (n_1, n_2)^t$ are two-vectors with integer components.

3.1 A Multiresolution Analysis and Wavelets of $L^2(\mathbb{R}^2)$

3.1.1 Multiresolution analysis

To design 2-D wavelets, it is natural to generalize the 1-D multiresolution analysis, $M1$, (see [46], [47]), defined in subsection 2.1.1 to a 2-D multiresolution analysis, $M2$. As in 1-D, where $M1$ depends on the dilation factor N, $M2$ is highly dependent on the choice of the dilation matrix $\boldsymbol{D}$, which is defined as follows.

Definition 6 *A matrix $\boldsymbol{D} \in \mathbb{Z}^{n\times n}$ is said to be a dilation matrix if all its singular values are larger than* 1*: $\sigma_i > 1$, $i = 1, 2, \ldots, n$.*

The condition on the singular values ensures that every direction in $\mathbb{R}^n$ is dilated, which is a very desirable property of the multiresolution concept. Moreover, $\|\boldsymbol{D}\|_2 = \sigma_1 > 1$, $\|\boldsymbol{D}^{-1}\|_2 = 1/\sigma_n < 1$ and $d = |\det \boldsymbol{D}| = \sigma_1\sigma_2\cdots\sigma_n$ is an integer. The condition $\|\boldsymbol{D}^{-1}\|_2 = 1/\sigma_n < 1$ is used in Theorems 4 and 5.

Under these conditions, $M2$ is defined as follows.

Definition 7 *A 2-D multiresolution analysis, $M2$, is a decreasing sequence of closed linear subspaces of $L^2(\mathbb{R}^2)$,*

$$\cdots \subset V_2 \subset V_1 \subset V_0 \subset V_{-1} \subset V_{-2} \subset \cdots,$$

with the following properties:

$(P1)$ $\bigcup_{-\infty}^{\infty} V_j$ *is dense in* $L^2(\mathbb{R}^2)$ *and* $\bigcap_{-\infty}^{\infty} V_j = \{0\}$;

$(P2)$ $\forall\, j \in \mathbf{Z}, \quad f(\boldsymbol{x}) \in V_{j+1} \Longleftrightarrow f(\boldsymbol{D}\boldsymbol{x}) \in V_j$;

$(P3)$ $\exists\, \phi \in V_0 \subset L^2(\mathbb{R}^2)$ *such that* $\phi_{0,\boldsymbol{n}}(\boldsymbol{x}) = \phi(\boldsymbol{x} - \boldsymbol{n})$, $\boldsymbol{n} \in \mathbf{Z}^2$, *is an orthonormal basis of* V_0.

If we define

$$\phi_{j,\boldsymbol{k}}(\boldsymbol{x}) = |\det \boldsymbol{D}|^{-j/2} \phi(\boldsymbol{D}^{-j}\boldsymbol{x} - \boldsymbol{k}), \qquad j \in \mathbf{Z}, \quad \boldsymbol{k} \in \mathbf{Z}^2, \tag{3.1}$$

by scaling and translation, then it is easily seen from $(P2)$ and $(P3)$ that, for fixed $j \in \mathbf{Z}$, the family of functions, $\phi_{j,\,\boldsymbol{k}}(\boldsymbol{x})$, $\boldsymbol{k} \in \mathbf{Z}^2$, form an orthonormal basis of V_j. It follows from these properties, that a sampling rate of $|\det \boldsymbol{D}|$ has to be achieved in order to go from one approximation level to the next. This means that the number of sampling points has to be multiplied by $|\det \boldsymbol{D}|$ in order to represent the signal in the next level. Note that the geometry of the sampling grid, $\Gamma = \mathbf{Z}^2/\boldsymbol{D}\mathbf{Z}^2$, is defined by means of the matrix $\boldsymbol{D}$. In other word, to achieve exact reconstruction, we need to construct one scaling function and $|\det \boldsymbol{D}| - 1$ wavelets by iterating one lowpass filter. In the interesting case $|\det \boldsymbol{D}| = 2$, only one elementary wavelet $\Psi_{0,0}(\boldsymbol{x}) = \Psi(\boldsymbol{x})$ has to be constructed.

Note that the family of functions

$$\Psi_{j,\boldsymbol{k}}(\boldsymbol{x}) = |\det \boldsymbol{D}|^{-j/2} \Psi(\boldsymbol{D}^{-j}\boldsymbol{x} - \boldsymbol{k}), \qquad j \in \mathbf{Z}, \quad \boldsymbol{k} \in \mathbf{Z}^2,$$

forms an orthonormal basis of the orthogonal complement, W_j, of V_j in V_{j-1}. If we define the scaling functions $\Phi_{j,k}$ as we have defined $\Psi_{j,k}$, then for $f(x) \in L^2(\mathbb{R}^2)$ and $J \in \mathbf{Z}$,

$$\begin{aligned} f(x) &= \sum_{j\in\mathbf{Z}} \sum_{k\in\mathbf{Z}^2} < f, \Psi_{j,k} > \Psi_{j,k}(x) \\ &= \sum_{k\in\mathbf{Z}^2} < f, \Phi_{J,k} > \Phi_{J,k}(x) + \sum_{j<J} \sum_{k\in\mathbf{Z}^2} < f, \Psi_{j,k} > \Psi_{j,k}(x), \end{aligned}$$

where the scalar product is defined by

$$< f, \Psi_{j,k} >= \int_{\mathbb{R}^2} f(x)\, \overline{\Psi_{j,k}(x)}\, dx.$$

A similar formula holds for $< f, \Phi_{j,k} >$. If in $(P2)$ we take $f = \Phi$ and use (P_3), then there exists a finite sequence of real numbers α_n such that

$$\Phi(x) = \sum_{n\in\mathbf{Z}^2} \alpha_n \Phi(Dx - n). \tag{3.2}$$

From now on, only the quincunx-decimation and the column-decimation dilation matrices will be considered.

For quincunx decimation (Fig. 3.1 (a)), the sampling sublattice $Q = \mathbf{Z}^2/D\mathbf{Z}^2$, where $|\det D| = 2$, is defined by

$$Q = \{(a,b)^t \in \mathbf{Z}^2; \quad a, b \text{ have the same parity}\}.$$

By using the results of the next section, the elementary wavelet Ψ associated with Q is given by

$$\Psi(x) = \sum_{(n,m)\in\mathbf{Z}^2} (-1)^n \alpha_{1-n,-m} \Phi\big(Dx - (n,m)^t\big). \tag{3.3}$$

Similarly, for column decimation (Fig. 3.1 (b)), the sampling sublattice $C = \mathbf{Z}^2/D\mathbf{Z}^2$, where $|\det D| = 2$, is defined as

$$C = \{(a,b)^t \in \mathbf{Z}^2; \quad a \text{ is even}\},$$

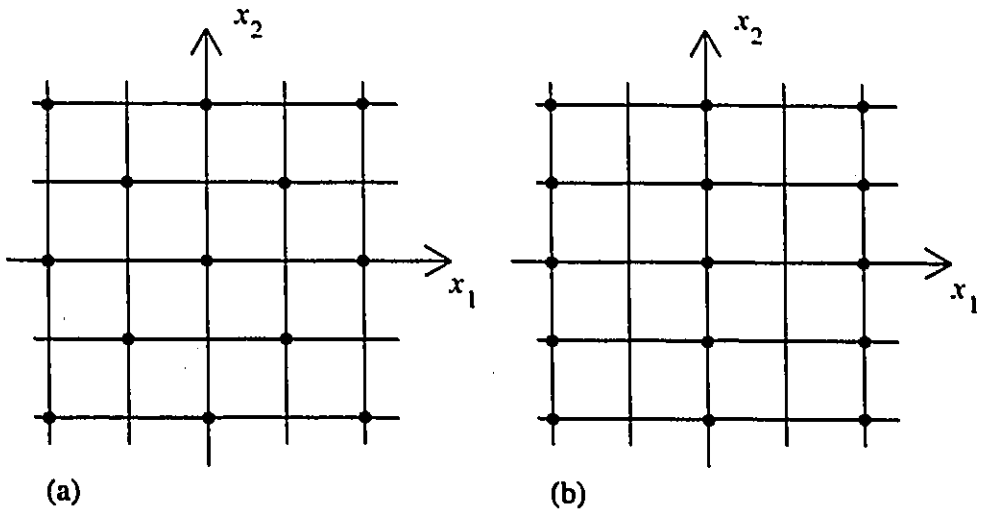

Figure 3.1: (a) The Quincunx sampling lattice, (b) The Column sampling lattice.

and the elementary wavelet is given by

$$\Psi(\boldsymbol{x}) = \sum_{(n,m)\in\mathbb{Z}^2} (-1)^{n+m} \alpha_{1-n,1-m} \Phi\big(\boldsymbol{D}\boldsymbol{x} - (n,m)^t\big). \tag{3.4}$$

In general, $\Phi(\boldsymbol{x})$ is not known exactly. However, under some conditions on the filter $H(\boldsymbol{\omega})$ and on the matrix $\boldsymbol{D}$, the 2-D cascade algorithm given in [40] produces a good numerical approximation to $\Phi(\boldsymbol{x})$.

As in filter bank theory, where the analyzing and synthetizing filters may be different, in the present case it is possible to use two different families of wavelets, one to decompose and the other to reconstruct a signal. Such wavelets are called biorthogonal wavelets and are described in the following subsection.

3.1.2 Biorthogonal wavelets for $L^2(\mathbb{R}^2)$

We first generalize the 2-D orthonormal multiresolution analysis to a 2-D biorthogonal multiresolution analysis.

Definition 8 *A 2-D biorthogonal multiresolution analysis is a decreasing pair of families, $(V_j)_{j\in\mathbf{Z}}$, and $(\tilde{V}_j)_{j\in\mathbf{Z}}$, of linear subspaces of $L^2(\mathbb{R}^2)$:*

$$\cdots \subset V_2 \subset V_1 \subset V_0 \subset V_{-1} \subset V_{-2} \subset \cdots, \tag{3.5}$$

$$\cdots \subset \tilde{V}_2 \subset \tilde{V}_1 \subset \tilde{V}_0 \subset \tilde{V}_{-1} \subset \tilde{V}_{-2} \subset \cdots, \tag{3.6}$$

where each family satisfies properties $(P1)$ and $(P2)$ of Definition 6. Moreover, the two families are related to each other by the following orthogonality conditions:

$$\widetilde{W}_j \perp V_j, \qquad W_j \perp \tilde{V}_j,$$

where W_j and $\widetilde{W}_j$ are the (in general non-orthonormal) complements of V_j and $\tilde{V}_j$ in V_{j-1} and $\tilde{V}_{j-1}$, respectively.

If $|\det \boldsymbol{D}| = 2$, and $\Phi(\boldsymbol{x})$ and $\tilde{\Phi}(\boldsymbol{x})$ are the scaling functions whose $\mathbf{Z}^2$-translates generate biorthogonal bases of V_0 and $\tilde{V}_0$, respectively, then the reconstruction formula is written as:

$$\begin{aligned}
f(\boldsymbol{x}) &= \sum_{j\in\mathbf{Z}}\sum_{k\in\mathbf{Z}^2} < f, \Psi_{j,k} > \tilde{\Psi}_{j,k}(\boldsymbol{x}) \\
&= \sum_{j\in\mathbf{Z}}\sum_{k\in\mathbf{Z}^2} < f, \tilde{\Psi}_{j,k} > \Psi_{j,k}(\boldsymbol{x}), \\
&= \sum_{k\in\mathbf{Z}^2} < f, \Phi_{J,k} > \tilde{\Phi}_{J,k}(\boldsymbol{x}) + \sum_{j<J}\sum_{k\in\mathbf{Z}^2} < f, \Psi_{j,k} > \tilde{\Psi}_{j,k}(\boldsymbol{x}), \\
&= \sum_{k\in\mathbf{Z}^2} < f, \tilde{\Phi}_{J,k} > \Phi_{J,k}(\boldsymbol{x}) + \sum_{j<J}\sum_{k\in\mathbf{Z}^2} < f, \tilde{\Psi}_{j,k} > \Psi_{j,k}(\boldsymbol{x}).
\end{aligned}$$

With the notation of the previous section, the elementary biorthogonal wavelets are given by

$$\begin{aligned}
\Psi(\boldsymbol{x}) &= \sum_{(n,m)\in\mathbf{Z}^2} (-1)^{n+m} \tilde{\alpha}_{1-n,1-m} \Phi\big(\boldsymbol{D}\boldsymbol{x} - (n,m)^t\big), \\
\tilde{\Psi}(\boldsymbol{x}) &= \sum_{(n,m)\in\mathbf{Z}^2} (-1)^{n+m} \alpha_{1-n,1-m} \tilde{\Phi}\big(\boldsymbol{D}\boldsymbol{x} - (n,m)^t\big),
\end{aligned} \tag{3.7}$$

for column decimation, and by

$$\begin{aligned}\Psi(x) &= \sum_{(n,m)\in\mathbb{Z}^2} (-1)^n \bar{\alpha}_{1-n,-m}\Phi\big(Dx-(n,m)^t\big),\\ \tilde{\Psi}(x) &= \sum_{(n,m)\in\mathbb{Z}^2} (-1)^n \alpha_{1-n,-m}\tilde{\Phi}\big(Dx-(n,m)^t\big),\end{aligned} \tag{3.8}$$

for quincunx decimation (see [10]).

The theoretical results of this section will be used in the design of 2-D biorthogonal wavelets in the next section.

3.2 A Design of 2-D Nonseparable Wavelets

3.2.1 The McClellan transformation

As mentioned earlier, our design is based on the McClellan transformation and consequently only biorthogonal wavelet bases will be considered from now on. We obtain symmetric compactly supported wavelets since we use symmetric 1-D wavelet filters of finite length. To proceed further, the following definition is needed

Definition 9 *An n-D zero-phase filter is a compactly supported filter with frequency response $H(\omega)$ satisfying*

$$H(\omega) = \sum_{k\in\mathbb{Z}^n} \alpha_k \cos(k\cdot\omega), \qquad \alpha_k \in \mathbb{R}.$$

McClellan's transformation, which is widely used for designing and implementing multidimentional FIR filters, [48], [49], [50], can be defined as follows.

Definition 10 *Let $h(\omega) = \sum_0^N \alpha_n \cos(n\omega)$ be the frequency response of a 1-D zero-phase FIR filter. Then $h(\omega)$ can be rewritten in the form $h(\omega) = \sum_0^N \alpha_n T_n[\cos(\omega)]$, where T_n is the nth Chebyshev polynomial. Now, if $F(\omega)$ is a given frequency response of a zero-phase 2-D FIR filter, and FIR_1, FIR_2 denote the set of 1-d and 2-D zero-phase FIR filters, respectively, then $M_f : FIR_1 \longrightarrow FIR_2$, and defined by*

$$M_F(h(\omega)) = \sum_{n=0}^{N} \alpha_n T_n[F(\omega)]$$

is the McClellan transformation associated to $F(\omega)$ and applied to $h(\omega)$.

Note that the function $F(\omega)$ in the above definition is also known as a transfer function. Finally, unlike filter bank theory, some extra conditions on the function $F(\omega)$ are needed to construct 2-D wavelet filters. These conditions are derived by using the two following properties.

(α) Let $h(\omega) = \sum_0^N \alpha_n \cos(n\omega)$ and $\tilde{h}(\omega) = \sum_0^{\tilde{N}} \tilde{\alpha}_n \cos(n\omega)$.
Then

$$h(\omega)\tilde{h}(\omega) + h(\omega+\pi)\tilde{h}(\omega+\pi) = 1, \qquad \forall \omega \in [0,\pi], \tag{3.9}$$

if and only if

$$\left(\sum_{n=0}^{N} \alpha_n T_n[x]\right)\left(\sum_{n=0}^{\tilde{N}} \tilde{\alpha}_n T_n[x]\right) + \left(\sum_{n=0}^{N} \alpha_n T_n[-x]\right)\left(\sum_{n=0}^{\tilde{N}} \tilde{\alpha}_n T_n[-x]\right) = 1, \tag{3.10}$$

for all $-1 \le x \le 1$. In fact, (3.10) is equivalent to the identity

$$\left(\sum_{n=0}^{N} \alpha_n T_n[\cos\omega]\right)\left(\sum_{n=0}^{\tilde{N}} \tilde{\alpha}_n T_n[\cos\omega]\right) + \left(\sum_{n=0}^{N} \alpha_n T_n[\cos(\omega+\pi)]\right)\left(\sum_{n=0}^{\tilde{N}} \tilde{\alpha}_n T_n[\cos(\omega+\pi)]\right) = 1. \tag{3.11}$$

Since $\cos : [0,\pi] \to [-1,1]$ is a bijection, then (3.9) is equivalent to (3.10).

(β) Let $h(\omega) = \sum_0^N \alpha_n \cos(n\omega)$. Then $h(\omega)$ has a zero of order $2m$ at π if and only if, for $0 \le x \le 1$,

$$\sum_{n=0}^{N} \alpha_n T_n[2x^2 - 1] = x^{2m} P_{2(N-m)}(x), \tag{3.12}$$

where $P_{2(N-m)}(x)$ is a polynomial of degree $2(N-m)$. In fact, by writing

$$h(\omega) = \sum_0^N \alpha_n T_n[\cos(\omega)] = \sum_0^N \alpha_n T_n\left[2\cos^2\left(\frac{\omega}{2}\right) - 1\right], \tag{3.13}$$

it is easy to prove that $h(\omega)$ has a zero of order 2m at π if and only if $\sum_{n=0}^N \alpha_n T_n[2x^2-1]$ has a zero of order 2m at zero which proves the equality (3.12).

Remark 4 *Property* (α) *provides necessary conditions on* $F(\omega)$ *to have exact 2-D reconstruction.*

Remark 5 *Property* (β) *shows how to preserve the number of vanishing moments. Suppose that*

$$F(\omega) = 2f^2(\omega) - 1 \tag{3.14}$$

and $h(\omega)$ *has a zero of order* $2m$ *at* π*, then the frequency response of the corresponding filter factors as*

$$H(\omega) = f^{2m}(\omega) P_{2(N-m)}\big(f(\omega)\big), \tag{3.15}$$

where, here and in the following, $f^m(\omega)$ *denotes the* m*th power of* f

$$f^m(\omega) := [f(\omega)]^m.$$

Hence by choosing an appropriate $f(\omega)$*, the 1-D and the corresponding 2-D wavelets have the same number of vanishing moments.*

3.2.2 A 2-D wavelet design

From 1-D to 2-D filters

From now on, we assume that the dilation matrix $\boldsymbol{D}$ satisfies $|\det \boldsymbol{D}| = 2$. We shall use the quincunx and the column decimations to illustrate the design techniques. It is known (see [10]) that the construction of 2-D biorthogonal wavelets reduces to the design of a pair of 2-D low-pass filters whose frequency responses $H(\omega_1, \omega_2)$, $\widetilde{H}(\omega_1, \omega_2)$ satisfy, for $\omega_1, \omega_2 \in [0, 2\pi]$, the equations

$$H(\omega_1, \omega_2)\widetilde{H}(\omega_1, \omega_2) + H(\omega_1 + \pi, \omega_2 + \pi)\widetilde{H}(\omega_1 + \pi, \omega_2 + \pi) = 1, \tag{3.16}$$

for quincunx decimation, and

$$H(\omega_1, \omega_2)\widetilde{H}(\omega_1, \omega_2) + H(\omega_1 + \pi, \omega_2)\widetilde{H}(\omega_1 + \pi, \omega_2) = 1, \tag{3.17}$$

for column decimation. Note that H and $\widetilde{H}$ are obtained by applying the McClellan transformation on a 1-D biorthogonal filter and its dual, respectively. If

$$h(\omega) = \sum_{n=0}^{N} \alpha_n \cos(n\omega), \qquad \tilde{h}(\omega) = \sum_{n=0}^{\tilde{N}} \tilde{\alpha}_n \cos(n\omega) \tag{3.18}$$

denote the Fourier transform of the 1-D filter and its dual, respectively, then

$$h(\omega)\tilde{h}(\omega) + h(\omega+\pi)\tilde{h}(\omega+\pi) = 1. \tag{3.19}$$

Thus, for quincunx decimation, H and $\widetilde{H}$ will satisfy (3.16) if the transformation function $F(\omega_1, \omega_2)$ satisfies

$$F(\omega_1 + \pi, \omega_2 + \pi) = -F(\omega_1, \omega_2). \tag{3.20}$$

The wavelets will be in $L^2(\mathbb{R}^2)$ only if the infinite product

$$\prod_{j=1}^{\infty} H({}^t\boldsymbol{D}^{-j}\omega),$$

converges; thus necessarily

$$F(0,0) = 1. \tag{3.21}$$

In terms of the auxiliary transformation function $f(\omega_1, \omega_2)$, conditions (3.20) and (3.21) are written as

$$f^2(\omega_1 + \pi, \omega_2 + \pi) = 1 - f^2(\omega_1, \omega_2), \qquad f(0,0) = 1. \tag{3.22}$$

For column decimation, conditions (3.20) and (3.21) become

$$f^2(\omega_1 + \pi, \omega_2) = 1 - f^2(\omega_1, \omega_2), \qquad f(0,0) = 1. \tag{3.23}$$

We remark that conditions of type (3.22) and (3.23) are necessary, but not sufficient, for exact reconstruction. In fact, they do not ensure that the constructed wavelets are regular or even in $L^2(\mathbb{R}^2)$. However, by imposing extra conditions on $f(\omega)$, $H(\omega)$ and $\widetilde{H}(\omega)$, the construction of $L^2(\mathbb{R}^2)$ biorthogonal wavelets is ensured, as shown in the following paragraph.

Wavelet bases of $L^2(\mathbb{R}^2)$

Under the assumption that the dual scaling functions, ψ^0, $\tilde{\psi}^0$, and the $(d-1)$ different dual mother wavelets, ψ^i, $\tilde{\psi}^i$, $i = 0, \ldots, d-1$, satisfy

$$\psi^i(\boldsymbol{x}) = \sum_{\boldsymbol{l}} \alpha^i_{\boldsymbol{l}} \psi^0(\boldsymbol{D}\boldsymbol{x} - \boldsymbol{l}), \quad \tilde{\psi}^i(\boldsymbol{x}) = \sum_{\boldsymbol{l}} \tilde{\alpha}^i_{\boldsymbol{l}} \tilde{\psi}^0(\boldsymbol{D}\boldsymbol{x} - \boldsymbol{l}).$$

The following theorem which is a generalization of the one given in [11], provides us with some necessary and sufficient conditions for the construction of biorthogonal wavelets of $L^2(\mathbb{R}^n)$.

Theorem 4 *Let $\boldsymbol{D}$ be a dilation matrix and set $d = |\det \boldsymbol{D}|$. Assume that for some positive numbers, ϵ and $\tilde{\epsilon} > 0$, and $0 \le i \le d-1$, we have*

$$|\widehat{\psi}^i(\boldsymbol{\xi})| < c\left(1 + |\boldsymbol{\xi}|^2\right)^{-\epsilon - n/4}, \qquad |\widehat{\tilde{\psi}}^i(\boldsymbol{\xi})| < c\left(1 + |\boldsymbol{\xi}|^2\right)^{-\tilde{\epsilon} - n/4}, \tag{3.24}$$

for some constant c. For $j \in \mathbb{Z}$ and $\boldsymbol{k} \in \mathbb{Z}^n$, define

$$\begin{aligned} \psi^i_{j,\boldsymbol{k}}(\boldsymbol{x}) &= |\det \boldsymbol{D}|^{-j/2} \psi^i(\boldsymbol{D}^{-j}\boldsymbol{x} - \boldsymbol{k}), \\ \tilde{\psi}^i_{j,\boldsymbol{k}}(\boldsymbol{x}) &= |\det \boldsymbol{D}|^{-j/2} \tilde{\psi}^i(\boldsymbol{D}^{-j}\boldsymbol{x} - \boldsymbol{k}), \end{aligned}$$

where the compactly supported wavelets ψ^i, $\tilde{\psi}^i$ are as defined in (5.37) *and assume that*

$$\sum_{i=0}^{d-1} \sum_{\boldsymbol{l} \in \mathbb{Z}^n} \alpha^i_{\boldsymbol{l} - \boldsymbol{D}\boldsymbol{j}} \tilde{\alpha}^i_{\boldsymbol{l} - \boldsymbol{D}\boldsymbol{k}} = \delta_{\boldsymbol{j} - \boldsymbol{k}}. \tag{3.25}$$

Then for $f \in L^2(\mathbb{R}^n)$, we have

$$f = \sum_{i=1}^{d-1} \sum_{j \in \mathbb{Z}} \sum_{\boldsymbol{k} \in \mathbb{Z}^n} \left\langle f, \tilde{\psi}^i_{j,\boldsymbol{k}} \right\rangle \psi^i_{j,\boldsymbol{k}} = \sum_{i=1}^{d-1} \sum_{j \in \mathbb{Z}} \sum_{\boldsymbol{k} \in \mathbb{Z}^n} \left\langle f, \psi^i_{j,\boldsymbol{k}} \right\rangle \tilde{\psi}^i_{j,\boldsymbol{k}}. \tag{3.26}$$

Proof: See the next chapter.

By the factorization formula (3.15), the following theorem whose proof is given in the next chapter, provides us with a way of designing wavelet bases of $L^2(\mathbb{R}^2)$.

Theorem 5 *Let $\boldsymbol{D}$ be a dilation matrix and assume that the frequency response, $H(\boldsymbol{\xi})$, of an n-D FIR wavelet filter factors in the form*

$$H(\boldsymbol{\xi}) = f^{2N}(\boldsymbol{\xi})\mathcal{F}(\boldsymbol{\xi}), \tag{3.27}$$

where

$$\prod_{j=1}^{\infty} f^2({}^t\boldsymbol{D}^{-j}\boldsymbol{\xi}) \leq \frac{c}{1+|\boldsymbol{\xi}|^2}, \tag{3.28}$$

and for some $k \geq 1$ we have the bound

$$B_k := \max_{\boldsymbol{\xi}\in\mathbb{R}^n} \left|\mathcal{F}(\boldsymbol{\xi})\mathcal{F}({}^t\boldsymbol{D}\boldsymbol{\xi})\cdots\mathcal{F}({}^t\boldsymbol{D}^{k-1}\boldsymbol{\xi})\right|^{1/k} < \|\boldsymbol{D}^{-1}\|_2^{-2N+n/2}. \tag{3.29}$$

Then, the Fourier transform

$$\widehat{\phi}(\boldsymbol{\xi}) = \prod_{j=1}^{\infty} H({}^t\boldsymbol{D}^{-j}\boldsymbol{\xi}),$$

of the scaling function $\phi(\boldsymbol{\xi})$ satisfies the inequality

$$\left|\widehat{\phi}(\boldsymbol{\xi})\right| \leq C(1+|\boldsymbol{\xi}|^2)^{-\epsilon-n/2}, \qquad \epsilon < N - \frac{n}{2} + \frac{\log(B_k)}{2\log(\|\boldsymbol{D}^{-1}\|_2)}. \tag{3.30}$$

Under the hypothesis of the above theorem, Note that $n = d = 2$ in our case.

Remark 6 *If the hypotheses of Theorem 5 are satisfied, then the constructed wavelets are r-Hölder continuous for all real r satisfying*

$$0 \leq r < 2N - 2 + \frac{\log(B_k)}{\log\left(\|\boldsymbol{D}^{-1}\|_2\right)}.$$

However, this estimate is far from being optimal and, in practice, does not generally provide a good estimate for the regularity of the wavelets.

Example 1. The following example makes use of Theorem 5.
Consider the 1-D biorthogonal wavelet filters with frequency responses $h_1(\omega)$, $\widetilde{h}_1(\omega)$ and whose coefficients are given in Table 3.1. Then, by choosing the dilation matrix

$$\boldsymbol{D}_1 = \begin{bmatrix} 1 & 1 \\ 1 & -1 \end{bmatrix},$$

Table 3.1: The coefficients a_n of $h_1(\omega)$ for $-3 \leq n \leq 3$, and the coefficients $\tilde{a}_n$ of $\tilde{h}_1(\omega)$ for $-8 \leq n \leq 8$.

n	a_n	$\tilde{a}_n$
0	0.593 750 000	0.534 189 260 4
±1	0.304 687 500	0.283 911 990 7
±2	−0.046 875 000	−0.047 869 427 8
±3	−0.054 687 500	−0.048 717 700 9
±4		0.038 357 801 0
±5		0.015 976 353 5
±6		−0.008 948 753 9
±7		−0.001 170 643 2
±8		0.001 365 750 5

Table 3.2: The coefficients $\alpha_{n,m}$ of $H_1(\omega_1, \omega_2)$ for $-3 \leq n, m \leq 3$.

$n\backslash m$	0	±1	±2	±3
±0	0.640625000000	0.172851562500	−0.011718750000	−0.006835937500
±1	0.172851562500	−0.023437500000	−0.020507812500	−0.000000000000
±2	−0.011718750000	−0.020507812500	−0.000000000000	0.000000000000
±3	−0.006835937500	−0.000000000000	0.000000000000	−0.000000000000

and applying the McClellan transformation with the transfer function

$$F_q(\omega_1, \omega_2) = \frac{1}{2}(\cos\omega_1 + \cos\omega_2),$$

one obtains 2-D biorthogonal filters with frequency responsses $H_1(\omega_1, \omega_2)$ and $\widetilde{H}_1(\omega_1, \omega_2)$ and whose respective coefficients are given in Table 3.2 and Table 3.3. By applying Theorem 5, where the B_k are estimated numerically, the regularity of the corresponding 2-D biorthogonal wavelets is given by 0.2233 and 1.8342, respectively.

Table 3.3: The coefficients $\tilde{\alpha}_{n,m}$, of $\widetilde{H}_1(\omega_1,\omega_2)$ for $-8 \leq n,m \leq 8$.

$n\backslash m$	0	±1	±2	±3	±4
0	0.594077408314	0.160289153457	−0.009699273854	−0.003273309674	0.000463392964
±1	0.160289153457	−0.045047584921	−0.023325767368	0.010257677175	0.002432285575
±2	−0.009699273854	−0.023325767368	0.017953356728	0.005312708206	−0.002268082928
±3	−0.003273309674	0.010257677175	0.005312708206	−0.003223282751	−0.000320097781
±4	0.000463392964	0.002432285575	−0.002268082928	−0.000320097781	0.000373447430
±5	0.000307202397	−0.000668226858	−0.000192058666	0.000298757921	0.000000000000
±6	0.000030894538	−0.000064019550	0.000149378960	0.000000000000	0.000000000000
±7	−0.000009145650	0.000042679705	0.000000000000	0.000000000000	0.000000000000
±8	0.000000533496	0.000000000000	0.000000000000	0.000000000000	0.000000000000

$n\backslash m$	±5	±6	±7	±8
0	0.000307202397	0.000030894538	−0.000009145650	0.000000533496
±1	−0.000668226858	−0.000064019550	0.000042679705	0.000000000000
±2	−0.000192058666	0.000149378960	0.000000000000	0.000000000000
±3	0.000298757921	0.000000000000	0.000000000000	0.000000000000
±4	0.000000000000	0.000000000000	0.000000000000	0.000000000000
±5	0.000000000000	0.000000000000	0.000000000000	0.000000000000
±6	0.000000000000	0.000000000000	0.000000000000	0.000000000000
±7	0.000000000000	0.000000000000	0.000000000000	0.000000000000
±8	0.000000000000	0.000000000000	0.000000000000	0.000000000000

A design example

In this paragraph, we design the auxiliary transformation functions $f_q(\omega_1,\omega_2)$ and $f_c(\omega_1,\omega_2)$ for the construction of 2-D biorthogonal wavelet bases associated to matrices for the quincunx and column decimations, respectively. As seen from the results of the previous paragraph, to construct biorthogonal wavelets for $L^2(\mathbb{R}^2)$ it is enough that the dual frequency responses $H(\omega)$, $\widetilde{H}(\omega)$ satisfy the conditions of Theorem 5. Hence, one needs an auxiliary transformation function, $f(\omega)$, such that

$$\prod_{j=1}^{\infty} f^2\left({}^tD^{-j}\omega\right) \leq \frac{c}{1+\|\omega\|^2}.$$

Since one is interested in symmetric 2-D wavelets with minimal support, a trivial choice of the auxiliary transformation function is

$$f^2(\omega_1,\omega_2) = a_0 + a_1\cos\omega_1 + a_2\cos\omega_2 + a_3\cos\omega_1\cos\omega_2,$$

where the coefficients a_0, a_1, a_2 and a_3 are to be fixed later.

For quincunx decimation, we have

$$f^2(\omega_1, \omega_2) = 1 - f^2(\omega_1 + \pi, \omega_2 + \pi).$$

Thus, a direct computation shows that $a_0 = \frac{1}{2}$ and $a_1 + a_2 = \frac{1}{2}$. Consequently,

$$F_q(\omega_1, \omega_2) = 2f_q^2(\omega_1, \omega_2) - 1 = a_1 \cos\omega_1 + (1 - a_1)\cos\omega_2,$$

where $a_1 \in [0, \frac{1}{2}]$. To have symmetry, it is appropriate to choose $a_1 = \frac{1}{2}$. Thus,

$$f_q^2(\omega_1, \omega_2) = 1 - \frac{1}{2}\sin^2\left(\frac{\omega_1}{2}\right) - \frac{1}{2}\sin^2\left(\frac{\omega_2}{2}\right).$$

It only remains to choose a dilation matrix $\boldsymbol{D}$ that defines the quincunx sampling lattice and satisfies

$$\prod_{j=1}^{\infty} f_q^2\left({}^t\boldsymbol{D}^{-j}\omega\right) \leq \frac{c}{1 + \|\omega\|^2}.$$

It is proved in [11] that the matrix $\boldsymbol{D}_1$ satisfies the above inequality. Since, furthermore, $\|\boldsymbol{D}_1^{-1}\|_2 = 1/\sqrt{2} < 1$, then $\boldsymbol{D}_1$ is an appropriate dilation matrix for designing 2-D wavelets.

For column decimation, by following the analysis done in the quincunx case, one easily sees that the auxiliary transformation function $f_c(\omega_1, \omega_2)$, defined by

$$f_c^2(\omega_1, \omega_2) = \frac{1}{2}\left(1 + \cos\omega_1 \cos\omega_2\right),$$

is appropriate for the McClellan transformation in the design of 2-D biorthogonal wavelets.

Finally, we note that the proposed transformation function for designing 2-D wavelets associated to the quincunx sampling strategy is the transformation function $F_q(\omega)$ used in [2] and [10]. Hence, this section can be used to justify the choice of $F(\omega)$ made in [2] and [10].

3.3 Numerical Results

This last section is devoted to the numerical construction of 2-D biorthogonal wavelet bases by means of the theoretical results of the previous section. The numerical

approximation of the scaling functions and wavelets is done by the following 2-D generalization of the 1-D cascade algorithm [15], pp. 202–205.

Algorithm 1 (2-D Cascade Algorithm). Let $\Phi(\boldsymbol{x})$ be a compactly supported scaling function and $\boldsymbol{D}$ the dilation matrix of Definition 1. Define

$$\Phi_{j,\boldsymbol{k}}(\boldsymbol{x}) = |\det \boldsymbol{D}|^{-j/2}\Phi(\boldsymbol{D}^{-j}\boldsymbol{x} - \boldsymbol{k}), \qquad j \in \mathbf{Z}, \quad \boldsymbol{k} \in \mathbf{Z}^2,$$

where

$$\Phi(\boldsymbol{x}) = \sum_{\boldsymbol{n}\in\mathbf{Z}^2} \alpha_{\boldsymbol{n}}\Phi(\boldsymbol{D}\boldsymbol{x} - \boldsymbol{n}).$$

If we denote the scalar product by

$$A_{\boldsymbol{k}}^{-j} := < \Phi, \Phi_{-j,\boldsymbol{k}} >,$$

then

$$A_{\boldsymbol{k}}^{-j} = |\det \boldsymbol{D}|^{1/2} \sum_{\boldsymbol{n}\in\mathbf{Z}^2} \alpha_{\boldsymbol{k}-\boldsymbol{D}\boldsymbol{n}} A_{\boldsymbol{n}}^{1-j}.$$

Imposing the starting value $A_{\boldsymbol{k}}^{0} = 1$ if $\boldsymbol{k} = 0$, and zero otherwise, and iterating the above equation, one obtains an approximation

$$\Phi(\boldsymbol{D}^{-j}\boldsymbol{x}) \approx |\det \boldsymbol{D}|^{j/2} A_{\boldsymbol{n}}^{-j}$$

to the value of the scaling function at $\boldsymbol{x} = \boldsymbol{n}$. Moreover, it is proved in [40] that if Φ is r-times differentiable and $\|\boldsymbol{D}^{-1}\|_2 < 1$, then the convergence of the cascade algorithm is ensured with the following error bound

$$\left|\Phi(\boldsymbol{D}^{-j}\boldsymbol{x}) - |\det \boldsymbol{D}|^{j/2} A_{\boldsymbol{n}}^{-j}\right| \leq \text{const}\, \|\boldsymbol{D}^{-1}\|_2^{jr}.$$

For our numerical tests, we have considered the dilation matrix $\boldsymbol{D}_1$ of the previous section. The transformation function

$$F(\omega_1, \omega_2) = \frac{1}{2}(\cos\omega_1 + \cos\omega_2)$$

has been used in the McClellan transformation to generate 2-D biorthogonal wavelet filters from 1-D filters. Among the numerical tests we have performed, the following

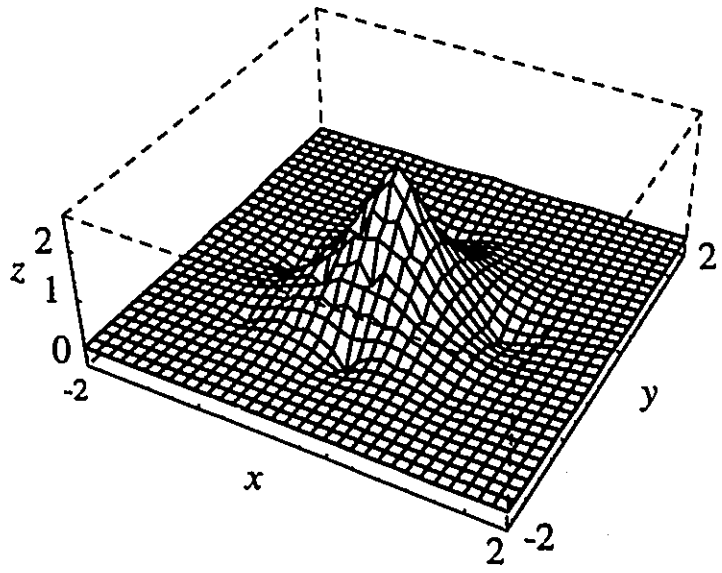

Figure 3.2: Graph of the scaling function $\Phi_1(\boldsymbol{x})$.

three examples are chosen to illustrate the proposed construction method.

Example 2.

In this example, the 2-D biorthogonal wavelet filters, are those of Example 1. Six iterations of the 2-D cascade algorithm were used to approximate the dual scaling functions, $\Phi_1(\boldsymbol{x})$ and $\tilde{\Phi}_1(\boldsymbol{x})$, and the corresponding wavelets, $\Psi_1(\boldsymbol{x})$ and $\tilde{\Psi}_1(\boldsymbol{x})$, shown in Figs. 3.2 to 3.5, where $x = x_1$ and $y = x_2$.

Example 3.

In this example, the coefficients of the frequency responses, $h_2(\omega)$, $\tilde{h}_2(\omega)$, of the 1-D biorthogonal wavelet filters to be used in the design process are given in Table 3.4. The coefficients of the corresponding 2-D biorthogonal wavelet filters with frequency responses $H_2(\omega_1, \omega_2)$ and $\widetilde{H}_2(\omega_1, \omega_2)$ are given in Table 3.5 and Table 3.6, respectively. As in Example 2, six iterations of the cascade algorithm have been performed in order to construct the 2-D biorthogonal scaling functions $\Phi_2(\boldsymbol{x})$ and $\tilde{\Phi}_2(\boldsymbol{x})$, and the corresponding wavelets, $\Psi_2(\boldsymbol{x})$ and $\tilde{\Psi}_2(\boldsymbol{x})$, as shown in Figs. 3.6 to 3.9. The numerical techniques given in [37] show that the analysing 1-D wavelets generated by $h_2(\omega)$ are smoother than those generated by $h_1(\omega)$ of Example 2, the regularity estimates are

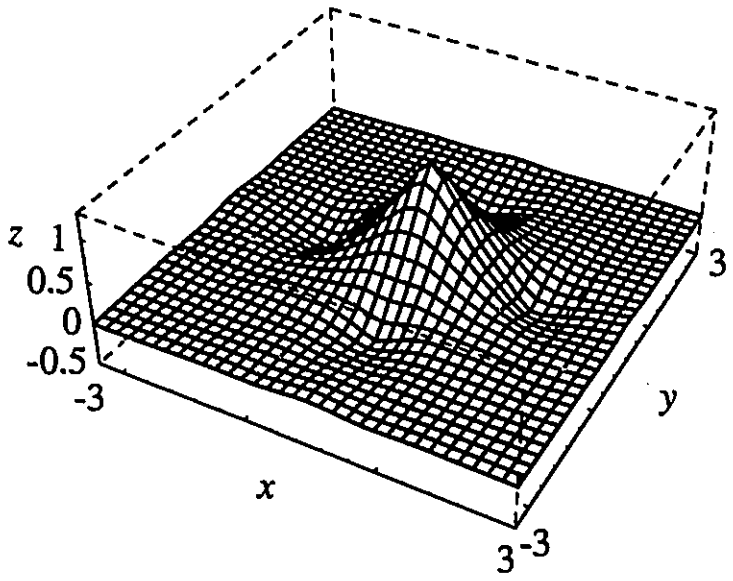

Figure 3.3: Graph of the scaling function $\tilde{\Phi}_1(x)$.

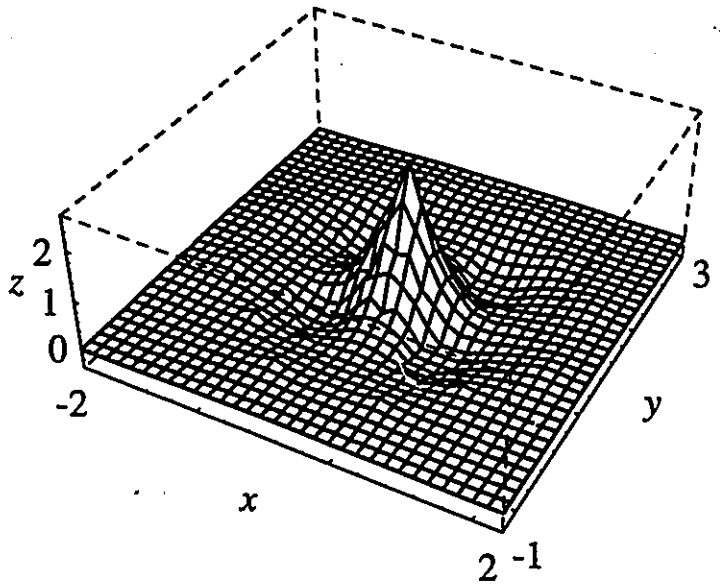

Figure 3.4: Graph of the wavelet $\Psi_1(x)$.

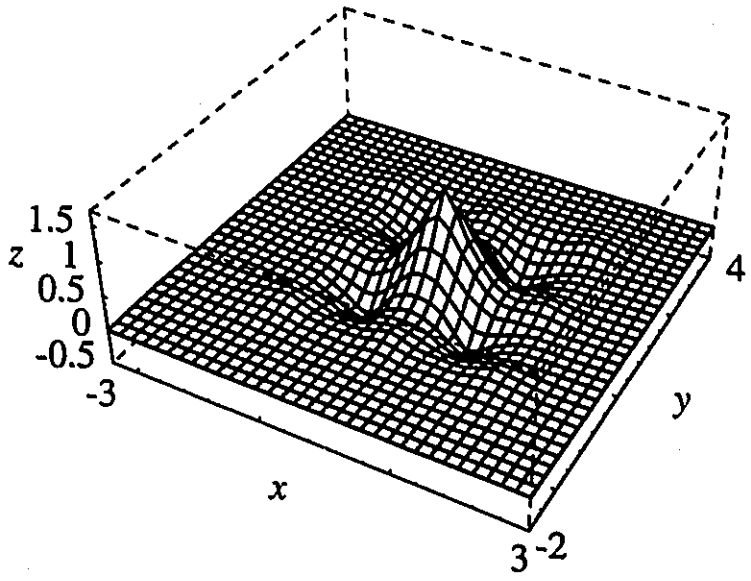

Figure 3.5: Graph of the wavelet $\tilde{\Psi}_1(x)$.

Table 3.4: The coefficients α_n of $h_2(\omega)$ for $-4 \leq n \leq 4$, and the coefficients $\tilde{\alpha}_n$ of $\tilde{h}_2(\omega)$ for $-11 \leq n \leq 11$.

n	α_n	$\tilde{\alpha}_n$
0	0.480 468 750	0.657 635 569 572
±1	0.301 562 500	0.308 584 809 303
±2	0.026 562 500	−0.149 226 635 694
±3	−0.051 562 500	−0.089 541 628 956
±4	−0.016 796 875	0.101 056 776 941
±5		0.034 959 517 419
±6		−0.041 568 409 651
±7		−0.002 760 077 826
±8		0.012 585 756 368
±9		−0.001 785 110 798
±10		−0.001 665 276 009
±11		0.000 542 476 366

Table 3.5: The coefficients $\alpha_{n,m}$ of $H_2(\omega_1, \omega_2)$ for $-4 \leq n, m \leq 4$.

$n\backslash m$	0	±1	±2	±3	±4
±0	0.449707031250	0.170117184520	0.006640625186	−0.006445312407	−0.001049804734
±1	0.170117184520	0.021679688245	−0.019335936755	−0.004199218936	0.000000000000
±2	0.006640625186	−0.019335936755	−0.006298827939	0.000000000000	0.000000000000
±3	−0.006445312407	−0.004199218936	0.000000000000	0.000000000000	0.000000000000
±4	−0.001049804734	0.000000000000	0.000000000000	0.000000000000	0.000000000000

Table 3.6: The coefficients $\tilde{\alpha}_{n,m}$ of $\widetilde{H}_2(\omega_1, \omega_2)$ for $-11 \leq n, m \leq 11$.

$n\backslash m$	0	±1	±2	±3	±4	±5
0	0.844522535801	0.188009798527	−0.025763168931	−0.005243036896	−0.003837857628	0.000703987724
±1	0.188009798527	−0.135490760207	−0.044516731054	0.027457913384	0.005752130877	−0.001998569584
±2	−0.025763168931	−0.044516731054	0.055711168796	0.011513250880	−0.011201978661	−0.000540236011
±3	−0.005243036896	0.027457913384	0.011513250880	−0.017150850967	−0.000274612481	0.002980808727
±4	−0.003837857628	0.005752130877	−0.011201978661	−0.000274612481	0.003896766575	−0.000561679655
±5	0.000703987724	−0.001998569584	−0.000540236011	0.002980808727	−0.000561679655	−0.000409814005
±6	0.000883057015	−0.000468987855	0.001246467466	−0.000310351897	−0.000341511681	0.000122375044
±7	−0.000134752234	0.000181892887	−0.000064328080	−0.000195149536	0.000087410743	0.000000000000
±8	−0.000048411657	0.000023981236	−0.000073181072	0.000043705371	0.000000000000	0.000000000000
±9	0.000016909295	−0.000016262462	0.000014568457	0.000000000000	0.000000000000	0.000000000000
±10	−0.000001626246	0.000002913691	0.000000000000	0.000000000000	0.000000000000	0.000000000000
±11	0.000000264881	0.000000000000	0.000000000000	0.000000000000	0.000000000000	0.000000000000

$n\backslash m$	±6	±7	±8	±9	±10	±11
0	0.000883057015	−0.000134752234	−0.000048411657	0.000016909295	−0.000001626246	0.000000264881
±1	−0.000468987855	0.000181892887	0.000023981236	−0.000016262462	0.000002913691	0.000000000000
±2	0.001246467466	−0.000064328080	−0.000073181072	0.000014568457	0.000000000000	0.000000000000
±3	−0.000310351897	−0.000195149536	0.000043705371	0.000000000000	0.000000000000	0.000000000000
±4	−0.000341511681	0.000087410743	0.000000000000	0.000000000000	0.000000000000	0.000000000000
±5	0.000122375044	0.000000000000	0.000000000000	0.000000000000	0.000000000000	0.000000000000
±6	0.000000000000	0.000000000000	0.000000000000	0.000000000000	0.000000000000	0.000000000000
±7	0.000000000000	0.000000000000	0.000000000000	0.000000000000	0.000000000000	0.000000000000
±8	0.000000000000	0.000000000000	0.000000000000	0.000000000000	0.000000000000	0.000000000000
±9	0.000000000000	0.000000000000	0.000000000000	0.000000000000	0.000000000000	0.000000000000
±10	0.000000000000	0.000000000000	0.000000000000	0.000000000000	0.000000000000	0.000000000000
±11	0.000000000000	0.000000000000	0.000000000000	0.000000000000	0.000000000000	0.000000000000

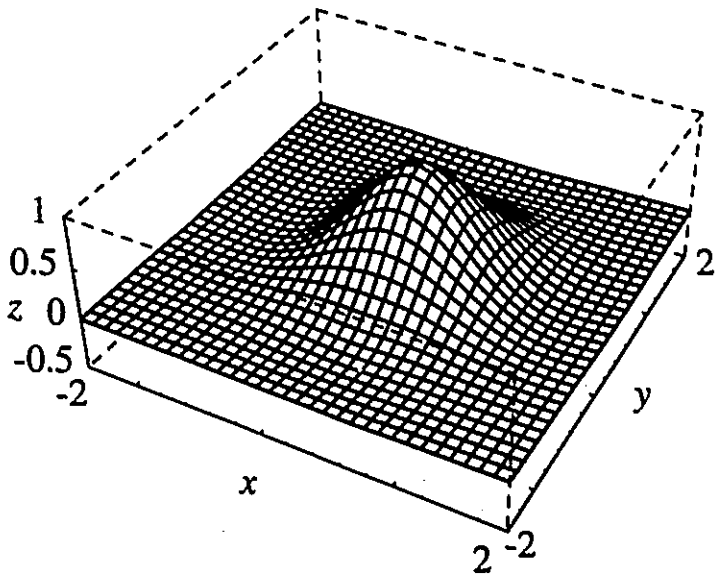

Figure 3.6: Graph of the scaling function $\Phi_2(\boldsymbol{x})$.

3.0217 and 1.1115 respectively. Unlike the analysing 1-D wavelets, the synthetezing 1-D wavelets of Example 2 are smoother than those of this example, the regularity estimates being 1.9166 and 1.5443, respectively. Finally, we remark that the analysing and synthetezing 2-D biorthogonal wavelets satisfy the same regularity properties as their corresponding 1-D wavelets. This is essentially due to the way we have applied the McClellan transformation in our design.

Example 4.

Since our design is limited to biorthogonal 2-D wavelets, we have designed biorthogonal 1-D wavelet filters with frequency responses $h_3(\omega)$ and $\widetilde{h}_3(\omega)$. These filters generate almost orthonormal 1-D wavelet bases. The coefficients, β_n and $\widetilde{\beta}_n$ of $h_3(\omega)$ and $\widetilde{h}_3(\omega)$, are listed in Table 3.7.

The filters have been used to construct nonseparable 2-D biorthogonal wavelet filters with frequency responses $H_3(\omega_1, \omega_2)$ and $\widetilde{H}_3(\omega_1, \omega_2)$. These filters are very close 2-D orthonormal wavelet bases and their coefficients are listed in Table 3.8 and 3.9, respectively. The graphs of the scaling function, $\phi(\boldsymbol{x})$, and associated wavelet, $\psi(\boldsymbol{x})$, are shown in Fig. 3.10 and 3.11, where $x = x_1$ and $y = x_2$. Since these wavelets are almost orthonormal, the graphs of the dual scaling function and wavelet, $\widetilde{\phi}(\boldsymbol{x})$

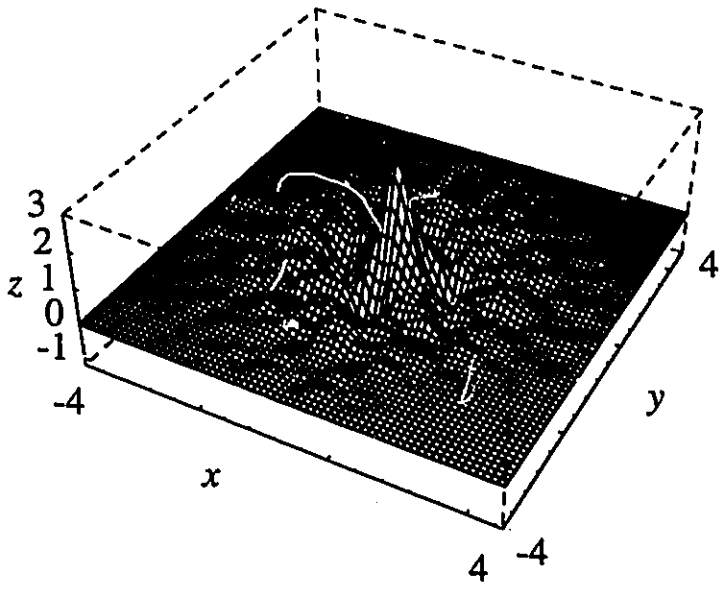

Figure 3.7: Graph of the scaling function $\tilde{\Phi}_2(x)$.

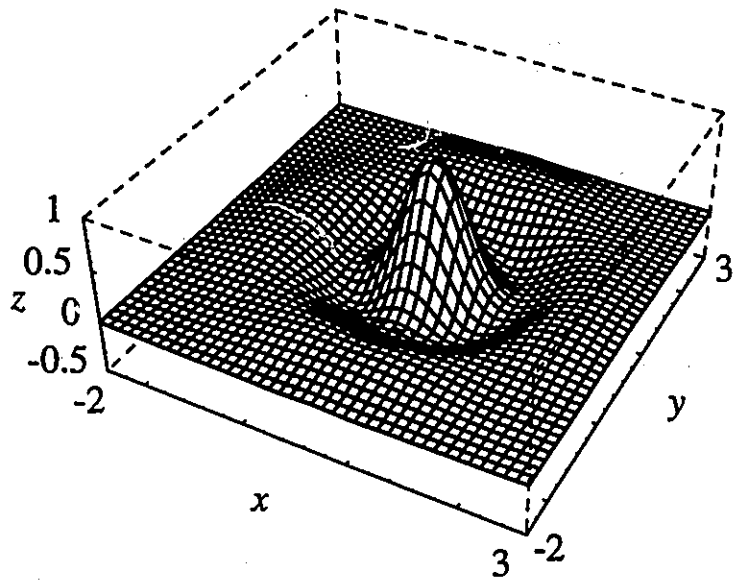

Figure 3.8: Graph of the wavelet $\Psi_2(x)$.

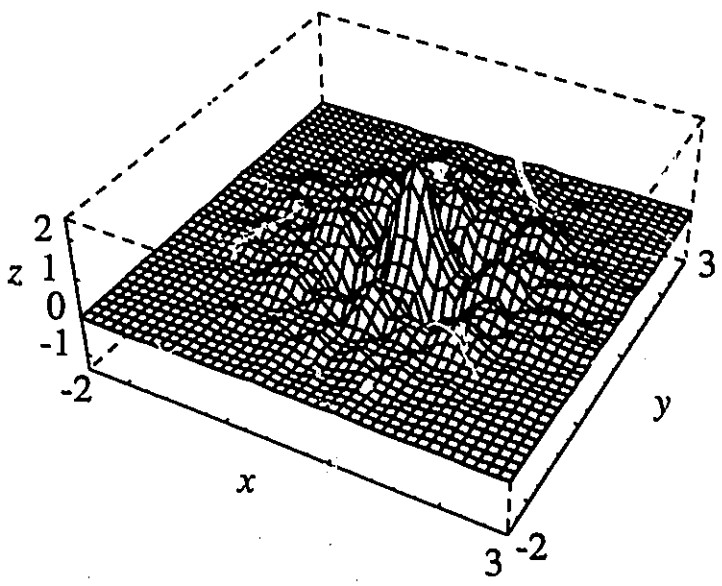

Figure 3.9: Graph of the wavelet $\bar{\Psi}_2(\boldsymbol{x})$.

Table 3.7: The coefficients, β_n of $h_3(\omega)$ for $-3 \leq n \leq 3$, and the coefficients $\tilde{\beta}_n$ of $\tilde{h}_3(\omega)$ for $-4 \leq n \leq 4$.

n	β_n	$\tilde{\beta}_n$
0	0.603 513 642 8	0.602 196 264 8
± 1	0.255 301 328 8	0.256 818 852 5
± 2	−0.051 756 821 0	−0.051 796 571 4
± 3	−0.005 301 328 0	−0.006 818 852 5
± 4		0.000 698 438 0

Table 3.8: The coefficients $\alpha_{n,m}$ of $\widetilde{H}_3(\omega_1, \omega_2)$ for $-3 \leq n, m \leq 3$.

$n \backslash m$	0	± 1	± 2	± 3
0	0.655270457268	0.129638656974	−0.012939205393	−0.000662665989
± 1	0.129638656974	−0.025878410786	−0.001987997908	0.000000000000
± 2	−0.012939205393	−0.001987997908	0.000000000000	0.000000000000
± 3	−0.000662665989	0.000000000000	0.000000000000	0.000000000000

Table 3.9: The coefficients $\tilde{\alpha}_{n,m}$ of $\widetilde{H}_3(\omega_1, \omega_2)$ for $-4 \leq n, m \leq 4$.

$n \backslash m$	0	± 1	± 2	± 3	± 4
± 0	0.654167473316	0.130966499448	−0.012949142605	−0.000852356548	0.000043652373
± 1	0.130966499448	−0.026247505099	−0.002557069762	0.000174609493	0.000000000000
± 2	−0.012949142605	−0.002557069762	0.000261914247	0.000000000000	0.000000000000
± 3	−0.000852356548	0.000174609493	0.000000000000	0.000000000000	0.000000000000
± 4	0.000043652373	0.000000000000	0.000000000000	0.000000000000	0.000000000000

and $\tilde{\psi}(\boldsymbol{x})$, are almost identical to those of $\phi(\boldsymbol{x})$ and $\psi(\boldsymbol{x})$, respectively, and are not shown. Finally, numerical results indicate that the almost orthonormal wavelets $\psi(\boldsymbol{x})$ and $\tilde{\psi}(\boldsymbol{x})$ are continuous.

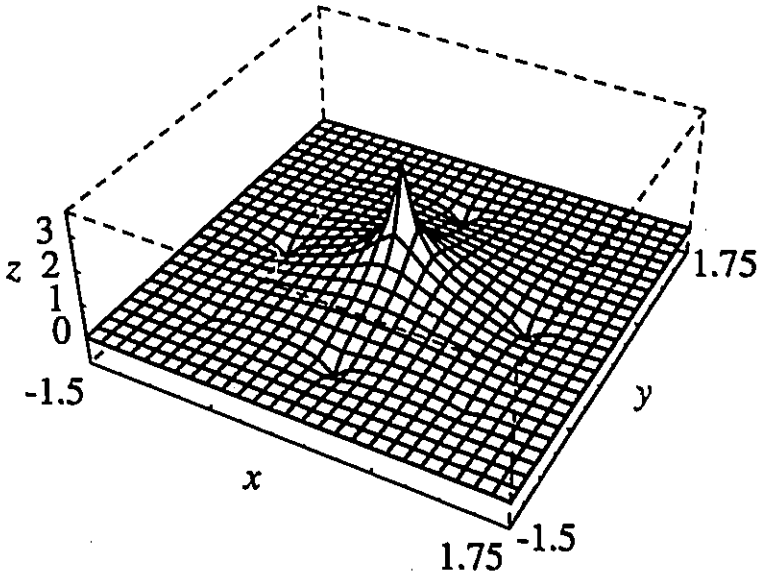

Figure 3.10: Graph of the scaling function $\phi(x, y)$.

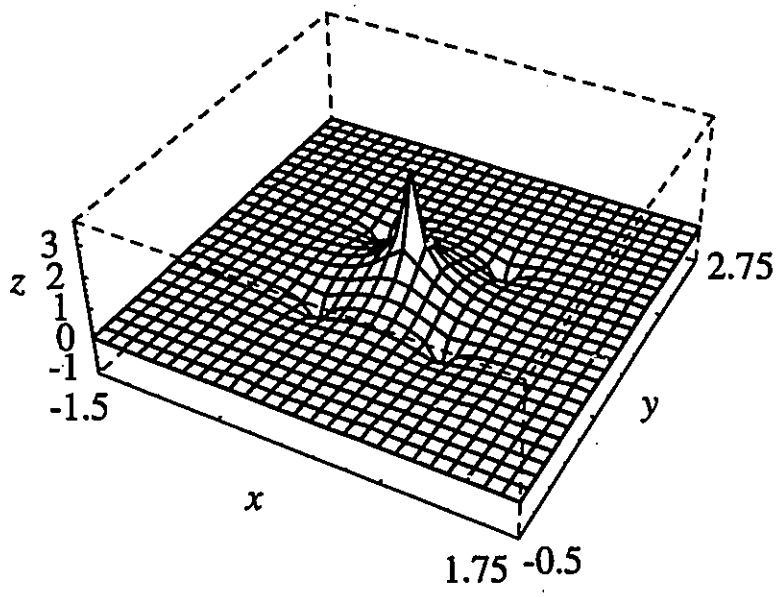

Figure 3.11: Graph of the wavelet $\psi(x, y)$.

Chapter 4

Nonseparable Biorthogonal Wavelet Bases of $L^2(\mathbb{R}^n)$

Due to the growing interest in nonseparable multidimensional wavelets in many applications, we consider that it is of interest to generalize some theoritical and technical results that are useful in the study of multidimensional wavelets. We also should give an overview of the design of nonseparable wavelet bases of $L^2(\mathbb{R}^n)$ where n is a positive integer satisfying $n > 1$. Unfortunately, this design is complicated because many techniques and results do not generalize from the 1-D case to higher dimensions. Moreover, the design of n-D wavelets depends critically on a dilation matrix $\boldsymbol{D}$ which defines the n-D sampling lattice (see [68]). The eigenvalues $\{\lambda_i\}_{i=1,\ldots,n}$, the absolute value of the determinant of $\boldsymbol{D}$ $|\det \boldsymbol{D}|$ and the norm $\|\boldsymbol{D}^{-1}\|_2$ play important roles in the design process and regularity estimates of wavelets, and the convergence of the n-D version of the cascade algorithm. Unlike the 1-D case, where it is relatively easy to design the lowpass wavelet filter that generates the scaling function and consequently the wavelets (see [14], [11], [67], [60], etc.), for the n-D case, with $n \geq 2$, the construction of the equivalent general lowpass filter is hard to achieve without using special techniques as it is done in the previous chapter. Due to the flexibility of their design, only biorthogonal wavelets are considered in this chapter. However many of the theoretical results of this chapter are still valid for the case of n-D orthonormal wavelet bases.

4.1 Biorthogonal Wavelets of $L^2(\mathbb{R}^n)$

4.1.1 Preliminaries

For better understanding biorthogonal wavelet bases and for the aims of this chapter, it is essential to give the definition of a biorthogonal basis of a general Hilbert space and also to briefly review the n-D multiresolution analysis whose 1-D and 2-D versions were given in the previous two chapters.

Definition 11 *We say that the sequences* $\{f_n\}$, $\{g_n\}$, $n \in \mathbb{N}$, *of elements of a Hilbert space* $\mathcal{H}$ *form a biorthogonal system if*

$$< f_n, g_m >= \delta_{n-m}. \tag{4.1}$$

The biorthogonal system is said to be complete if each of the systems $\{f_n\}$, $\{g_n\}$ *is complete in* $\mathcal{H}$, *that is, if the linear combinations of the* f_n, *as well as those of the* g_n, *are everywhere dense in* $\mathcal{H}$.
Then we have the biorthogonal expansions:

$$f = \sum_{n=1}^{\infty} < f, g_n > f_n, \qquad f = \sum_{n=1}^{\infty} < f, f_n > g_n, \tag{4.2}$$

valid whenever the series on the rigth-hand side converge.

For a simple proof, see [55], p. 208.

Multiresolution analysis

One way of designing n-D wavelets is to generalize the 1-D multiresolution analysis (MRA) (see [46], [47]), to the n-D case. It is known that an n-D MRA is critically dependent on the choice of the dilation matrix $\boldsymbol{D}$ of definition 6.

As in the 1-D case, there are two types of n-D MRA, generating n-D orthonormal and biorthogonal wavelet bases, respectively.

Definition 12 *An n-D orthogonal MRA is a decreasing sequence of closed linear subspaces of $L^2(\mathbb{R}^n)$,*

$$\cdots \subset V_2 \subset V_1 \subset V_0 \subset V_{-1} \subset V_{-2} \subset \cdots, \tag{4.3}$$

with the following properties:

(P1) $\bigcup_{-\infty}^{\infty} V_j$ *is dense in* $L^2(\mathbb{R}^n)$ *and* $\bigcap_{-\infty}^{\infty} V_j = \{0\}$;

(P2) $\forall\, j \in \mathbf{Z},\ \forall\, \boldsymbol{x} \in \mathbb{R}^n \quad f(\boldsymbol{x}) \in V_{j+1} \Longleftrightarrow f(\boldsymbol{D}\boldsymbol{x}) \in V_j$;

(P3) $\exists\, \phi \in V_0 \subset L^2(\mathbb{R}^n)$ *such that* $\phi_{0,\boldsymbol{k}}(\boldsymbol{x}) = \phi(\boldsymbol{x} - \boldsymbol{k})$, $\boldsymbol{k} \in \mathbf{Z}^n$, *is an orthonormal basis of* V_0.

Definition 13 *An n-D biorthogonal MRA is a pair of decreasing families $\{V_j\}$, $\{\tilde{V}_j\}$, $j \in \mathbf{Z}$, of closed linear subspaces of $L^2(\mathbb{R}^n)$, each satisfying the inclusions* (4.3), *properties* (*P*1) *and* (*P*2) *of Definition 12, and, instead of* (*P*3), *property* (*P*3′):

(P3′) There exist $\phi \in V_0$ and $\tilde{\phi} \in \tilde{V}_0$ such that $\{\phi_{0,\boldsymbol{n}}\}_{\boldsymbol{n}\in\mathbf{Z}^n}$ and $\left\{\tilde{\phi}_{0,\boldsymbol{n}}\right\}_{\boldsymbol{n}\in\mathbf{Z}^n}$ is a biorthogonal basis of V_0.

Moreover, the two families are related to each other by the following orthogonality conditions:

$$\widetilde{W}_j \perp V_j, \qquad W_j \perp \tilde{V}_j, \tag{4.4}$$

where W_j and $\widetilde{W}_j$ are the (non-orthonormal) complements of V_j and $\tilde{V}_j$ in V_{j-1} and $\tilde{V}_{j-1}$, respectively.

4.1.2 From a multiresolution analysis to biorthogonal scaling functions and wavelets

From now on, we restrict ourselves to the biorthogonal n-D case. But, the results of this paragraph also apply to the orthonormal n-D case.

Given an n-D biorthogonal MRA, the construction of a biorthogonal wavelet basis of $L^2(\mathbb{R}^n)$ can proceed as follows.

Because of the inclusions

$$\phi \in V_0 \subset V_{-1}, \qquad \tilde{\phi} \in \tilde{V}_0 \subset \tilde{V}_{-1},$$

there exist two sequences of real numbers $\{\alpha_k^0\}$, $\{\tilde{\alpha}_k^0\}$, $k \in \mathbf{Z}^n$, such that

$$\phi(x) = \sum_{k \in \mathbf{Z}^n} \alpha_k^0 \phi(Dx - k), \qquad \tilde{\phi}(x) = \sum_{k \in \mathbf{Z}^n} \tilde{\alpha}_k^0 \tilde{\phi}(Dx - k). \tag{4.5}$$

Taking Fourier transforms, we have

$$\begin{aligned} \widehat{\phi}(\xi) &= \frac{1}{|\det D|} \sum \alpha_n^0 e^{-i D^{-1} n \cdot \xi} \widehat{\phi}({}^t D^{-1} \xi) \\ &= H_0({}^t D^{-1} \xi) \widehat{\phi}({}^t D^{-1} \xi) \end{aligned} \tag{4.6}$$

and, similarly,

$$\widehat{\tilde{\phi}}(\xi) = \widetilde{H}_0({}^t D^{-1} \xi) \widehat{\tilde{\phi}}({}^t D^{-1} \xi), \tag{4.7}$$

where $H_0(\xi)$ and $\widetilde{H}_0(\xi)$ are $2\pi\mathbf{Z}^n$-periodic functions.

Note that if the scaling functions have compact support, then H_0 and $\widetilde{H}_0$ are trigonometric polynomials.

If $\widehat{\phi}(0) = 1$ and $\widehat{\tilde{\phi}}(0) = 1$, by iterating (4.6) and (4.7) infinitely often, one obtains

$$\widehat{\phi}(\xi) = \prod_{j=1}^{\infty} H_0({}^t D^{-j} \xi), \qquad \widehat{\tilde{\phi}}(\xi) = \prod_{j=1}^{\infty} \widetilde{H}_0({}^t D^{-j} \xi). \tag{4.8}$$

Hence, by designing appropriate dual lowpass filters, H_0 and $\widetilde{H}_0$, the construction of the dual scaling functions ϕ and $\tilde{\phi}$ is straightforward.

Following [29], since $|\det D| = d$ is the number of cosets in $\mathbf{Z}^n / D\mathbf{Z}^n$, then two families, each containing $d - 1$ elementary wavelets $\{\psi^i\}_{i=1}^{d-1}$, $\{\tilde{\psi}^i\}_{i=1}^{d-1}$, are needed in order that the following pair of d-families:

$$\{\phi_k, \psi_k^i\}_{k \in \mathbf{Z}^n}, \qquad \{\tilde{\phi}_k, \tilde{\psi}_k^i\}_{k \in \mathbf{Z}^n}, \qquad i = 1, \ldots, d-1, \tag{4.9}$$

to form a biorthogonal basis of V_{-1}. For convenience, we shall denote the scaling functions ϕ, $\tilde{\phi}$ by ψ^0, $\tilde{\psi}^0$, respectively.

By definition, biorthogonal wavelets satisfy the following relations:

$$\left\langle \psi_k^i, \tilde{\psi}_l^j \right\rangle = \delta_{i-j}\delta_{k-l}, \qquad k, l \in \mathbf{Z}^n, \quad i, j = 0, \ldots, d-1. \tag{4.10}$$

Once the scaling functions have been constructed, one is concerned with the design of the dual wavelets $\{\psi^i\}$, $\{\tilde{\psi}^i\}$, $i = 1, \ldots, d-1$. This is the subject of the next section.

4.2 An Algorithm for the Construction of n-D Biorthogonal Wavelets

In this section, we generalize Gröchenig's algorithm [28] for the construction of n-dimensional orthonormal wavelet bases with dilation matrix $\boldsymbol{D} = 2\boldsymbol{I}_n$ to a similar algorithm with an arbitrary dilation matrix in $\mathbf{Z}^{n\times n}$.

Formulation of the problem.— Given dual scaling functions, ψ^0 and $\tilde{\psi}^0$, can one construct dual wavelets, ψ^i and $\tilde{\psi}^i$, and, consequently, a biorthogonal basis of V_{-1}?

The answer is given in two steps. In the first step, we intuitively provide necessary conditions on the wavelets ψ^i, $\tilde{\psi}^i$, for $i = 1, \ldots, d-1$. In the second step, a proof similar to the one given in [51], pp. 83–87, ensures that the necessary conditions are also sufficient.

4.2.1 Necessary conditions for the existence of an n-dimensional biorthogonal basis

Since V_0, $W_0 \subset V_{-1}$ and $\tilde{V}_0$, $\tilde{W}_0 \subset \tilde{V}_{-1}$, one easily sees that for each i, $i = 0, \ldots, d-1$, there are two sequences, $\{\alpha_m^i\}_{m\in\mathbf{Z}^n}$ and $\{\tilde{\alpha}_m^i\}_{m\in\mathbf{Z}^n}$, of real numbers such that

$$\psi^i(\boldsymbol{x}) = \sum_{m\in\mathbf{Z}^n} \alpha_m^i \psi^0(\boldsymbol{D}\boldsymbol{x} - \boldsymbol{m}), \qquad \tilde{\psi}^i(\boldsymbol{x}) = \sum_{m\in\mathbf{Z}^n} \tilde{\alpha}_m^i \tilde{\psi}^0(\boldsymbol{D}\boldsymbol{x} - \boldsymbol{m}). \tag{4.11}$$

Taking Fourier transforms, we have

$$\widehat{\psi}^i({}^t\boldsymbol{D}\boldsymbol{\xi}) = H_i(\boldsymbol{\xi})\widehat{\psi}^0(\boldsymbol{\xi}), \qquad \widehat{\tilde{\psi}}^i({}^t\boldsymbol{D}\boldsymbol{\xi}) = \widetilde{H}_i(\boldsymbol{\xi})\widehat{\tilde{\psi}}^0(\boldsymbol{\xi}).$$

for some $2\pi\mathbf{Z}^n$-periodic functions $H_i(\boldsymbol{\xi})$ and $\widetilde{H}_i(\boldsymbol{\xi})$. Now, for $\boldsymbol{k} \in \mathbf{Z}^n$,

$$\begin{aligned}\delta_{\boldsymbol{k}} = \left\langle \psi^0(\cdot), \tilde{\psi}^0(\cdot - \boldsymbol{k}) \right\rangle &= \left\langle \widehat{\psi}^0(\cdot), \widehat{\tilde{\psi}}^0(\cdot)\, e^{-i\boldsymbol{k}\cdot(\cdot)} \right\rangle \\ &= \int_{[0,2\pi]^n} e^{i\boldsymbol{k}\cdot\boldsymbol{\xi}} \sum_{\boldsymbol{l}\in\mathbf{Z}^n} \widehat{\psi}^0(\boldsymbol{\xi} + 2\pi\boldsymbol{l})\overline{\widehat{\tilde{\psi}}^0(\boldsymbol{\xi} + 2\pi\boldsymbol{l})}. \qquad (4.12)\end{aligned}$$

Hence, if we define Γ by $\mathbf{Z}^n = {}^t\boldsymbol{D}\mathbf{Z}^n + \Gamma$, ${}^t\boldsymbol{D}\mathbf{Z}^n \cap \Gamma = \emptyset$, then

$$\sum_{\boldsymbol{\eta}\in\Gamma} \sum_{\boldsymbol{l}\in\mathbf{Z}^n} \widehat{\psi}^0({}^t\boldsymbol{D}\boldsymbol{\xi} + 2\pi({}^t\boldsymbol{D}\boldsymbol{l} + \boldsymbol{\eta}))\overline{\widehat{\tilde{\psi}}^0({}^t\boldsymbol{D}\boldsymbol{\xi} + 2\pi({}^t\boldsymbol{D}\boldsymbol{l} + \boldsymbol{\eta}))} = 1, \qquad \text{a.e.}$$

Thus

$$\sum_{\boldsymbol{\eta}\in\Gamma} H_0(\boldsymbol{\xi} + 2\pi{}^t\boldsymbol{D}^{-1}\boldsymbol{\eta})\overline{\widetilde{H}_0(\boldsymbol{\xi} + 2\pi{}^t\boldsymbol{D}^{-1}\boldsymbol{\eta})} = 1, \qquad \text{a.e.} \qquad (4.13)$$

By the same manipulations on the wavelets ψ^i, $\tilde{\psi}^i$, $i = 1, \ldots, d-1$, one can easily prove that the $2\pi\mathbf{Z}^n$-periodic functions $H_i(\boldsymbol{\xi})$, $\widetilde{H}_i(\boldsymbol{\xi})$ satisfy

$$\sum_{\boldsymbol{\eta}\in\Gamma} H_i(\boldsymbol{\xi} + 2\pi{}^t\boldsymbol{D}^{-1}\boldsymbol{\eta})\overline{\widetilde{H}_j(\boldsymbol{\xi} + 2\pi{}^t\boldsymbol{D}^{-1}\boldsymbol{\eta})} = \delta_{i-j}, \qquad \text{a.e.} \qquad (4.14)$$

Letting $\boldsymbol{\eta}_j$ denote the different points of the set $\{2\pi{}^t\boldsymbol{D}^{-1}\boldsymbol{\eta};\ \boldsymbol{\eta} \in \Gamma\}$ and combining (4.13), (4.14), we conclude that if the entries of the matrices $\boldsymbol{U}$ and $\boldsymbol{V}$ are

$$H_{i,j}(\boldsymbol{\xi}) = H_j(\boldsymbol{\xi} + \boldsymbol{\eta}_i), \qquad \widetilde{H}_{i,j}(\boldsymbol{\xi}) = \widetilde{H}_j(\boldsymbol{\xi} + \boldsymbol{\eta}_i), \qquad i, j = 0, \ldots, d-1,$$

respectively, then to construct a biorthogonal wavelet basis of V_{-1}, it is necessary that

$$\overline{{}^t\boldsymbol{V}}\boldsymbol{U} = \boldsymbol{I}_d, \qquad (4.15)$$

that is

$$\begin{bmatrix} \overline{\widetilde{H}_0(\xi)} & \overline{\widetilde{H}_0(\xi+\eta_1)} & \cdots & \overline{\widetilde{H}_0(\xi+\eta_{d-1})} \\ \overline{\widetilde{H}_1(\xi)} & \overline{\widetilde{H}_1(\xi+\eta_1)} & \cdots & \overline{\widetilde{H}_1(\xi+\eta_{d-1})} \\ \vdots & \vdots & & \vdots \\ \overline{\widetilde{H}_{d-1}(\xi)} & \overline{\widetilde{H}_{d-1}(\xi+\eta_1)} & \cdots & \overline{\widetilde{H}_{d-1}(\xi+\eta_{d-1})} \end{bmatrix} \times$$
$$\begin{bmatrix} H_0(\xi) & H_1(\xi) & \cdots & H_{d-1}(\xi) \\ H_0(\xi+\eta_1) & H_1(\xi+\eta_1) & \cdots & H_{d-1}(\xi+\eta_1) \\ \vdots & \vdots & & \vdots \\ H_0(\xi+\eta_{d-1}) & H_1(\xi+\eta_{d-1}) & \cdots & H_{d-1}(\xi+\eta_{d-1}) \end{bmatrix} = I_d.$$

Remark 7 Relation (4.15) generalizes the relation $\overline{U}^t U = I_n$ given in [28] and [51] for the construction of an n-dimensional orthonormal wavelet basis of V_{-1} with dilation matrix $D = 2I_n$.

Remark 8 A relation similar to (4.15) has been derived in [68] by using the polyphase decomposition for different analysis and synthesis filters.

To prove that condition (4.15) is also sufficient for generating a biorthogonal wavelet basis of V_{-1}, we need the following analysis which is an adaptation to the biorthogonal case of the one made in [51], pp. 83–87.

4.2.2 Sufficient conditions for the existence of a biorthogonal wavelet basis

In this subsection, we show that Gröchenig's algorithm, given in [51], pp. 83–87, for the construction of a multidimensional orthonormal wavelet basis can be generalized to the case of a multidimensional biorthogonal wavelet basis with arbitrary dilation matrix D.

The generalized algorithm.— Let $D \in \mathbb{Z}^{n\times n}$ be a dilation matrix and write $\Gamma_0 = \mathbb{Z}^n$, $\Gamma = D^{-1}\mathbb{Z}^n$. We consider the translation operator

$$T_\alpha : l^2(\Gamma) \longrightarrow l^2(\Gamma)$$

operating on the Hilbert space $l^2(\Gamma)$. By considering the inclusions $V_0 \subset V_{-1}$, $\tilde{V}_0 \subset \tilde{V}_{-1}$, the scaling functions ψ^0, $\tilde{\psi}^0$ become, respectively, two vectors, v_0 and $\tilde{v}_0$, which satisfy the relation

$$\sum_{\alpha \in \Gamma_0} [T_\alpha v_0]^t \overline{T_\alpha \tilde{v}_0} = 1.$$

Thus, the problem reduces to the one of finding two families of vectors $\{v_i\}$, $\{\tilde{v}_i\}$, $i = 1, \ldots, d-1$, in $l^2(\Gamma)$ such that

$$\{T_\alpha v_i, \alpha \in \Gamma_0\}, \qquad \{T_\alpha \tilde{v}_i, \alpha \in \Gamma_0\}, \qquad i = 0, \ldots, d-1,$$

form a biorthogonal basis of $l^2(\Gamma)$.

For $0 \leq j \leq d-1$, let $\Gamma_j = \Gamma_0 + \eta_j$, where η_j, $j = 0, 1, \ldots, d-1$, are the residues modulo Γ_0 in Γ, and let $\mathcal{H}_j = l^2(\Gamma_j)$. Hence $l^2(\Gamma)$ is the direct sum of the $\mathcal{H}_j$. By identifying each $\mathcal{H}_j$ with $\mathcal{H}_0$, the elements of $l^2(\Gamma)$ become d-vectors. Consequently, for $\alpha \in \Gamma_0$ and $0 \leq i \leq d-1$, we have

$$T_\alpha v_i = (v_{i,0}(\alpha), \ldots, v_{i,d-1}(\alpha))^t,$$

and a similar expression holds for $T_\alpha \tilde{v}_i$. By taking the Fourier transform of $T_\alpha v_i$ and $T_\alpha \tilde{v}_i$, two matrices,

$$U(\xi) = (u_{j,k}(\xi))_{0 \leq j,k \leq d-1}, \qquad \widetilde{U}(\xi) = (\tilde{u}_{j,k}(\xi))_{0 \leq j,k \leq d-1},$$

are constructed with elements

$$u_{i,j}(\xi) = \sum_{\alpha \in \Gamma_0} v_{i,j}(\alpha)\beta(\xi), \qquad \tilde{u}_{i,j}(\xi) = \sum_{\alpha \in \Gamma_0} \tilde{v}_{i,j}(\alpha)\beta(\xi),$$

where $\beta(\xi)$ has modulus 1. With this notation, the following proposition holds.

Proposition 2 *The pair*

$$\{T_\alpha v_i, \alpha \in \Gamma_0\}_{i=0}^{d-1}, \qquad \{T_\alpha \tilde{v}_i, \alpha \in \Gamma_0\}_{i=0}^{d-1} \tag{4.16}$$

is a biorthogonal basis of $l^2(\Gamma)$ *if and only if*

$$\overline{\widetilde{U}(\xi)}^t U(\xi) = I_d. \tag{4.17}$$

Proof: For the proof of the "if part", the reader is referred to the first part of the proof of Proposition 1 in [51].

To prove the result in the other direction, by contradiction, we assume that the biorthogonal system (4.16) is not a basis of $l^2(\Gamma)$. Hence there exists $u \in l^2(\Gamma)$, $u \neq 0$, such that

$$u \neq \sum_{i=0}^{d-1} \sum_{\alpha \in \Gamma_0} < u, T_\alpha v_i > T_\alpha \tilde{v}_i,$$

and the family $\{T_\alpha v_i,\ \alpha \in \Gamma_0\}_{i=0}^{d-1}$ is not complete. Thus, there exists a nonzero vector w in $l^2(\Gamma)$ whose Fourier transform, $\widehat{w}(\xi)$, is orthogonal to the columns of $\boldsymbol{U}(\xi)$. But this is impossible by assumption (4.17). Thus, $\widehat{w}(\xi) = 0$ and $w = 0$ a.e. □

Remark 9 It is clear that our derivation of the necessary conditions for the construction of a biorthogonal wavelet basis of V_{-1} followed step by step the generalized algorithm and consequently these conditions are also sufficient.

The construction of a biorthogonal wavelet basis of $L^2(\mathbb{R}^n)$ is done by the following generalization of Theorem 3.2 [11] to the n-D case. Recall Th. 4 :

Let $\boldsymbol{D}$ be a dilation matrix and set $d = |\det \boldsymbol{D}|$. Assume that for some positive numbers, ϵ and $\tilde{\epsilon} > 0$, and $0 \leq i \leq d-1$, we have

$$|\widehat{\psi}^i(\xi)| < c\left(1 + |\xi|^2\right)^{-\epsilon - n/4}, \qquad |\widehat{\tilde{\psi}}^i(\xi)| < c\left(1 + |\xi|^2\right)^{-\tilde{\epsilon} - n/4}, \tag{4.18}$$

for some constant c. For $j \in \mathbb{Z}$ and $\boldsymbol{k} \in \mathbb{Z}^n$, define

$$\begin{aligned} \psi^i_{j,\boldsymbol{k}}(\boldsymbol{x}) &= |\det \boldsymbol{D}|^{-j/2} \psi^i(\boldsymbol{D}^{-j}\boldsymbol{x} - \boldsymbol{k}), \\ \tilde{\psi}^i_{j,\boldsymbol{k}}(\boldsymbol{x}) &= |\det \boldsymbol{D}|^{-j/2} \tilde{\psi}^i(\boldsymbol{D}^{-j}\boldsymbol{x} - \boldsymbol{k}), \end{aligned}$$

where the compactly supported wavelets ψ^i, $\tilde{\psi}^i$ are as defined in (5.37) and assume that

$$\sum_{i=0}^{d-1} \sum_{l \in \mathbb{Z}^n} \alpha^i_{l - \boldsymbol{D}j} \tilde{\alpha}^i_{l - \boldsymbol{D}k} = \delta_{j-k}. \tag{4.19}$$

Then for $f \in L^2(\mathbb{R}^n)$, we have

$$f = \sum_{i=1}^{d-1} \sum_{j\in\mathbb{Z}} \sum_{k\in\mathbb{Z}^n} \left\langle f, \tilde{\psi}^i_{j,k} \right\rangle \psi^i_{j,k} = \sum_{i=1}^{d-1} \sum_{j\in\mathbb{Z}} \sum_{k\in\mathbb{Z}^n} \left\langle f, \psi^i_{j,k} \right\rangle \tilde{\psi}^i_{j,k}. \tag{4.20}$$

Proof: The proof is carried out in three parts denoted by (a), (b) and (c).

(a) We first prove that, for all $f_1,\ f_2 \in L^2(\mathbb{R}^n)$,

$$\begin{aligned} &\sum_{k\in\mathbb{Z}^n} \langle f_1, \phi_{-1,k} \rangle \left\langle \tilde{\phi}_{-1,k}, f_2 \right\rangle \\ &\quad = \sum_{l\in\mathbb{Z}^n} \left[\langle f_1, \phi_{0,l} \rangle \left\langle \tilde{\phi}_{0,l}, f_2 \right\rangle + \sum_{i=1}^{d-1} \left\langle f_1, \psi^i_{0,l} \right\rangle \left\langle f_2, \tilde{\psi}^i_{0,l} \right\rangle \right]. \end{aligned} \tag{4.21}$$

To do this, we remark that

$$\begin{aligned} \left\langle f_1, \psi^i_{0,l} \right\rangle &= \int f_1(x) \overline{\psi^i(x-l)}\, dx \\ &= \int f_1(x) \overline{\sum_{n\in\mathbb{Z}^n} \alpha^i_{l-Dn} \psi^0(Dx-n)}\, dx, \qquad i = 0, \ldots, d-1, \end{aligned}$$

and, similarly,

$$\begin{aligned} \left\langle \tilde{\psi}^i_{0,l}, f_2 \right\rangle &= \int \tilde{\psi}^i(x-l) \overline{f_2(x)}\, dx \\ &= \int \sum_{n\in\mathbb{Z}^n} \left[\tilde{\alpha}^i_{l-Dn} \tilde{\psi}^0(Dx-n) \right] \overline{f_2(x)}\, dx, \qquad i = 0, \ldots, d-1. \end{aligned}$$

Hence,

$$\begin{aligned} &\sum_{l\in\mathbb{Z}^n} \sum_{i=0}^{d-1} \left\langle f_1, \psi^i_{0,l} \right\rangle \left\langle \tilde{\psi}^i_{0,l}, f_2 \right\rangle \\ &\quad = \sum_{l\in\mathbb{Z}^n} \sum_{i=0}^{d-1} \left[\sum_{n\in\mathbb{Z}^n} \alpha^i_{l-Dn} \left\langle f_1, \psi^0_{-1,n} \right\rangle \right] \left[\sum_{n\in\mathbb{Z}^n} \tilde{\alpha}^i_{l-Dn} \left\langle \tilde{\psi}^0_{-1,n}, f_2 \right\rangle \right] \\ &\quad = \sum_{l\in\mathbb{Z}^n} \sum_{i=0}^{d-1} \sum_{j,k\in\mathbb{Z}^n} \alpha^i_{l-Dj} \tilde{\alpha}^i_{l-Dk} \left\langle f_1, \psi^0_{-1,j} \right\rangle \left\langle \tilde{\psi}^0_{-1,k}, f_2 \right\rangle. \end{aligned}$$

Finally, equality (4.22) follows from (4.21).

(b) We prove that, for all $f_1,\ f_2 \in L^2(\mathbb{R}^n)$, the following equality holds:

$$\sum_{k\in\mathbb{Z}^n} \sum_{j\in\mathbb{Z}} \sum_{i=1}^{d-1} \left\langle f_1, \psi^i_{j,k} \right\rangle \left\langle \tilde{\psi}^i_{j,k}, f_2 \right\rangle = \langle f_1, f_2 \rangle.$$

Using the techniques of part (a), one shows that

$$\sum_{k\in\mathbf{Z}^n} \langle f_1, \phi_{j-1,k}\rangle \left\langle \tilde{\phi}_{j-1,k}, f_2\right\rangle = \sum_{l\in\mathbf{Z}^n}\sum_{i=0}^{d-1} \left\langle f_1, \psi^i_{j,l}\right\rangle \left\langle f_2, \tilde{\psi}^i_{j,l}\right\rangle \tag{4.22}$$

which implies that

$$\begin{aligned}&\sum_{k\in\mathbf{Z}^n} \langle f_1, \phi_{-J-1,k}\rangle \left\langle \tilde{\phi}_{-J-1,k}, f_2\right\rangle \\ &\quad = \sum_{j=-J}^{J}\sum_{l\in\mathbf{Z}^n}\sum_{i=1}^{d-1} \left\langle f_1, \psi^i_{j,l}\right\rangle \left\langle \tilde{\psi}^i_{j,l}, f_2\right\rangle + \sum_{l\in\mathbf{Z}^n} \left\langle f_1, \psi^0_{J,l}\right\rangle \left\langle \tilde{\psi}^0_{J,l}, f_2\right\rangle .\end{aligned} \tag{4.23}$$

To prove the d inequalities

$$\lim_{J\to+\infty} \sum_{j=-J}^{J}\sum_{l\in\mathbf{Z}^n} \left|\left\langle f_1, \psi^i_{j,l}\right\rangle \left\langle \tilde{\psi}^i_{j,l}, f_2\right\rangle\right| < \infty, \qquad i = 0,\dots,d-1,$$

it suffices to consider the case $i = 0$. By the n-D version of Parseval's equality, we have

$$\sum_{j=-J}^{J}\sum_{l\in\mathbf{Z}^n} \left|\left\langle f_1, \psi^0_{j,l}\right\rangle \left\langle \tilde{\psi}^0_{j,l}, f_2\right\rangle\right| = \sum_{j=-J}^{J}\sum_{l\in\mathbf{Z}^n} \left|\left\langle \hat{f}_1, \hat{\psi}^0_{j,l}\right\rangle \left\langle \hat{\tilde{\psi}}^0_{j,l}, \hat{f}_2\right\rangle\right|,$$

where

$$\hat{\psi}^0_{j,l}(\xi) = |\det \boldsymbol{D}|^{j/2} e^{-i\xi\cdot \boldsymbol{D}^j l}\hat{\psi}^0({}^t\boldsymbol{D}^j\xi).$$

Consider the set $C_j = \{2\pi\, {}^t\boldsymbol{D}^{-j}x;\ x\in[0,1]^n\}$, and use the n-D version of Plancherel's identity to obtain

$$\begin{aligned}&\sum_{j=-J}^{J}\sum_{l\in\mathbf{Z}^n} \left|\left\langle \hat{f}_1, \hat{\psi}^0_{j,l}\right\rangle \left\langle \hat{\tilde{\psi}}^0_{j,l}\hat{f}_2\right\rangle\right| \\ &\quad = \sum_{-J}^{J}\left|\int_{C_j}\sum_{l,k\in\mathbf{Z}^n}\Big[\overline{\hat{f}_2(\xi+2\pi\,{}^t\boldsymbol{D}^{-j}k)}\hat{f}_1(\xi+2\pi\,{}^t\boldsymbol{D}^{-j}l) \\ &\qquad \times\overline{\hat{\psi}^0({}^t\boldsymbol{D}^j\xi+2\pi l)}\hat{\tilde{\psi}}^0({}^t\boldsymbol{D}^j\xi+2\pi k)d\xi\Big]\right| \\ &\quad \le \sum_{-J}^{J}\int_{C_j}\sum_{l,k\in\mathbf{Z}^n}\left|\hat{f}_1(\xi+2\pi\,{}^t\boldsymbol{D}^{-j}l)\overline{\hat{f}_2(\xi+2\pi\,{}^t\boldsymbol{D}^{-j}k)}\right| \\ &\qquad \times\left|\overline{\hat{\psi}^0({}^t\boldsymbol{D}^j\xi+2\pi l)}\hat{\tilde{\psi}}^0({}^t\boldsymbol{D}^j\xi+2\pi k)d\xi\right|^{\delta} \\ &\qquad \times\sum_{l,k\in\mathbf{Z}^n}\left|\overline{\hat{\psi}^0({}^t\boldsymbol{D}^j\xi+2\pi l)}\hat{\tilde{\psi}}^0({}^t\boldsymbol{D}^j\xi+2\pi k)d\xi\right|^{1-\delta},\end{aligned} \tag{4.24}$$

where $\delta \in (0,1)$ is to be fixed later. By (4.18), the series

$$\sum_{l,k\in\mathbb{Z}^n} \left|\overline{\widehat{\psi}^0({}^t\boldsymbol{D}^j\boldsymbol{\xi}+2\pi\boldsymbol{l})}\widehat{\tilde{\psi}}^0({}^t\boldsymbol{D}^j\boldsymbol{\xi}+2\pi\boldsymbol{k})d\boldsymbol{\xi}\right|^{1-\delta}$$

is uniformly bounded in $\boldsymbol{\xi}$ for all $\delta < 2\epsilon(n+2\epsilon)^{-1}$. Hence the left-most term of (4.24) is bounded by

$$\|f_1\|_2\|f_2\|_2\Big(\sup_{\boldsymbol{\xi}\in[1,2]^n}\sum_{j\in\mathbb{Z}}\left|\widehat{\psi}^0({}^t\boldsymbol{D}^j\boldsymbol{\xi})\right|\Big)^{\delta}\Big(\sup_{\boldsymbol{\xi}\in[1,2]^n}\sum_{j\in\mathbb{Z}}\left|\widehat{\tilde{\psi}}^0({}^t\boldsymbol{D}^j\boldsymbol{\xi})\right|\Big)^{\delta}.$$

Since ψ has compact support, then $\psi \in L^1(\mathbb{R}^n)$. By the n-D version of the Paley–Wiener theorem, $\widehat{\psi}(\boldsymbol{\xi})$ can be extended to a holomorphic function satisfying

$$\left|\widehat{\psi}(\boldsymbol{\xi}+i\boldsymbol{\eta})\right| \le c(1+|\boldsymbol{\xi}|+|\boldsymbol{\eta}|)\,e^{i|\boldsymbol{\eta}|}, \qquad \boldsymbol{\xi},\,\boldsymbol{\eta}\in\mathbb{R}^n.$$

Since $\widehat{\psi}(0)=0$, there exists a constant A such that

$$\left|\widehat{\psi}^0(\boldsymbol{\xi})\right| \le A|\boldsymbol{\xi}|, \qquad \left|\widehat{\tilde{\psi}}^0(\boldsymbol{\xi})\right| \le A|\boldsymbol{\xi}|.$$

Therefore, for $\boldsymbol{\xi}\in[1,2]^n$, we have

$$\begin{aligned}
&\sum_{j=-\infty}^{0}\left|\widehat{\psi}^0({}^t\boldsymbol{D}^j\boldsymbol{\xi})\right|^{\delta}\\
&\quad\le CA^{\delta}\sum_{j=-\infty}^{0}\left|({}^t\boldsymbol{D}^j\boldsymbol{\xi})\right|^{\delta}\\
&\quad\le CA^{\delta}\sum_{j=-\infty}^{0}\|\boldsymbol{D}\|_2^{\delta j}\le C',
\end{aligned}$$

because $\|\boldsymbol{D}\|_2 > 1$. Similarly

$$\sum_{j=-\infty}^{0}\left|\widehat{\tilde{\psi}}^{0\iota}\boldsymbol{D}^j\boldsymbol{\xi})\right|^{\delta} \le C''.$$

On the other hand, since $\|\boldsymbol{D}\|_2 > \eta > 1$, then for $\boldsymbol{\xi}\in[1,2]^n$, we have

$$\sum_{j=1}^{\infty}\left|\widehat{\psi}^0({}^t\boldsymbol{D}^j\boldsymbol{\xi})\right|^{\delta} \le C^{\delta}\sum_{j=1}^{\infty}\left(1+\eta^{2j}\right)^{-n\delta/4} < \infty.$$

Similarly we can prove that

$$\sum_{j=1}^{\infty} \left| \widehat{\tilde{\psi}}^0({}^t\boldsymbol{D}^j\boldsymbol{\xi}) \right|^{\delta} < \infty.$$

Combining these results we have that for all integer $J \geq 1$

$$\sum_{j=-J}^{J} \sum_{k\in\mathbb{Z}^n} \left| \left\langle f_1, \psi^0_{j,k} \right\rangle \left\langle \tilde{\psi}^0_{j,k}, f_2 \right\rangle \right| < \infty.$$

Finally, by the same techniques one can prove that

$$\sum_{j=-J}^{J} \sum_{k\in\mathbb{Z}^n} \left| \left\langle f_1, \psi^i_{j,k} \right\rangle \left\langle \tilde{\psi}^i_{j,k}, f_2 \right\rangle \right| < \infty, \qquad i = 1, \ldots, d-1.$$

(c) To complete the proof of the theorem, we first show that

$$\lim_{J\to+\infty} \sum_{k\in\mathbb{Z}^n} \left\langle f_1, \psi^0_{J,k} \right\rangle \left\langle \tilde{\psi}^0_{J,k}, f_2 \right\rangle = 0.$$

Using the Cauchy–Schwarz inequality, we have

$$\sum_{k\in\mathbb{Z}^n} \left\langle f_1, \psi^0_{J,k} \right\rangle \left\langle \tilde{\psi}^0_{J,k}, f_2 \right\rangle \leq \left[\sum_{k\in\mathbb{Z}^n} \left| \left\langle f_1, \psi^0_{J,k} \right\rangle \right|^2 \right]^{1/2} \left[\sum_{k\in\mathbb{Z}^n} \left| \left\langle \tilde{\psi}^0_{J,k}, f_2 \right\rangle \right|^2 \right]^{1/2}.$$

Hence, following the proof in (b), we have

$$\begin{aligned} &\sum_{k\in\mathbb{Z}^n} \left\langle f_1, \psi^0_{J,k} \right\rangle \left\langle \tilde{\psi}^0_{J,k}, f_2 \right\rangle \\ &\quad \leq \; K \left[\int |\hat{f}_1(\boldsymbol{\xi})| (1 + |{}^t\boldsymbol{D}^J\boldsymbol{\xi}|^2)^{-n\delta/2} \, d\boldsymbol{\xi} \right]^{1/2} \left[\int |\hat{f}_2(\boldsymbol{\xi})| (1 + |{}^t\boldsymbol{D}^J\boldsymbol{\xi}|^2)^{-n\delta/2} \, d\boldsymbol{\xi} \right]^{1/2} \\ &\quad \to \; 0, \qquad \text{as} \quad J \to +\infty, \end{aligned} \tag{4.25}$$

where the limit to zero follows by the Lebesgue dominated convergence theorem and the fact $\|\boldsymbol{D}\|_2 > 1$. It remains to be proved that

$$\lim_{J\to+\infty} \sum_{k\in\mathbb{Z}^n} \left\langle f_1, \psi^0_{-J-1,k} \right\rangle \left\langle \tilde{\psi}^0_{-J-1,k}, f_2 \right\rangle = \langle f_1, f_2 \rangle .$$

Using the techniques of part (b), one can easily show that

$$\begin{aligned} &\sum_{k\in\mathbb{Z}^n} \left\langle f_1, \psi^0_{-J-1,k} \right\rangle \left\langle \tilde{\psi}^0_{-J-1,k}, f_2 \right\rangle \\ &\quad = \int \hat{f}_1(\boldsymbol{\xi}) \overline{\hat{f}_2(\boldsymbol{\xi}) \widehat{\psi}^0({}^t\boldsymbol{D}^{-J-1}\boldsymbol{\xi})} \widehat{\tilde{\psi}}^0({}^t\boldsymbol{D}^{-J-1}\boldsymbol{\xi}) \, d\boldsymbol{\xi} \\ &\qquad + \sum_{0\neq k\in\mathbb{Z}^n} \int \overline{\hat{f}_2(\boldsymbol{\xi} + 2\pi {}^t\boldsymbol{D}^{J+1}k)} \hat{f}_1(\boldsymbol{\xi}) \overline{\widehat{\psi}^0({}^t\boldsymbol{D}^{-J-1}\boldsymbol{\xi})} \widehat{\tilde{\psi}}^0({}^t\boldsymbol{D}^{-J-1}\boldsymbol{\xi} \\ &\qquad + 2\pi k) \, d\boldsymbol{\xi}. \end{aligned} \tag{4.26}$$

Since $\widehat{\psi}^0(0) = 1$ and $\widehat{\tilde{\psi}}(0) = 1$, and $\|D^{-1}\|_2 < 1$, then the limit of the first term on the rigth-hand side of (5.49), as J goes to infinity, is equal to

$$\int \hat{f}_1(\xi)\overline{\hat{f}_2(\xi)}\, d\xi = \langle f_1, f_2 \rangle .$$

From the results of part (b) one concludes that the absolute value of the second term (that is, the summation) on the rigth-hand side of (4.26) is bounded by a constant.

Hence by approximating $\hat{f}_1(\xi)$ and $\hat{f}_2(\xi)$ by compactly supported functions in $L^2(\mathbb{R}^n)$ and remembering that $\|D\|_2 > 1$, we may assume that for $k \in \mathbb{Z}^n$, with $k \neq 0$,

$$\text{supp } \hat{f}_1(\cdot) \cap \text{supp } \hat{f}_2(\cdot + 2\pi\, {}^tD^J k) = \emptyset, \qquad \text{as } J \to +\infty;$$

thus, the second term of the sum in (5.49) goes to 0 as J goes to infinity.

Combining the above results, we conclude that

$$\lim_{J\to+\infty} \sum_{k\in\mathbb{Z}^n} \left\langle f_1, \psi^0_{-J-1,k} \right\rangle \left\langle \tilde{\psi}^0_{-J-1,k}, f_2 \right\rangle = \langle f_1, f_2 \rangle ,$$

and, consequently, (4.20) follows. □

4.2.3 Regular $L^2(\mathbb{R}^n)$ wavelets

One of the challenging problems in wavelet theory is to find a good estimate for the order of regularity of wavelets. We generalize the estimate given in [10] to the n-D case. Recall th. 5:

Let D be a dilation matrix and assume that the frequency response, $H(\xi)$, of an n-D FIR wavelet filter factors in the form

$$H(\xi) = f^{2N}(\xi)\mathcal{F}(\xi), \tag{4.27}$$

where

$$\prod_{j=1}^{\infty} f^2({}^tD^{-j}\xi) \leq \frac{c}{1+|\xi|^2}, \tag{4.28}$$

and for some $k \geq 1$ we have the bound

$$B_k := \max_{\xi \in \mathbb{R}^n} \left| \mathcal{F}(\xi)\mathcal{F}({}^tD\xi) \cdots \mathcal{F}({}^tD^{k-1}\xi) \right|^{1/k} < \|D^{-1}\|_2^{-2N+n/2}. \tag{4.29}$$

Then, the Fourier transform

$$\widehat{\phi}(\xi) = \prod_{j=1}^{\infty} H({}^tD^{-j}\xi),$$

of the scaling function $\phi(\xi)$ satisfies the inequality

$$\left|\widehat{\phi}(\xi)\right| \leq C(1+|\xi|^2)^{-\epsilon-n/2}, \qquad \epsilon < N - \frac{n}{2} + \frac{\log(B_k)}{2\log(\|D^{-1}\|_2)}. \tag{4.30}$$

Proof. If $H(\xi)$ has finite length, then clearly

$$|H(\xi)| \leq 1 + C|\xi|.$$

Hence, if $|\xi| \leq 1$, then

$$\left|\widehat{\phi}(\xi)\right| \leq \prod_{j=1}^{\infty} \exp\left(C\left|{}^tD^{-j}\xi\right|\right) \leq \exp\left(C\sum_{j=1}^{\infty}\|D^{-1}\|_2^j\right) < \infty.$$

On the other hand, if $|\xi| > 1$, we have

$$\begin{aligned} |\widehat{\phi}(\xi)| &= \prod_{j=1}^{\infty} \left|f^{2N}\left({}^tD^{-j}\xi\right)\right| \prod_{k=1}^{\infty} \left|\mathcal{F}\left({}^tD^{-k}\xi\right)\right| \\ &\leq \frac{C}{(1+|\xi|^2)^N} \prod_{j=1}^{\infty} \left|\mathcal{F}\left(D^{-j}\xi\right)\right|. \end{aligned} \tag{4.31}$$

Let

$$\mathcal{G}(\xi) = \mathcal{F}({}^tD^{-1}\xi) \cdots \mathcal{F}({}^tD^{-k}\xi).$$

Since $\|D^{-1}\|_2 < 1$, given $\xi \in \mathbb{R}^n$ with $|\xi| > 1$, there exists $l_0 \in N$ such that

$$\|D^{-1}\|_2^{-kl_0} \leq |\xi| \leq \|D^{-1}\|_2^{-k(l_0+1)}. \tag{4.32}$$

To bound the infinite product on the right-hand side of (4.31), we factor it as

$$\prod_{j=1}^{\infty} \left|\mathcal{F}\left({}^tD^{-j}\xi\right)\right| = \prod_{l=0}^{l_0} \left|\mathcal{G}\left({}^tD^{-kl}\xi\right)\right| \prod_{j=0}^{\infty} \left|\mathcal{G}\left(\left[{}^tD^{-jk}\right]\left[{}^tD^{-(l_0+1)k}\right]\xi\right)\right|. \tag{4.33}$$

Since $\left|{}^t\boldsymbol{D}^{-(l_0+1)k}\boldsymbol{\xi}\right| \leq 1$ by the second inequality in (4.32), we have

$$\prod_{j=0}^{\infty}\left|\mathcal{G}\left({}^t\boldsymbol{D}^{-jk}({}^t\boldsymbol{D}^{-(l_0+1)k}\boldsymbol{\xi})\right)\right| \leq \exp\Big(C\sum_{j=1}^{\infty}\|\boldsymbol{D}^{-1}\|_2^{jk}\Big) < \infty.$$

By definition (4.29) of B_k, the finite product in (4.33) is bounded by

$$\prod_{l=0}^{l_0}\left|\mathcal{G}({}^t\boldsymbol{D}^{-kl}\boldsymbol{\xi})\right| \leq B_k^{k(l_0+1)}. \tag{4.34}$$

Since, by the first inequality in (4.32), one has

$$kl_0 \leq -\frac{\log|\boldsymbol{\xi}|}{\log\|\boldsymbol{D}^{-1}\|_2}, \tag{4.35}$$

then one can easily conclude from (4.34) that

$$\begin{aligned}\prod_{0}^{l_0}\left|\mathcal{G}({}^t\boldsymbol{D}^{-kl}\boldsymbol{\xi})\right| &\leq B_k^{k-\log|\boldsymbol{\xi}|/\log\|\boldsymbol{D}^{-1}\|_2}\\ &\leq B_k^k\exp\left(-\log|\boldsymbol{\xi}|\frac{\log B_k}{\log\|\boldsymbol{D}^{-1}\|_2}\right)\\ &\leq C\left(1+|\boldsymbol{\xi}|^2\right)^{-\log B_k/\log\|\boldsymbol{D}^{-1}\|_2^2}.\end{aligned} \tag{4.36}$$

Inserting (4.36) in (4.31), we have

$$\begin{aligned}\left|\widehat{\phi}(\boldsymbol{\xi})\right| &\leq C\left(\frac{1}{1+|\boldsymbol{\xi}|^2}\right)^N\left(1+|\boldsymbol{\xi}|^2\right)^{-\log B_k/\log\|\boldsymbol{D}^{-1}\|_2^2}\\ &\leq C\left(1+|\boldsymbol{\xi}|^2\right)^{-N-\log B_k/\log\|\boldsymbol{D}^{-1}\|_2^2}.\end{aligned}$$

Consequently, if $B_k < \|\boldsymbol{D}^{-1}\|_2^{-2N+n/2}$, inequality (4.30) holds. □

Remark 10 Under the hypotheses of the theorem, it is easily seen that the scaling function and, consequently, the wavelets are r-Hölder continuous with

$$r < 2N - n + \frac{\log(B_k)}{\log(\|\boldsymbol{D}^{-1}\|_2)}.$$

Remark 11 The above method for estimating the regularity of the wavelets is a brute force method and has the disadvantage of not being optimal in the sense that, in general, it cannot provide the best approximation to the exact order of regularity. However, unlike other known methods (see [17], [56]), it has the advantage of being a general method in the sense that it can be used in the n-D case, where $n \geq 1$, and for arbitrarily long filter $H(\boldsymbol{\xi})$.

4.3 Examples of Design of n-D Biorthogonal Wavelets

In the n-D case with $n \geq 3$, one may consider using McClellan's transformation with a suitable choice of 1-D dual filters and transformation function $F(\xi_1, \ldots, \xi_n)$. Unfortunately, due to the large number of constraints, in practice it is not possible to choose $F(\xi_1, \ldots, \xi_n)$ and the method becomes inefficient. However, if the dilation matrix $\boldsymbol{D}$ satisfies $|\det \boldsymbol{D}| = 2^p$, with $p \geq 2$, then it is possible to construct the dual filters, $H_0^n(\boldsymbol{\xi})$, $\widetilde{H}_0^n(\boldsymbol{\xi})$, by combining two families $H_0^{n-1}(\xi_1, \ldots, \xi_{n-1})$, $\widetilde{H}_0^{n-1}(\xi_1, \ldots, \xi_{n-1})$ and $h_0(\xi)$, $\tilde{h}_0(\xi)$ as follows:

$$\begin{aligned} H_0^n(\xi_1, \ldots, \xi_n) &= H_0^{n-1}(\xi_1, \ldots, \xi_{n-1}) h_0(\xi_n), \\ \widetilde{H}_0^n(\xi_1, \ldots, \xi_n) &= \widetilde{H}_0^{n-1}(\xi_1, \ldots, \xi_{n-1}) \tilde{h}_0(\xi_n). \end{aligned}$$

Here the dilation matrix associated to the $(n-1)$-D dual filters satisfies $|\det \boldsymbol{D}| = 2^{p-1}$ and the dilation factor of the 1-D dual filters is equal to 2. Note that for an arbitrary dilation matrix $\boldsymbol{D}$ satisfying $|\det \boldsymbol{D}| = 2^p$, $p \geq 2$, the designed biorthogonal wavelets, in general, have nonseparable variables.

As an example of this design in 3-D, we consider the dilation matrix $\boldsymbol{D}$ given by

$$\boldsymbol{D} = \begin{pmatrix} 1 & -1 & 1 \\ 1 & 1 & -1 \\ 1 & 1 & 1 \end{pmatrix}.$$

The dual lowpass filters $H_0^3(\boldsymbol{\xi})$ and $\widetilde{H}_0^3(\boldsymbol{\xi})$ satisfy the equation

$$\sum_{i=0}^{3} H_0^3(\boldsymbol{\xi} + \boldsymbol{\eta}_i) \overline{\widetilde{H}_0^3(\boldsymbol{\xi} + \boldsymbol{\eta}_i)} = 1,$$

where

$$\boldsymbol{\eta}_0 = (0,0,0)^t, \qquad \boldsymbol{\eta}_1 = (\pi,0,\pi)^t, \qquad \boldsymbol{\eta}_2 = (0,\pi,\pi)^t, \qquad \boldsymbol{\eta}_3 = (\pi,\pi,0)^t.$$

By taking m_0^3 and $\widetilde{m}_0^3$ of the form

$$\begin{aligned} H_0^3(\xi_1, \xi_2, \xi_3) &= H_0^2(\xi_1, \xi_2) h_0(\xi_3), \\ \widetilde{H}_0^3(\xi_1, \xi_2, \xi_3) &= \widetilde{H}_0^2(\xi_1, \xi_2) \tilde{h}_0(\xi_3), \end{aligned}$$

where $H_0^2(\xi_1, \xi_2)$ and $\widetilde{H}_0^2(\xi_1, \xi_2)$ are obtained by using McClellan's transformation and satisfy the identity

$$H_0^2(\boldsymbol{\xi})\overline{\widetilde{H}_0^2(\boldsymbol{\xi})} + H_0^2\left(\boldsymbol{\xi} + (\pi,\pi)^t\right)\overline{\widetilde{H}_0^2\left(\boldsymbol{\xi} + (\pi,\pi)^t\right)} = 1,$$

and the dual 1-D filters, $h_0(\xi)$ and $\widetilde{h}_0(\xi)$, satisfy the identity

$$h_0(\xi)\overline{\widetilde{h}_0(\xi)} + h_0(\xi+\pi)\overline{\widetilde{h}_0(\xi+\pi)} = 1.$$

It is not possible, in general, to know the exact values of the n-D dual scaling functions and wavelets $\psi^i(\boldsymbol{x})$, $\widetilde{\psi}^i(\boldsymbol{x})$, $i = 0, \ldots, d-1$; however, under some conditions on the dilation matrix $\boldsymbol{D}$ and on the dual lowpass filters, it is possible to get a good numerical approximation to these values as will be shown in the next section.

4.4 The Cascade Algorithm for the n-D Case

In this section, we generalize the 1-D cascade algorithm given in [15], pp. 202–205, to the n-D case. To do so, the following proposition is needed.

Proposition 3 *Assume that $\boldsymbol{D}$ is the dilation matrix of Definition 6 and that $\|\boldsymbol{D}^{-1}\|_2 < 1$. Let $\phi(\boldsymbol{x})$ be an n-D compactly supported scaling function. If f is a continuous function on $\mathbb{R}^n$, then for $\boldsymbol{x} \in \mathbb{R}^n$*

$$\lim_{j\to\infty} |\det \boldsymbol{D}|^j \int f(\boldsymbol{x}+\boldsymbol{y})\overline{\phi(\boldsymbol{D}^j\boldsymbol{y})}\, d\boldsymbol{y} = f(\boldsymbol{x}). \tag{4.37}$$

If f is uniformly continuous, then this pointwise convergence is uniform. Finally, if f is r-Hölder continuous, then

$$\left| f(\boldsymbol{x}) - |\det \boldsymbol{D}|^j \int f(\boldsymbol{x}+\boldsymbol{y})\overline{\phi(\boldsymbol{D}^j\boldsymbol{y})} d\boldsymbol{y} \right| \leq C\|\phi\|_1 \|\boldsymbol{D}^{-1}\|_2^{jr}. \tag{4.38}$$

Proof: Since ϕ is compactly supported, we may assume that $\text{supp}\phi := \mathcal{K} \subset [R_1, R_2]^n$ for some real numbers R_1, R_2. Since $\|\boldsymbol{D}^{-1}\|_2 = \beta < 1$, then $\|\boldsymbol{D}^{-j}\| \leq \beta^{-j}$ for all

positive integer $j \geq 1$. Since $\int \phi(\boldsymbol{x})d\boldsymbol{x} = 1$, then it is clear that $|\det \boldsymbol{D}|^j \phi(\boldsymbol{D}^j \boldsymbol{y})$ is an approximation of the δ function. Also

$$\begin{aligned}\left| f(\boldsymbol{x}) - |\det \boldsymbol{D}|^j \int f(\boldsymbol{x}+\boldsymbol{y})\overline{\phi(\boldsymbol{D}^j\boldsymbol{y})}d\boldsymbol{y} \right| &= \left| \int \left[f(\boldsymbol{x}) - f(\boldsymbol{x}+\boldsymbol{D}^{-j}\boldsymbol{z}) \right] \overline{\phi(\boldsymbol{z})} \right| \\ &\leq \|\phi\|_1 \sup_{\boldsymbol{z}\in\mathcal{K}} \left| f(\boldsymbol{x}) - f(\boldsymbol{x}+\boldsymbol{D}^{-j}\boldsymbol{z}) \right|.\end{aligned}$$

Since the diameter of $\boldsymbol{D}^{-j}\mathcal{K} \to 0$ as $j \to +\infty$, then, if f is continuous,

$$\sup_{\boldsymbol{z}\in\mathcal{K}} \left| f(\boldsymbol{x}) - f(\boldsymbol{x}+\boldsymbol{D}^{-j}\boldsymbol{z}) \right| \to 0 \qquad \text{as } j \to +\infty.$$

This proves pointwise convergence. Now, if f is uniformly continuous, then it is clear that

$$|\det \boldsymbol{D}|^j \int f(\boldsymbol{x}+\boldsymbol{y})\overline{\phi(\boldsymbol{D}^j\boldsymbol{y})}\, d\boldsymbol{y} \to f(\boldsymbol{x}), \qquad \text{uniformly as } j \to \infty.$$

Finally, if f is r-Hölder continuous, then

$$\begin{aligned}\left| f(\boldsymbol{x}) - |\det \boldsymbol{D}|^j \int f(\boldsymbol{x}+\boldsymbol{y})\overline{\phi(\boldsymbol{D}^j\boldsymbol{y})}\, d\boldsymbol{y} \right| &\leq \|\phi\|_1 \sup_{\boldsymbol{z}\in\mathcal{K}} \left| f(\boldsymbol{x}) - f(\boldsymbol{x}+\boldsymbol{D}^{-j}\boldsymbol{z}) \right| \\ &\leq C\|\phi\|_1 \sup_{\boldsymbol{y}\in\boldsymbol{D}^{-j}\mathcal{K}} \|\boldsymbol{y}\|_2^r, \\ &\leq C\|\phi\|_1 \|\boldsymbol{D}^{-1}\|_2^{jr}.\end{aligned}$$

The proof is complete. □

We now state the n-D cascade algorithm.

Algorithm (n-D cascade algorithm): Let $\phi(\boldsymbol{x})$ be a compactly supported scaling function and $\boldsymbol{D}$ be as defined in the previous proposition. We assume that

$$\phi(\boldsymbol{x}) = \sum_{\boldsymbol{l}\in\mathbb{Z}^n} \alpha_{\boldsymbol{l}} \phi(\boldsymbol{D}\boldsymbol{x} - \boldsymbol{l}) \tag{4.39}$$

with

$$\sum_{\boldsymbol{k}\in\mathbb{Z}^n} \alpha_{\boldsymbol{l}-\boldsymbol{D}\boldsymbol{k}}\alpha_{\boldsymbol{m}-\boldsymbol{D}\boldsymbol{k}} = \frac{1}{|\det \boldsymbol{D}|}\delta_{\boldsymbol{l}-\boldsymbol{m}}. \tag{4.40}$$

Also, for $j \in \mathbb{Z}$ and $\boldsymbol{k} \in \mathbb{Z}^n$, let

$$\phi_{j\boldsymbol{k}}(\boldsymbol{x}) = |\det \boldsymbol{D}|^{-j/2}\phi(\boldsymbol{D}^{-j}\boldsymbol{x} - \boldsymbol{k}).$$

If we denote the scalar product $\langle \phi, \phi_{j\boldsymbol{k}} \rangle$ by $A_{\boldsymbol{k}}^{-j}$. Then under the above conditions, it is easy to prove that

$$A_{\boldsymbol{l}}^{-j} = |\det \boldsymbol{D}|^{3/2} \sum_{\boldsymbol{k} \in \mathbb{Z}^n} \alpha_{\boldsymbol{l}-\boldsymbol{D}\boldsymbol{k}} A_{\boldsymbol{k}}^{-j+1}.$$

If we take the starting value $A_{\boldsymbol{k}}^{0} = 1$ if $\boldsymbol{k} = 0$ and 0 otherwise and by using the new variable $C_{\boldsymbol{k}} = |\det \boldsymbol{D}|^{1/2}\alpha_{\boldsymbol{k}}$, then the n-D cascade algorithm becomes:

$$\begin{aligned} A_{\boldsymbol{k}} &= \delta_{\boldsymbol{k}}, \\ A_{\boldsymbol{l}}^{-j} &= |\det \boldsymbol{D}|^{1/2} \sum_{\boldsymbol{k} \in \mathbb{Z}^n} C_{\boldsymbol{l}-\boldsymbol{D}\boldsymbol{k}} A_{\boldsymbol{k}}^{-j+1}, \qquad j \geq 1. \end{aligned}$$

This algorithm provides a good numerical approximation of the scaling function and, consequently, of the wavelets. If, in the previous proposition, $f = \phi$ is r-Hölder continuous and $\boldsymbol{x} = \boldsymbol{D}^{-j}\boldsymbol{k}$ for some $j \in \mathbb{Z}$ and $\boldsymbol{k} \in \mathbb{Z}^n$, then we have the approximation

$$\phi(\boldsymbol{x}) \approx A_{\boldsymbol{k}}^{-j} |\det \boldsymbol{D}|^{j/2}.$$

Moreover

$$\left| \phi(\boldsymbol{x}) - |\det \boldsymbol{D}|^{j/2} A_{\boldsymbol{k}}^{-j} \right| \leq C \|\boldsymbol{D}^{-1}\|_2^{jr}.$$

4.5 Numerical Results

In this last section, we construct three examples of nonseparable 2-D biorthogonal wavelets.

A. First Example.— We consider the dilation matrix

$$\boldsymbol{D}_1 = \begin{pmatrix} 1 & 1 \\ 1 & -1 \end{pmatrix} \tag{4.41}$$

with eigenvalues $\lambda_1 = \sqrt{2}$, $\lambda_2 = -\sqrt{2}$, and $\|\boldsymbol{D}^{-1}\|_2 = \frac{1}{\sqrt{2}} < 1$ and the transformation function

$$F(\xi_1, \xi_2) = \frac{1}{2}(\cos \xi_1 + \cos \xi_2).$$

Table 4.1: The coefficients $\alpha_{n,m}$ of $H_0^2(\xi_1,\xi_2)$ for $-6 \le n,m \le 6$.

$n\backslash m$	0	±1	±2	±3
0	0.543945312500	0.200439453125	−0.000189208979	−0.000994873000
±1	0.200439453125	0.001049804734	−0.003747558687	−0.000622558582
±2	−0.000189208979	−0.003747558687	−0.001025390578	0.000305175781
±3	−0.000994873000	−0.000622558582	0.000305175781	0.000122070312
±4	−0.000073242190	0.000152587891	0.000091552734	0.000000000000
±5	0.000030517578	0.000036621095	0.000000000000	0.000000000000
±6	0.000006103516	0.000000000000	0.000000000000	0.000000000000

$n\backslash m$	±4	±5	±6
0	−0.000073242190	0.000030517578	0.000006103516
±1	0.000152587891	0.000036621095	0.000000000000
±2	0.000091552734	0.000000000000	0.000000000000
±3	0.000000000000	0.000000000000	0.000000000000
±4	0.000000000000	0.000000000000	0.000000000000
±5	0.000000000000	0.000000000000	0.000000000000
±6	0.000000000000	0.000000000000	0.000000000000

The 1-D dual wavelet filters with frequency responses $h_0(\xi)$, $\tilde{h}_0(\xi)$ are taken from [38] and their coefficients are listed in Table 2.3. The coefficients of the corresponding 2-D filters with frequency responses $H_0^2(\xi_1,\xi_2)$ and $\widetilde{H}_0^2(\xi_1,\xi_2)$ are listed in Table 4.1 and Table 4.2, respectively. Note that the 1-D dual filters $h_0(\xi)$, $\tilde{h}_0(\xi)$ factor in the form

$$h_0(\xi) = \cos^8\left(\frac{\xi}{2}\right)\mathcal{L}(\xi), \qquad \tilde{h}_0(\xi) = \cos^8\left(\frac{\xi}{2}\right)\tilde{\mathcal{L}}(\xi),$$

where $\mathcal{L}$ and $\tilde{\mathcal{L}}$ are polynomials in $\cos(\xi/2)$.

If we take for the function f^2 of Theorem 5, the function

$$f^2(\xi_1,\xi_2) = 1 - \frac{1}{2}\left[\sin^2\left(\frac{\xi_1}{2}\right) + \sin^2\left(\frac{\xi_2}{2}\right)\right],$$

then the Fourier transforms of the dual lowpass filters are

$$H_0^2(\xi_1,\xi_2) = f^8(\xi_1,\xi_2)\mathcal{F}(\xi_1,\xi_2), \qquad \widetilde{H}_0^2(\xi_1,\xi_2) = f^8(\xi_1,\xi_2)\tilde{\mathcal{F}}(\xi_1,\xi_2).$$

Table 4.2: The coefficients $\tilde{\alpha}_{n,m}$ of $\widetilde{H}_0^2(\xi_1, \xi_2)$ for $-13 \leq n, m \leq 13$.

$n\backslash m$	0	±1	±2	±3	±4
0	0.698936045170	0.150510951877	−0.001598281087	−0.000236869135	−0.000185325189
±1	0.150510951877	−0.009415543638	−0.001871916233	0.002125873463	0.000269698445
±2	−0.001598281087	−0.001871916233	0.004172427580	0.000477002410	−0.000749794533
±3	−0.000236869135	0.002125873463	0.000477002410	−0.001155607868	0.000025467329
±4	−0.000185325189	0.000269698445	−0.000749794533	0.000025467329	0.000264956616
±5	0.000047077032	−0.000132003901	−0.000011459812	0.000197393674	−0.000038863029
±6	0.000050880873	−0.000022985785	0.000073699382	−0.000020204701	−0.000033824283
±7	−0.000006656019	0.000004907151	−0.000003116560	−0.000017653665	0.000006692242
±8	−0.000004588285	0.000001790425	−0.000005263473	0.000002682504	0.000001627982
±9	0.000000662104	−0.000000494350	0.000000451757	0.000000723548	−0.000000510474
±10	0.000000163683	−0.000000102701	0.000000217064	−0.000000204190	0.000000000000
±11	−0.000000064181	0.000000039466	−0.000000055688	0.000000000000	0.000000000000
±12	0.000000003289	−0.000000009281	0.000000000000	0.000000000000	0.000000000000
±13	−0.000000000714	0.000000000000	0.000000000000	0.000000000000	0.000000000000

$n\backslash m$	±5	±6	±7	±8	±9
0	0.000047077032	0.000050880873	−0.000006656019	−0.000004588285	0.000000662104
±1	−0.000132003901	−0.000022985785	0.000004907151	0.000001790425	−0.000000494350
±2	−0.000011459812	0.000073699382	−0.000003116560	−0.000005263473	0.000000451757
±3	0.000197393674	−0.000020204701	−0.000017653665	0.000002682504	0.000000723548
±4	−0.000038863029	−0.000033824283	0.000006692242	0.000001627982	−0.000000510474
±5	−0.000041631047	0.000010165480	0.000002604771	−0.000000918854	0.000000000000
±6	0.000010165480	0.000003038900	−0.000001225139	0.000000000000	0.000000000000
±7	0.000002604771	−0.000001225139	0.000000000000	0.000000000000	0.000000000000
±8	−0.000000918854	0.000000000000	0.000000000000	0.000000000000	0.000000000000
±9	0.000000000000	0.000000000000	0.000000000000	0.000000000000	0.000000000000
±10	0.000000000000	0.000000000000	0.000000000000	0.000000000000	0.000000000000
±11	0.000000000000	0.000000000000	0.000000000000	0.000000000000	0.000000000000
±12	0.000000000000	0.000000000000	0.000000000000	0.000000000000	0.000000000000
±13	0.000000000000	0.000000000000	0.000000000000	0.000000000000	0.000000000000

$n\backslash m$	±10	±11	±12	±13
0	0.000000163683	−0.000000064181	0.000000003289	−0.000000000714
±1	−0.000000102701	0.000000039466	−0.000000009281	0.000000000000
±2	0.000000217064	−0.000000055688	0.000000000000	0.000000000000
±3	−0.000000204190	0.000000000000	0.000000000000	0.000000000000
±4	0.000000000000	0.000000000000	0.000000000000	0.000000000000
±5	0.000000000000	0.000000000000	0.000000000000	0.000000000000
±6	0.000000000000	0.000000000000	0.000000000000	0.000000000000
±7	0.000000000000	0.000000000000	0.000000000000	0.000000000000
±8	0.000000000000	0.000000000000	0.000000000000	0.000000000000
±9	0.000000000000	0.000000000000	0.000000000000	0.000000000000
±10	0.000000000000	0.000000000000	0.000000000000	0.000000000000
±11	0.000000000000	0.000000000000	0.000000000000	0.000000000000
±12	0.000000000000	0.000000000000	0.000000000000	0.000000000000
±13	0.000000000000	0.000000000000	0.000000000000	0.000000000000

It is proved in [10] that

$$\prod_{j=1}^{\infty} f^2\big({}^t\boldsymbol{D}^{-j}(\xi_1,\xi_2)\big) \le \frac{c}{1+\|(\xi_1,\xi_2)\|^2}.$$

According to the algorithm of Section 3, we choose the following dual highpass filters:

$$H_1^2(\xi_1,\xi_2) = e^{i\xi_1}\widetilde{H}_0^2(\xi_1+\pi,\xi_2+\pi), \quad \widetilde{H}_1^2(\xi_1,\xi_2) = e^{i\xi_1}H_0^2(\xi_1+\pi,\xi_2+\pi).$$

Six iterations of the cascade algorithm of the previous section are used for the numerical approximation of the dual scaling functions and wavelets $\phi_1(\boldsymbol{x})$, $\tilde{\phi}_1(\boldsymbol{x})$ and $\psi_1(\boldsymbol{x})$, $\tilde{\psi}_1(\boldsymbol{x})$, whose respective graphs are given in Figs. 4.1 to 4.4.

B. Second Example.— This example is the same as the first except that $\widetilde{m}_0(\xi)$ is replaced with the frequency response of a 31-tap filter whose coefficients are given in Table 4.3. The coefficients of the corresponding 2-D dual filter with frquency response $\widetilde{H}_0(\xi_1,\xi_2)$ are given in Table 4.4. The dual scaling function and wavelet, $\tilde{\phi}_2$ and $\tilde{\psi}_2$, are smoother than those of the first example as can be seen in Figs 4.5 and 4.6.

C. Third Example.— The dilation matrix

$$\boldsymbol{D}_2 = \begin{pmatrix} 1 & 3 \\ -1 & -1 \end{pmatrix} \tag{4.42}$$

gives rise to the same sampling lattice as $\boldsymbol{D}_1$. However, by using a result from [26], p. 58, $\boldsymbol{D}_2$ satisfies $\|\boldsymbol{D}_2^{-1}\|_2 \ge \sqrt{2} > 1$. Consequently, the condition $\|\boldsymbol{D}^{-1}\|_2 < 1$ is not satisfied. McClellan's transformation is used with the same 1-D dual filters and transformation function $F(\xi_1,\xi_2)$ as in Example 1. Six iterations of the cascade algorithm have been used to get an approximation to the dual scaling functions $\phi_3(\boldsymbol{x})$, $\tilde{\phi}_3(\boldsymbol{x})$ whose graphs are given in Figs. 4.7 and 4.8. These figures show that the constructed dual scaling functions are not regular, perhaps not even continuous. This is essentially due to the fact that $\|\boldsymbol{D}_2^{-1}\|_2 > 1$. Hence special attention has to be given to condition (??) in choosing the dilation matrix $\boldsymbol{D}$ for the construction of n-D wavelets.

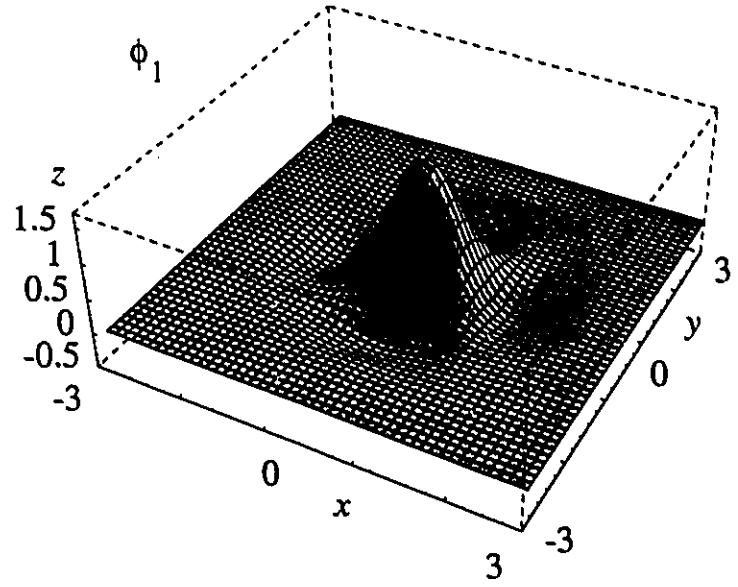

Figure 4.1: Graph of the scaling function $\phi_1(x, y)$.

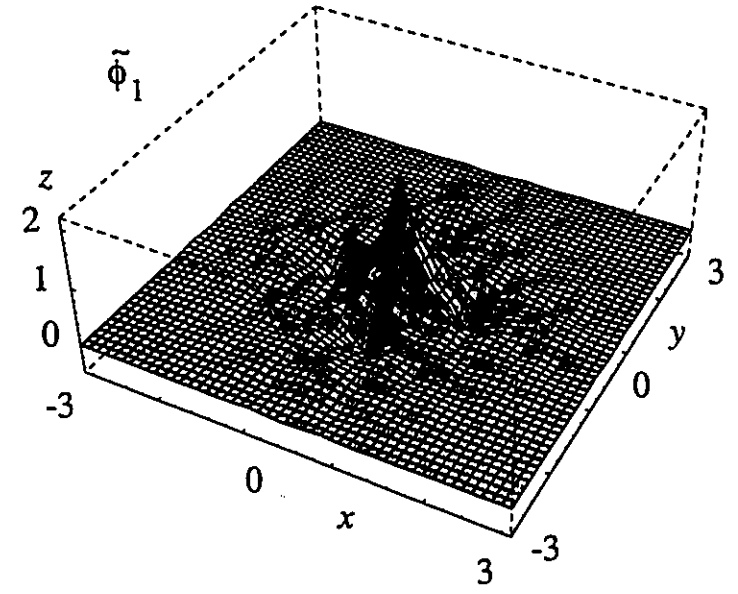

Figure 4.2: Graph of the scaling function $\tilde{\phi}_1(x, y)$.

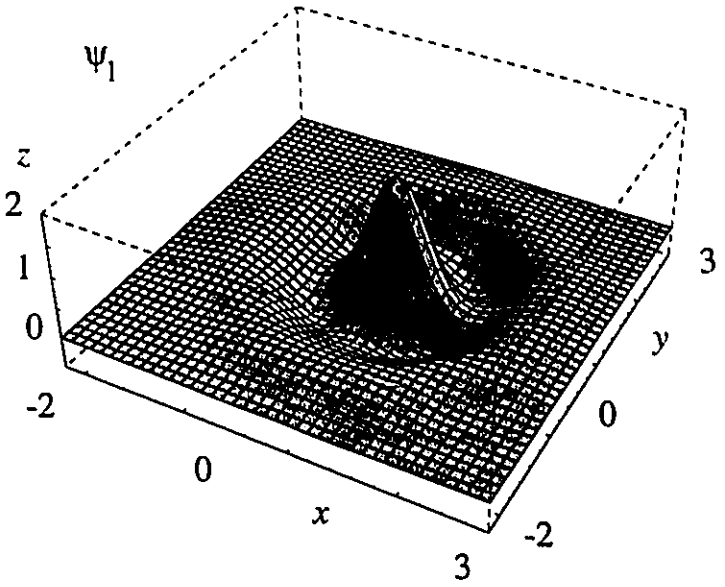

Figure 4.3: Graph of the wavelet $\psi_1(x, y)$.

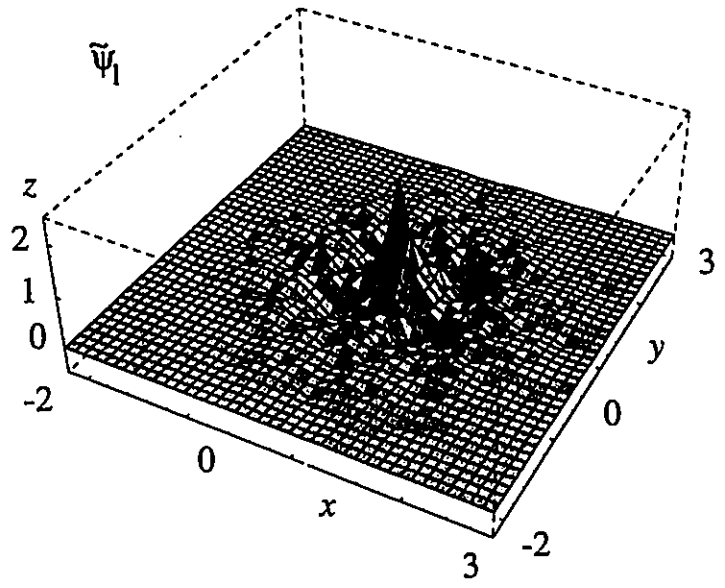

Figure 4.4: Graph of the scaling function $\tilde{\psi}_1(x, y)$.

Table 4.3: The coefficients α_n, $-6 \leq n \leq 6$, of $h_0(\xi)$ and $\tilde{\alpha}_n$, $-15 \leq n \leq 15$, of $\tilde{h}_0(\xi)$.

n	α_n	$\tilde{\alpha}_n$
0	0.5468 7500 0	0.5222 2994 74
±1	0.3320 3125 0	0.2986 6804 40
±2	−0.0039 0625 0	−0.0575 3858 12
±3	−0.0917 9687 5	−0.0981 4466 24
±4	−0.0234 3750 0	0.0753 3283 50
±5	0.0097 6562 5	0.0764 4168 60
±6	0.0039 0625 0	−0.0507 8782 69
±7	0.0000 0000 0	−0.0361 4520 76
±8	0.0000 0000 0	0.0340 5802 49
±9	0.0000 0000 0	0.0097 1072 70
±10	0.0000 0000 0	−0.0161 4736 92
±11	0.0000 0000 0	0.0002 9477 67
±12	0.0000 0000 0	0.0044 6650 04
±13	0.0000 0000 0	−0.0010 3936 83
±14	0.0000 0000 0	−0.0005 2635 86
±15	0.0000 0000 0	0.0002 1416 99

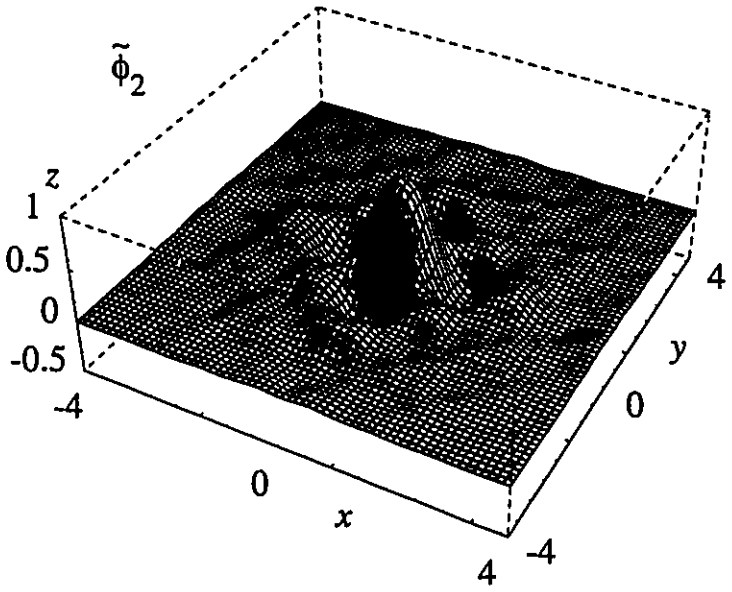

Figure 4.5: Graph of $\tilde{\phi}_2(x, y)$.

Table 4.4: The coefficients $\tilde{\alpha}_{n,m}$ of $\widetilde{H}(\xi_1, \xi_2)$ for $-15 \leq n, m \leq 15$.

$n\backslash m$	0	±1	±2	±3	±4	±5
0	0.618846416473	0.188106179237	0.004452986177	0.010592414066	−0.011140022427	−0.004373300355
±1	0.188106179237	−0.084804967046	−0.063309982419	0.017592664808	0.008086296730	0.002916741418
±2	0.004452986177	−0.063309982419	0.055651802570	0.034391172230	−0.014809003100	−0.006109273992
±3	0.010592414066	0.017592664808	0.034391172230	−0.029381206259	−0.012163926847	0.009487322532
±4	−0.011140022427	0.008086296730	−0.014809003100	−0.012163926847	0.014342392795	0.002227904741
±5	−0.004373300355	0.002916741418	−0.006109273992	0.009487322532	0.002227904741	−0.005132313818
±6	0.002288335003	−0.000593572797	0.001617449336	0.001731371041	−0.003932152409	0.000300393178
±7	0.000760148570	−0.001108572935	0.000865557580	−0.001611881191	0.000081437815	0.000937851670
±8	−0.000301132677	0.000144290316	−0.000144129735	−0.000098241755	0.000529879879	−0.000177309033
±9	−0.000084498592	0.000147450555	−0.000104570703	0.000185477838	−0.000076696742	−0.000064317013
±10	0.000042363565	−0.000036358673	0.000026993046	−0.000014619876	−0.000032158507	0.000019627449
±11	0.000000495516	−0.000006254630	0.000004123277	−0.000011694002	0.000008921567	0.000000000000
±12	−0.000003407239	0.000003546689	−0.000002923500	0.000002973856	0.000000000000	0.000000000000
±13	0.000000951555	−0.000000449769	0.000000686274	0.000000000000	0.000000000000	0.000000000000
±14	−0.000000032126	0.000000098039	0.000000000000	0.000000000000	0.000000000000	0.000000000000
±15	0.000000006536	0.000000000000	0.000000000000	0.000000000000	0.000000000000	0.000000000000

$n\backslash m$	±6	±7	±8	±9	±10	±11
0	0.002288335003	0.000760148570	−0.000301132677	−0.000084498592	0.000042363565	0.000000495516
±1	−0.000593572797	−0.001108572935	0.000144290316	0.000147450555	−0.000036358673	−0.000006254630
±2	0.001617449336	0.000865557580	−0.000144129735	−0.000104570703	0.000026993046	0.000004123277
±3	0.001731371041	−0.001611881191	−0.000098241755	0.000185477838	−0.000014619876	−0.000011694002
±4	−0.003932152409	0.000081437815	0.000529879879	−0.000076696742	−0.000032158507	0.000008921567
±5	0.000300393178	0.000937851670	−0.000177309033	−0.000064317013	0.000019627449	0.000000000000
±6	0.001126318821	−0.000259778055	−0.000096475516	0.000032712414	0.000000000000	0.000000000000
±7	−0.000259778055	−0.000110257737	0.000042058819	0.000000000000	0.000000000000	0.000000000000
±8	−0.000096475516	0.000042058819	0.000000000000	0.000000000000	0.000000000000	0.000000000000
±9	0.000032712414	0.000000000000	0.000000000000	0.000000000000	0.000000000000	0.000000000000
±10	0.000000000000	0.000000000000	0.000000000000	0.000000000000	0.000000000000	0.000000000000
±11	0.000000000000	0.000000000000	0.000000000000	0.000000000000	0.000000000000	0.000000000000
±12	0.000000000000	0.000000000000	0.000000000000	0.000000000000	0.000000000000	0.000000000000
±13	0.000000000000	0.000000000000	0.000000000000	0.000000000000	0.000000000000	0.000000000000
±14	0.000000000000	0.000000000000	0.000000000000	0.000000000000	0.000000000000	0.000000000000
±15	0.000000000000	0.000000000000	0.000000000000	0.000000000000	0.000000000000	0.000000000000

$n\backslash m$	±12	±13	±14	±15
0	−0.000003407239	0.000000951555	−0.000000032126	0.000000006536
±1	0.000003546689	−0.000000449769	0.000000098039	0.000000000000
±2	−0.000002923500	0.000000686274	0.000000000000	0.000000000000
±3	0.000002973856	0.000000000000	0.000000000000	0.000000000000
±4	0.000000000000	0.000000000000	0.000000000000	0.000000000000
±5	0.000000000000	0.000000000000	0.000000000000	0.000000000000
±6	0.000000000000	0.000000000000	0.000000000000	0.000000000000
±7	0.000000000000	0.000000000000	0.000000000000	0.000000000000
±8	0.000000000000	0.000000000000	0.000000000000	0.000000000000
±9	0.000000000000	0.000000000000	0.000000000000	0.000000000000
±10	0.000000000000	0.000000000000	0.000000000000	0.000000000000
±11	0.000000000000	0.000000000000	0.000000000000	0.000000000000
±12	0.000000000000	0.000000000000	0.000000000000	0.000000000000
±13	0.000000000000	0.000000000000	0.000000000000	0.000000000000
±14	0.000000000000	0.000000000000	0.000000000000	0.000000000000
±15	0.000000000000	0.000000000000	0.000000000000	0.000000000000

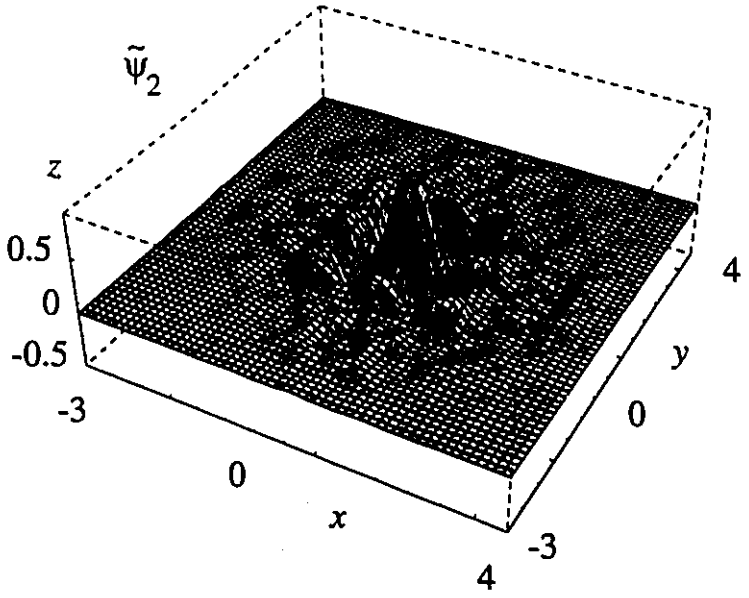

Figure 4.6: Graph of $\tilde{\psi}_2(x, y)$.

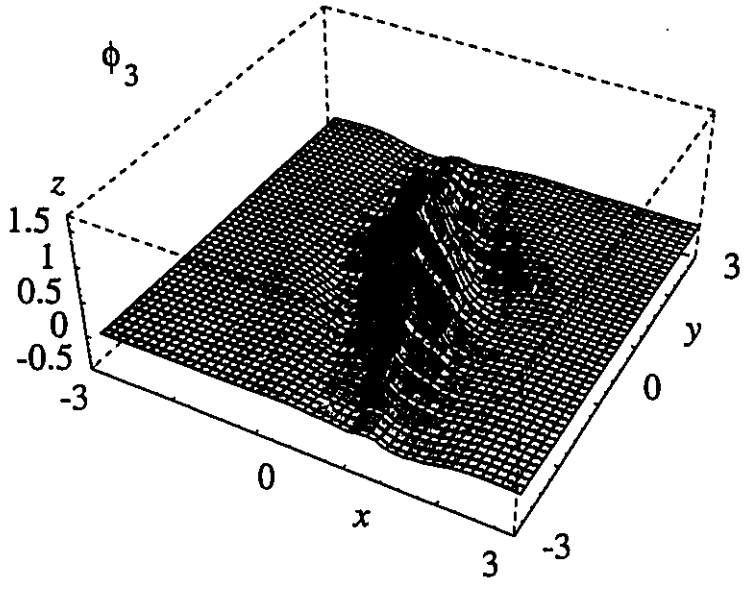

Figure 4.7: Graph of the scaling function $\phi_3(x, y)$.

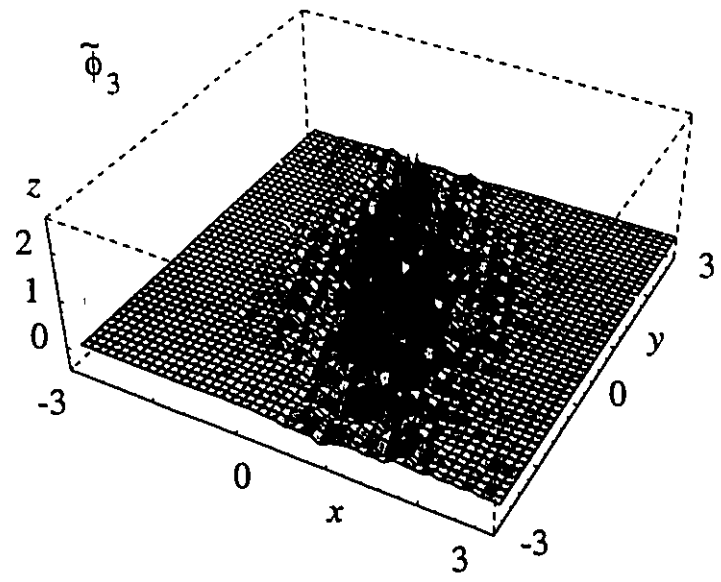

Figure 4.8: Graph of the scaling function $\tilde{\phi}_3(x, y)$.

C. Fourth Example.— In this example, the dilation matrix D is taken to be

$$D = \begin{bmatrix} 1 & 1 \\ 3 & -1 \end{bmatrix},$$

with eigenvalues $\lambda_1 = -2, \quad \lambda_2 = 2$, and $\|D^{-1}\|_2 < 1$. By applying the construction algorithm of Section 3, we find that

$$\eta_0 = (0,0), \qquad \eta_1 = \left(\frac{\pi}{2}, \frac{\pi}{2}\right), \qquad \eta_2 = (\pi, \pi), \qquad \eta_3 = \left(\frac{3\pi}{2}, \frac{3\pi}{2}\right).$$

Consequently, for $\xi_1, \xi_2 \in [0, 2\pi]$, the 2-D lowpass filters $H_0(\xi_1, \xi_2)$, $\widetilde{H}_0(\xi_1, \xi_2)$ have to satisfy the condition

$$H_0(\xi_1, \xi_2)\overline{\widetilde{H}_0(\xi_1, \xi_2)} + H_0\left(\xi_1 + \frac{\pi}{2}, \xi_2 + \frac{\pi}{2}\right)\overline{\widetilde{H}_0\left(\xi_1 + \frac{\pi}{2}, \xi_2 + \frac{\pi}{2}\right)} + H_0(\xi_1 + \pi, \xi_2 + \pi)$$

$$\overline{\widetilde{H}_0(\xi_1 + \pi, \xi_2 + \pi)} + H_0\left(\xi_1 + \frac{3\pi}{2}, \xi_2 + \frac{3\pi}{2}\right)\overline{\widetilde{H}_0\left(\xi_1 + \frac{3\pi}{2}, \xi_2 + \frac{3\pi}{2}\right)} = 1. \quad (4.43)$$

Once these filters are designed, the different highpass filters $H_1(\xi_1, \xi_2)$, $H_2(\xi_1, \xi_2)$ and $H_3(\xi_1, \xi_2)$, together with their duals are to be constructed. The approach taken to solve this problem is first to design symmetric 1-D biorthogonal wavelet filters $h_0(\xi)$

and $\tilde{h}_0(\xi)$ that satisfy the identity

$$h_0(\xi)\overline{\tilde{h}_0(\xi)} + h_0\left(\xi+\frac{\pi}{2}\right)\overline{\tilde{h}_0\left(\xi+\frac{\pi}{2}\right)} + h_0(\xi+\pi)\overline{\tilde{h}_0(\xi+\pi)} + h_0\left(\xi+\frac{3\pi}{2}\right)\overline{\tilde{h}_0\left(\xi+\frac{3\pi}{2}\right)} = 1, \tag{4.44}$$

then by applying the McClellan transformation with the transformation function $F(\xi_1,\xi_2) = \frac{1}{2}(\cos\xi_1 + \cos\xi_2)$, one generates nonseparable 2-D biorthogonal lowpass wavelet filters $H_0(\xi_1,\xi_2)$ and $\widetilde{H}_0(\xi_1,\xi_2)$, satisfying (4.43). The remaining difficult task is to choose the right highpass wavelet filters $H_i(\xi_1,\xi_2)$ and their duals $\widetilde{H}_i(\xi_1,\xi_2)$, $i = 1,2,3$. This problem can be considerably simplified if we assume that the 1-D biorthogonal wavelet filters $h_0(\xi)$, $\tilde{h}_0(\xi)$ factor in the form

$$h_0(\xi) = h(\xi)h(2\xi), \quad \tilde{h}_0(\xi) = \tilde{h}(\xi)\tilde{h}(2\xi), \tag{4.45}$$

where respectively, $h(\xi)$ and $\tilde{h}(\xi)$ are themselves biorthogonal wavelet filters. In this case, one possible choice for the highpass wavelet filters is the following,

$$\begin{aligned}
H_1(\xi_1,\xi_2) &= e^{i\xi_1}\widetilde{H}(\xi_1+\pi,\xi_2+\pi)H(2\xi_1,2\xi_2),\\
H_2(\xi_1,\xi_2) &= e^{2i\xi_1}H(\xi_1,\xi_2)\widetilde{H}(2\xi_1+\pi,2\xi_2+\pi),\\
H_3(\xi_1,\xi_2) &= e^{3i\xi_1}\widetilde{H}(\xi_1+\pi,\xi_2+\pi)\widetilde{H}(2\xi_1+\pi,2\xi_2+\pi),
\end{aligned}$$

where $H(\xi_1,\xi_2)$, $\widetilde{H}(\xi_1,\xi_2)$ are the McClellan transformations of $h(\xi)$ and $\tilde{h}(\xi)$, respectively. Note that similar formulae are used to compute the highpass wavelet filters $\widetilde{H}_i(\xi_1,\xi_2)$, $i = 1,2,3$. The above technique has been used first to compute 1-D biorthogonal wavelet filters $h_0(\xi)$ and $\tilde{h}_0(\xi)$, whose coefficients are given in Table 4.5. Then, the different lowpass and highpass wavelet filters have been computed via the McClellan transformation. The cascade algorithm has been used for the numerical approximation of the analysing and synthetizing scaling functions and wavelets $\phi_4(x)$, $\psi_4^i(x)$, $i = 1,2,3$, and $\tilde{\phi}_4(x)$, $\tilde{\psi}_4^i(x)$, $i = 1,2,3$, whose graphs are given in Figs. 4.9 and 4.10, respectively.

Table 4.5: The coefficients α_n $-9 \leq n \leq 9$, of $h_0(\xi)$ and β_n, $-12 \leq n \leq 12$, of $\tilde{h}_0(\xi)$.

n	α_n	β_n
0	0.3239 7460 9375 0000	0.2513 7417 3755 4881
±1	0.2596 4355 4687 5000	0.2244 9777 1460 1627
±2	0.1552 7343 7500 0000	0.1342 3837 7090 3279
±3	0.0490 7226 5625 0000	0.0473 9241 1665 4829
±4	−0.0395 5078 1250 0000	−0.0225 3310 1483 8100
±5	−0.0476 0742 1875 0000	−0.0360 4762 8103 2089
±6	−0.0302 7343 7500 0000	−0.0057 7671 2717 1035
±7	−0.0140 9912 1093 7500	0.0034 3429 9437 4677
±8	0.0025 6347 6562 5000	0.0203 6146 6841 2642
±9	0.0029 9072 2656 2500	0.0119 9561 5052 7827
±10	0.0000 0000 0000 0000	−0.0034 6166 4373 2244
±11	0.0000 0000 0000 0000	−0.0012 7246 9512 6872
±12	0.0000 0000 0000 0000	0.0014 8454 7764 8017

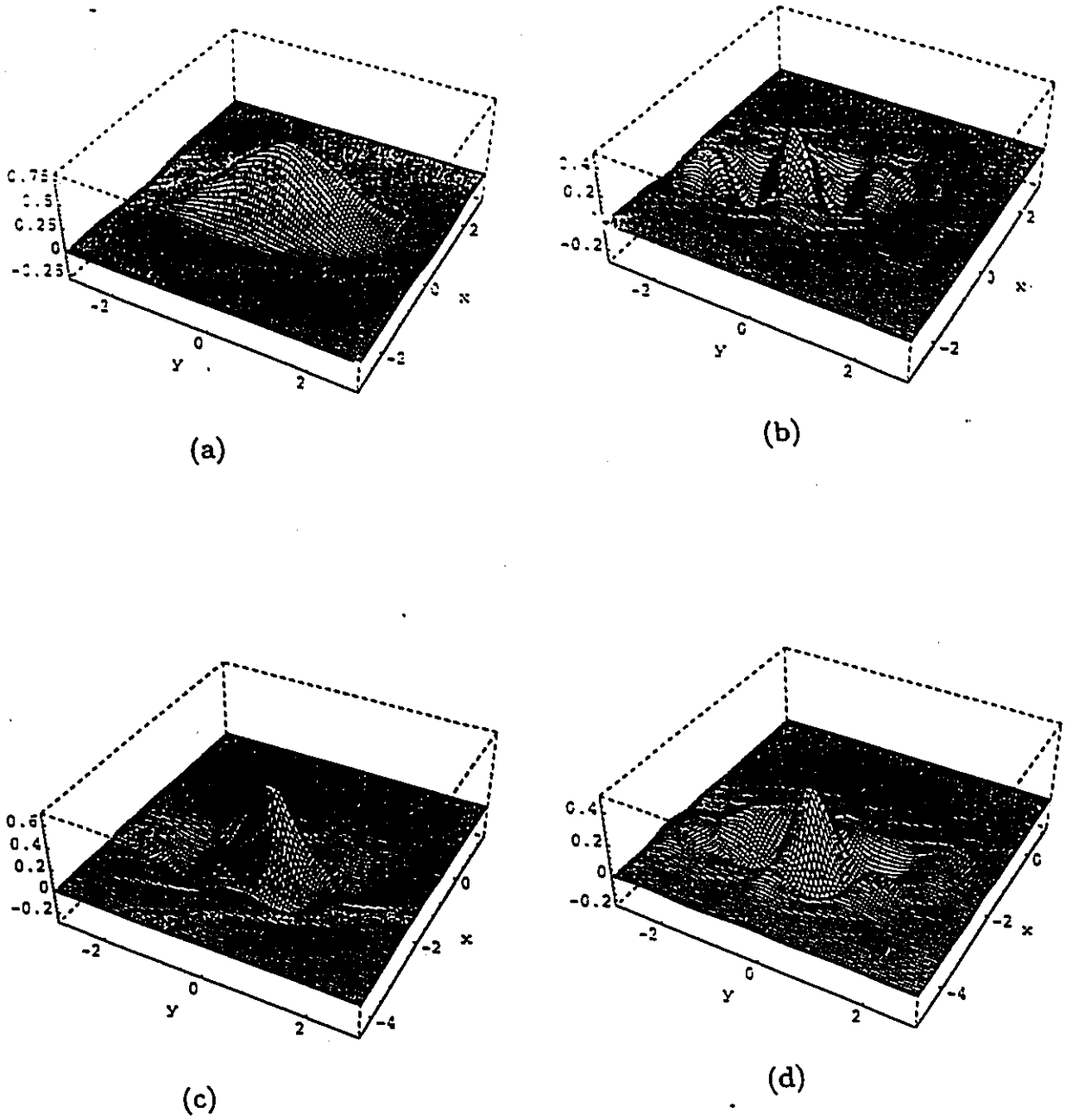

Figure 4.9: (a) graph of $\phi_4(x,y)$, (b) graph of $\psi_4^1(x,y)$, (c) graph of $\psi_4^2(x,y)$, (d) graph of $\psi_4^3(x,y)$.

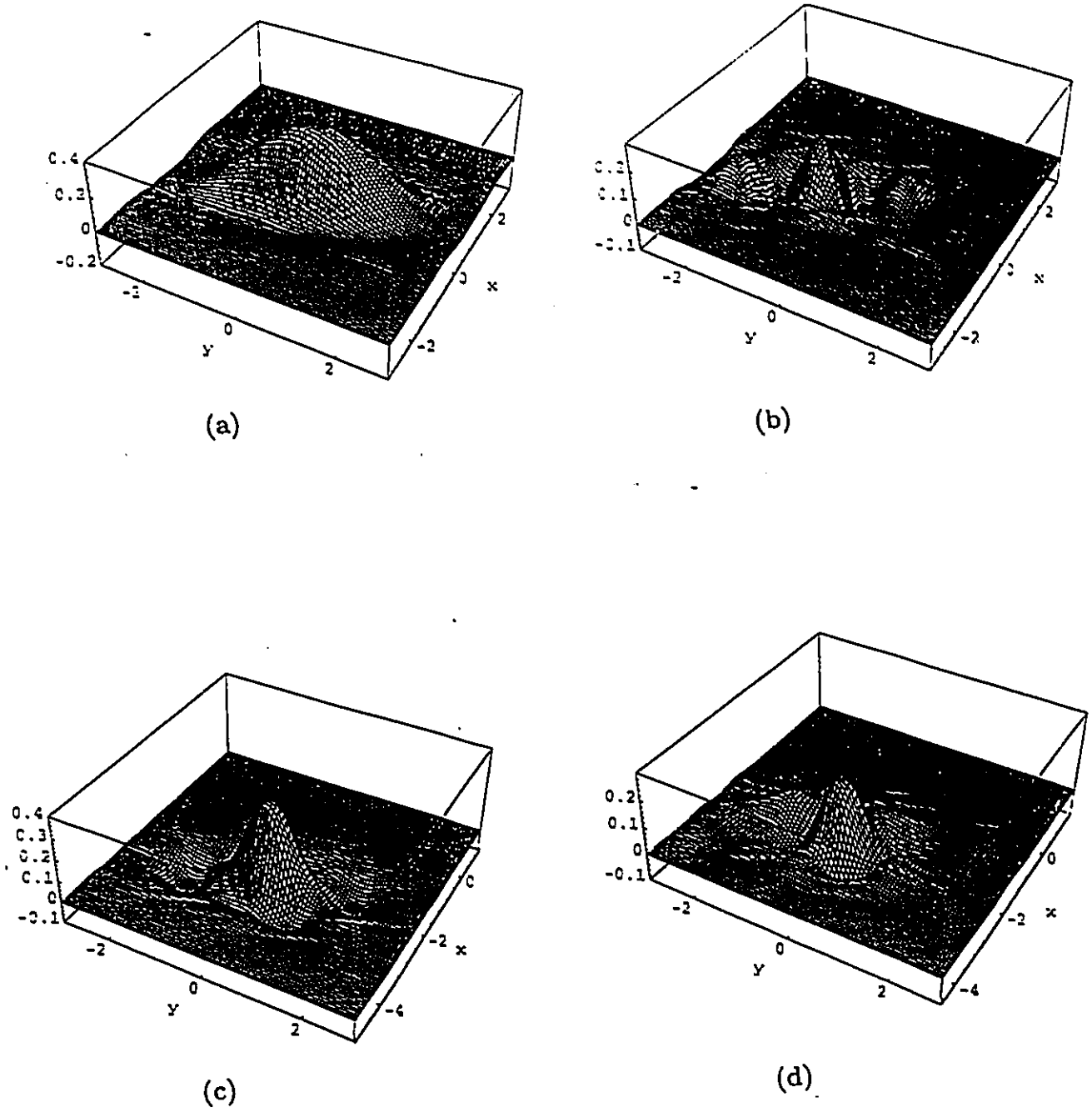

Figure 4.10: (a) graph of $\tilde{\phi}_4(x,y)$, (b) graph of $\tilde{\psi}_4^1(x,y)$, (c) graph of $\tilde{\psi}_4^2(x,y)$, (d) graph of $\tilde{\psi}_4^3(x,y)$.

Chapter 5

Fast 1-D and 2-D Discrete Biorthogonal Wavelet Transforms

Discrete wavelet transform (DWT) (see [58], [5], [3]) and discrete biorthogonal wavelet transform (DBWT) are closely related to subband coding (see [11], [15]). They are efficient practical tools for digital signal processing and are applied to sound analysis (see [43], [69]), image compression (see [20], [3]), and computer vision (see [47], [25]).

In DWT, the scaled translated mother wavelet $\psi(x)$ and scaling function $\phi(x)$,

$$\psi_{jk}(x) = 2^{-j/2}\psi(2^{-j}x - k), \quad \phi_{jk}(x) = 2^{-j/2}\phi(2^{-j}x - k), \qquad j, k \in \mathbb{Z},$$

form an orthonormal family in $L^2(\mathbb{R})$. It will be assumed that ϕ comes from a multiresolution analysis of $L^2(\mathbb{R})$, (see [46], [47], [51]).

For the reader's convenience, we briefly recall that a multiresolution analysis of $L^2(\mathbb{R})$ is a decreasing sequence of closed linear subspaces of $L^2(\mathbb{R})$,

$$\cdots \subset V_2 \subset V_1 \subset V_0 \subset V_{-1} \subset V_{-2} \subset \cdots, \tag{5.1}$$

with the following properties:

($P1$) $\bigcup_{-\infty}^{\infty} V_j$ is dense in $L^2(\mathbb{R})$ and $\bigcap_{-\infty}^{\infty} V_j = \{0\}$;

($P2$) $\forall\, j \in \mathbb{Z}, \quad f(x) \in V_{j+1} \Longleftrightarrow f(2x) \in V_j$;

($P3$) $\exists\, \Phi \in V_0 \subset L^2(\mathbb{R})$ such that $\forall n \in \mathbb{Z}$, $\Phi_{0,n}(x) = \phi(x - n)$ is an orthonormal basis of V_0.

Let W_j denote the orthogonal complement of V_j in V_{j-1}. Then the families ϕ_{jk} and ψ_{jk} form orthonormal bases of V_j and W_j, respectively, for all $k \in \mathbb{Z}$.

An n-D multiresolution analysis with dilation matrix $\boldsymbol{D} \in \mathbb{Z}^{n\times n}$ is a generalization to $L^2(\mathbb{R}^n)$ of the 1-D case (see [40]).

Let $\phi, \tilde{\phi}$ and $\psi, \tilde{\psi}$ be dual scaling functions and dual mother wavelets, respectively. In DBWT, the two scaled and translates paires of functions

$$\left\{\phi_{jk}(x), \tilde{\phi}_{jk}(x)\right\}, \qquad \left\{\psi_{jk}(x), \tilde{\psi}_{jk}(x)\right\} \qquad j,k \in \mathbb{Z}, \tag{5.2}$$

form dual $L^2(\mathbb{R})$ bases. In this case, every $f \in L^2(\mathbb{R})$ has the wavelet expansions

$$f(x) = \sum_{j\in\mathbb{Z}}\sum_{k\in\mathbb{Z}} < f, \psi_{jk} > \tilde{\psi}_{jk}(x) = \sum_{j\in\mathbb{Z}}\sum_{k\in\mathbb{Z}} < f, \tilde{\psi}_{jk} > \psi_{jk}(x). \tag{5.3}$$

where $< \cdot, \cdot >$ denotes the L^2 scalar product,

$$< f, g >= \int_{-\infty}^{\infty} f(x)\overline{g(x)}\, dx \qquad f, g \in L^2(\mathbb{R}). \tag{5.4}$$

DWT has been extensively studied (see [5], [16], [58]), but only a few papers have dealt with DBWT (see [11], [3]).

DBWT possesses many attractive features absent from DWT. For example, flexibility in choosing the analysing and synthetezing wavelets and use of nonseparable compactly supported 2-D wavelets. Practical compactly-supported nonseparable 2-D wavelet bases have been designed for DBWT, but to our knowledge, none for DWT. For these reasons, in this chapter we are essentially concerned with 1-D and 2-D DBWT's.

Since, the efficiency of DBWT depends critically on the choice of the biorthogonal wavelets, we shall review the design of appropriate 1-D and nonseparable 2-D biorthogonal wavelets.

In this chapter, we assume that all 1-D and 2-D signals (to be analysed and synthetized) are supported on the interval $[0, 1]$ and the square $[0, 1] \times [0, 1]$, respectively. Moreover, all wavelets will be real, symmetric and compactly supported; in other terms, the wavelet filters are real and finite in length, that is, FIR filters.

In Section 5.1, we briefly review the 1-D DWT and DBWT and describe the general 2-D DBWT. Section 5.2 is devoted to the design of appropriate 1-D and 2-D biorthogonal wavelets and the derivation of a 2-D quatrature formula to accelerate the DBWT algorithm. Finally, in Section 5.3, the efficiency of the proposed algorithms is illustrated by means of a numerical example.

5.1 Wavelet Transforms

5.1.1 1-D DWT

We briefly review DWT. Given a signal $f(t) \in L^2(\mathbb{R})$ supported on $[0,1]$, the orthonormal wavelet transform of f can be described as successive computations of coarse approximations of f and the details which constitute the difference of information between two successive approximation levels. In the language of multiresolution analysis, the jth coarse approximation is the projection of the signal on V_j, and the details are the projection on W_j.

First, the signal is identified with its projection on some subspace, V_{-N}, of the multiresolution analysis. If the scaling function $\phi(t)$ is supported on $[m_1, m_2]$, then

$$f(t) \approx \sum_{k=-m_2}^{2^N-m_1} s_k^0 \phi(2^N t - k), \tag{5.5}$$

where the coefficients s_k^0 are given by the scalar products

$$s_k^0 = < f, \phi_{-N,k} > = 2^{N/2} \int_{-\infty}^{\infty} f(x)\overline{\phi(2^N x - k)}\, dx. \tag{5.6}$$

Let $N_0 \geq j > 0$ be the number of iterations used by the algorithm. If T_j and D_j are the projections operators on V_{j-N} and W_{j-N}, respectively, then

$$T_j f(t) = \sum_{k=-m_2}^{2^{N-j}-m_1} s_k^j \phi_{j-N,k}(t), \tag{5.7}$$

$$D_j f(t) = \sum_{k=-n_2}^{2^{N-j}-n_1} d_k^j \psi_{j-N,k}(t), \tag{5.8}$$

where the mother wavelet, $\psi(t)$ is supported on $[n_1, n_2]$ and the coefficients s_k^j and d_k^j are given by the scalar products

$$s_k^j =< f, \phi_{j-N,k} >, \qquad d_k^j =< f, \psi_{j-N,k} > .$$

Since $V_j \oplus W_j = V_{j-1}$, then $T_{j-1}f = (T_j + D_j)\, f$ or, equivalently,

$$\sum_k s_k^j \phi_{j-N,k}(t) + d_k^j \psi_{j-N,k}(t) = \sum_k s_k^{j-1} \phi_{j-1-N,k}(t). \tag{5.9}$$

An interesting property of wavelet transform is that the coefficients s_k^j and d_k^j are easily computed recursively from the coefficients s_n^{j-1}, $n \in \mathbf{Z}$, as follows:

$$s_k^j = \sum_{n=2k-m_2}^{2k-m_1} h_{n-2k} s_n^{j-1}, \qquad d_k^j = \sum_{n=2k+m_1-1}^{2k+m_2-1} g_{n-2k} s_n^{j-1}, \tag{5.10}$$

where, for $m_1 \leq n \leq m_2$, h_n and $g_n = (-1)^{n+1} h_{1-n}$ are the coefficients of the lowpass and highpass waveletfilter, respectively. Conversely, finer approximations of the signal are recovered by the repeated application of the following formulae

$$s_k^{j-1} = \sum_n h_{k-2n} s_n^j + \sum_n h_{k-2n} d_n^j, \quad k = -m_2, 2^{N-j+1} - m_1. \tag{5.11}$$

Thus, we have

$$f(t) \approx \sum_{k=-m_2}^{2^N - m_1} s_k^0 \phi_{-N,k}(t). \tag{5.12}$$

5.1.2 1-D DBWT

For DBWT, the dual pairs of functions (5.2) are used. We assume that

$$\text{supp}\phi \subset [m_1, m_2], \qquad \text{supp}\tilde{\phi} \subset [\tilde{m}_1, \tilde{m}_2],$$

$$\text{supp}\psi \subset [n_1, n_2], \qquad \text{supp}\tilde{\psi} \subset [\tilde{n}_1, \tilde{n}_2].$$

Moreover, we assume that the signal $f(t)$ is analysed by means of the pair $\phi_{j,k}$, $\psi_{j,k}$ and synthetize by means of the pair $\tilde{\phi}_{j,k}$, $\tilde{\psi}_{j,k}$. As for DWT, the DBWT algorithm

first identifies the signal with its projection on some subspace of the biorthogonal multiresolution analysis. More precisely,

$$f(t) \approx \sum_{k=-m_2}^{2^N-m_1} < f, \phi_{-N,k} > \tilde{\phi}_{-N,k}(t). \tag{5.13}$$

For $N_0 \geq j > 0$, let $\tilde{T}_j$ and $\tilde{D}_j$ denote the projection operators on the subspaces $\tilde{V}_{j-N}$ and $\tilde{W}_{j-N}$, respectively, of the biorthogonal multiresolution analysis. Then

$$T_j f(t) = \sum_{k=-m_2}^{2^{N-j}-m_1} s_k^j \tilde{\phi}_{j-N,k}(t), \tag{5.14}$$

$$D_j f(t) = \sum_{k=-n_2}^{2^{N-j}-n_1} d_k^j \tilde{\psi}_{j-N,k}(t). \tag{5.15}$$

If $\{h_n\}_n$, $\{\tilde{h}_n\}_n$ denote the dual lowpass filters and $g_n = (-1)^{n+1}\tilde{h}_{1-n}$, $\tilde{g}_n = (-1)^{n+1}h_{1-n}$ the highpass filters, then for DBWT, the coefficients s_k^j and d_k^j are computed recursively by the formulae:

$$s_k^j = \sum_{n=2k-m_2}^{2k-m_1} h_{n-2k} s_n^{j-1}, \qquad d_k^j = \sum_{n=2k+m_1-1}^{2k+m_2-1} g_{n-2k} s_n^{j-1}. \tag{5.16}$$

Finally, finer approximations of the signal are recovered by repeated applications of the formula

$$\tilde{s}_k^{j-1} = \sum_n \tilde{h}_{k-2n} s_n^j + \sum_n \tilde{g}_{k-2n} d_n^j, \qquad k = -m_2, 2^{N-j} - m_1. \tag{5.17}$$

We thus have

$$f(t) \approx \sum_{-\tilde{m}_2}^{2^N-\tilde{m}_1} \tilde{s}_k^0 \tilde{\phi}_{-N,k}(t). \tag{5.18}$$

5.1.3 2-D DBWT

We assume that the 2-D dual scaling functions and wavelets are derived from a 2-D biorthogonal multiresolution analysis with a dilation matrix $\boldsymbol{D} \in \mathbb{Z}^2$. Henceforth, we shall use the following notation:

$$t = (t_1, t_2) \in \mathbb{R}^2, \qquad k = (k_1, k_2) \in \mathbb{Z}^2, \qquad n = (n_1, n_2) \in \mathbb{Z}^2.$$

We note that if $|\det \boldsymbol{D}| = d$, then one scaling function $\Phi(\boldsymbol{x})$ and $d-1$ mother wavelets $\Psi^i(\boldsymbol{x})$, $i = 1, \ldots, d-1$ are needed to generate an orthonormal wavelet basis of $L^2(\mathbb{R}^2)$ [29]. For the biorthogonal case, one family of dual mother scaling function $\Phi(\boldsymbol{x})$, $\tilde{\Phi}(\boldsymbol{x})$ and $d-1$ families of dual mother wavelets $\Psi^i(\boldsymbol{x})$, $\tilde{\Psi}^i(\boldsymbol{x})$, $i = 1, \ldots, d-1$ are needed to generate a wavelet basis of $L^2(\mathbb{R}^2)$. The construction of these dual functions is the subject of the next section. We define

$$\Phi_{j,k}(t) = |\det \boldsymbol{D}|^{-j/2} \Phi(\boldsymbol{D}^{-j}t - k), \tag{5.19}$$

$$\Psi^i_{j,k}(t) = |\det \boldsymbol{D}|^{-j/2} \Psi^i(\boldsymbol{D}^{-j}t - k), \quad i = 1, \ldots, d-1. \tag{5.20}$$

The scaling functions and wavelets $\tilde{\Phi}_{j,k}(t)$, $\tilde{\Psi}^i_{j,k}(t)$, $i = 1, \ldots, d-1$, are defined in a similar way.

We assume that $\mathrm{supp}\Phi \subset [m_1, m_2]^2$, $\mathrm{supp}\tilde{\Phi} \subset [\tilde{m}_1, \tilde{m}_2]^2$, $\mathrm{supp}\Psi^i_{j,k} \subset [n^i_1, n^i_2]^2$ and $\mathrm{supp}\tilde{\Psi}^i_{j,k} \subset [\tilde{n}^i_1, \tilde{n}^i_2]^2$.

The general 2-D DBWT is described as follows. As in the 1-D case, the first step is to identify the given 2-D signal $f(t)$ with its projection on some subspace $\tilde{V}_{-N}$ of the 2-D biorthogonal multiresolution analysis described above. This projection, which is the finest approximation to the signal, can be defined by

$$T_0 f(t) = \sum_k s^0_k \tilde{\Phi}_{-N,k}(t), \quad k \in \mathbb{Z}^2 \cap \boldsymbol{D}^N[0,1]^2 + [-m_2, -m_1]^2, \tag{5.21}$$

where

$$s^0_k = < f, \Phi_{-N,k} > = |\det \boldsymbol{D}|^{N/2} \int f(t)\Phi(D^N t - k)\, dt. \tag{5.22}$$

Then for a positive integer $N_0 \geq j > 0$, the different projections of the signal on the spaces $\tilde{V}_{j-N}$, $\tilde{W}^i_{j-N}$ are given by

$$T_j f(t) = \sum_k s^j_k \tilde{\Phi}_{j-N,k}(t), \; k \in \mathbb{Z}^2 \cap \boldsymbol{D}^{N-j}[0,1]^2 + [-m_2, -m_1]^2, \tag{5.23}$$

$$D^i_j f(t) = \sum_k d^i_{j,k} \tilde{\Psi}^i_{j-N,k}(t), \; k \in \mathbb{Z}^2 \cap \boldsymbol{D}^{N-j}[0,1]^2 + [-n^i_2, -n^i_1]^2, \tag{5.24}$$

respectively, where

$$s_k^j =< f, \Phi_{j-N,k} >, \qquad d_{j,k}^i =< f, \Psi_{j-N,k}^i > . \tag{5.25}$$

If $\{H_n\}_n$, $\{\widetilde{H}_n\}_n$, $\{G_n^i\}_n$, $\{\widetilde{G}_n^i\}_n$ denote the dual lowpass and highpass 2-D wavelet filters, respectively, then the wavelet coefficients are recursively computed by the formulae:

$$s_k^j = \sum_n H_{n-Dk} s_n^{j-1}, \quad k \in \mathbb{Z}^2 \cap \boldsymbol{D}^{N-j}[0,1]^2 + [-m_2, -m_1]^2, \tag{5.26}$$

$$d_{j,k}^i = \sum_n G_{n-Dk} s_n^{j-1}, \quad k \in \mathbb{Z}^2 \cap \boldsymbol{D}^{N-j}[0,1]^2 + [-n_2^i, -n_1^i]^2. \tag{5.27}$$

Finally, to reconstruct the signal, the computation of the coefficients of the finest approximation of $f(t)$ is needed. This can be done simply by iterating the following formula,

$$\begin{aligned} \tilde{s}_k^{j-1} &= \sum_n \widetilde{H}_{k-Dn} s_n^j + \sum_n \sum_{i=1}^{d-1} \widetilde{G}_{k-Dn}^i d_{j,n}^i, \\ & \qquad k \in \mathbb{Z}^2 \cap \boldsymbol{D}^{N-j+1}[0,1]^2 + [-m_2, -m_1]^2. \end{aligned} \tag{5.28}$$

This allows us to reconstruct the signal $f(t)$ as follows:

$$f(t) \approx \sum_k \tilde{s}_k^0 \tilde{\Phi}_{-N,k}, \quad k \in \mathbb{Z}^2 \cap \boldsymbol{D}^N[0,1]^2 + [-m_2, -m_1]^2. \tag{5.29}$$

The proof of (5.26) and (5.27) goes as follows. By (5.25), we have

$$\begin{aligned} s_k^j &= |\det \boldsymbol{D}|^{(N-j)/2} \int f(t) \Phi(\boldsymbol{D}^{N-j} t - k) dt, \\ &= |\det \boldsymbol{D}|^{(N-j)/2} \int f(t) \Phi(\boldsymbol{D}^{-1}(\boldsymbol{D}^{N-j+1} t - \boldsymbol{D}k)) dt. \end{aligned}$$

Since the scaling function Φ satisfies

$$\Phi(t) = \sum_n \alpha_n \Phi(\boldsymbol{D}t - n), \tag{5.30}$$

then

$$\Phi(\boldsymbol{D}^{-1}t) = \sum_n \alpha_n \Phi(t - n), \tag{5.31}$$

and, consequently,

$$\begin{aligned} s_k^j &= |\det \boldsymbol{D}|^{-1/2} \int f(t) \sum a_{n-\boldsymbol{D}k} |\det \boldsymbol{D}|^{\frac{N-j+1}{2}} \Phi(\boldsymbol{D}^{N-j+1}t - n)dt, \\ &= \sum H_{n-\boldsymbol{D}k} s_k^{j-1}. \end{aligned}$$

Since $\mathrm{supp}\Phi \subset [m_1, m_2]^2$ and $\mathrm{supp}f \subset [0,1]^2$, then obviously in (5.26) we have

$$\boldsymbol{k} \in \mathbb{Z}^2 \cap \boldsymbol{D}^{N-j}[0,1]^2 + [-m_2, -m_1]^2.$$

We can prove (5.27) in a similar way.

The proof of (5.28) is straightforward. In fact, by (5.25),

$$\tilde{s}_k^{j-1} =< \Phi_{-N-1+j,k}, f > . \tag{5.32}$$

Since $\Phi_{-N-1+j,k} \in V_{j-1-N}$ and $V_{j-1-N} = V_{j-N} + W_{j-N}$, then

$$\begin{aligned} \Phi_{-N-1+j,k}(t) &= \sum_n < \Phi_{-N-1+j,k}, \tilde{\Phi}_{-N+j,n} > \tilde{\Phi}_{-N+j,n}(t) \\ &+ \sum_{i=1}^{d} \sum_n < \Phi_{-N-1+j,k}, \tilde{\Psi}^i_{-N+j,n} > \tilde{\Psi}^i_{-N+j,n}(t). \end{aligned}$$

Using (5.30), i.e.,

$$\tilde{\Phi}(t) = \sum_m \tilde{\alpha}_m \tilde{\Phi}(\boldsymbol{D}t - m), \tag{5.33}$$

one concludes that

$$\tilde{\Phi}_{j-N,n}(t) = \sum_m \tilde{\alpha}_{m-\boldsymbol{D}n} \tilde{\Phi}(\boldsymbol{D}^{N-j+1}t - m). \tag{5.34}$$

Similarly, there exist real sequences $\{\tilde{\beta}^i_m\}$ such that

$$\tilde{\Psi}^i_{j-N,n}(t) = \sum_m \tilde{\beta}^i_{m-\boldsymbol{D}n} \tilde{\Phi}(\boldsymbol{D}^{N-j+1}t - m). \tag{5.35}$$

Since, by hypothesis, the families $\{\Phi_{j,k}\}_{j,k}$ and $\{\tilde{\Phi}_{j,k}\}_{j,k}$ form a biorthogonal system, then

$$< \Phi_{j,k}, \tilde{\Phi}_{j',k'} >= \delta_{jj'}\delta_{kk'}. \tag{5.36}$$

Hence, by combining (5.34), (5.35) and (5.36), one can easily see that

$$\begin{aligned} \tilde{s}_k^{j-1} &= < \Phi_{-N-1+j,k}, f > \\ &= \sum_n \widetilde{H}_{k-Dn} s_n^j + \sum_n \sum_{i=1}^{d-1} \tilde{G}_{k-Dn}^i d_{j,n}^i. \end{aligned}$$

Remark 12 In the interesting case, where the dilation matrix satisfies $d = |\det \boldsymbol{D}| = 2$, only one family of dual wavelets is needed, in the 2-D biorthogonal wavelet transform algorithm. This leads to a reduced number of operations per iteration.

Remark 13 It is clear that the whole DBWT algorithm is based on the computation of the coefficients (5.22). In practice, this cannot be done analytically and, consequently, a quadrature formula has to be used for this purpose. In the next section, we shall construct a one-point quadrature formula which approximates well the coefficients s_k^0 and accelerates the 1-D and 2-D DBWT.

Remark 14 For practical reasons, it is desirable that only the numerically significant wavelet coefficients $d_{j,n}^i$ be computed, while the sufficiently small ones be set to zero. In the next section, we shall design biorthogonal wavelet filters with fast decaying coefficients suitable for compression purposes.

5.2 Fast DBWT

The efficiency of the DBWT algorithm depends critically on the choice of the biorthogonal wavelets or equivalently on the dual wavelet filters. As it will be seen in this section, this choice has to take the following three main considerations into account.

(a) The biorthogonal wavelet filters have to be designed in such a way that they automatically generate a one-point quadrature formula to be used in the computation of the coefficients of the finest approximation of the signal $f(t)$. This is extremely important for a fast wavelet transform algorithm.

(b) The analysing wavelets have to have a reasonably high number of vanishing moments. This condition is necessary for the achievement of a considerable signal compression ratio.

(c) The biorthogonal wavelet filters have to be as short as possible in order to reduce as much as possible the number of multiplications and additions required by the DBWT algorithm.

5.2.1 Wavelet-based quadrature

We shall follow the idea used in [5] for designing a one-point quadrature formula to approximate s_k^0 in the 1-D case and generalize it to the 2-D case with general dilation matrix $\boldsymbol{D}$. In [5], it is proved that if the first $M-1$ shifted moments of the scaling function $\phi(t)$ are equal to zero, that is, for some constant τ_M, we have

$$\int \phi(x+\tau_M)x^m dx = 0, \qquad m = 1, \ldots, M-1, \tag{5.37}$$

then

$$\begin{aligned} s_k^0 &= 2^{N/2} \int f(x)\phi(2^N x - k)\, dx, \\ &= 2^{-N/2} f\left(2^{-N}(k+\tau_M)\right) + O\left(2^{-N(M+(1/2))}\right). \end{aligned} \tag{5.38}$$

In our 2-D case, the shift constant is simply taken to be the constant vector $(0,0)$, the dilation factor 2 is replaced with an arbitrary dilation matrix $\boldsymbol{D}$ in $\mathbb{Z}^{2\times 2}$. The generalized one-point quadrature formula is then given by the following proposition.

Proposition 4 *Assume that $f \in C^{M-1}([0,1]^2)$ and that the derivatives*

$$\frac{\partial^M f(t)}{\partial t_1^{M-j} \partial t_2^j}, \qquad j = 0, \ldots, M,$$

are bounded on $[0,1]^2$. Moreover, assume that the scaling function $\Phi(t)$ satisfies

$$\int t_1^{m_1} t_2^{m_2} \Phi(t_1, t_2) dt_1 dt_2 = 0, \qquad 1 \le m_1 + m_2 \le M,\ m_1, m_2 \ge 0. \tag{5.39}$$

Then we have the one-point quadrature formula

$$\begin{aligned} s_k^0 &= |\det \boldsymbol{D}|^{N/2} \int f(t)\Phi(\boldsymbol{D}^N t - k)\, dt, \\ &= |\det \boldsymbol{D}|^{-N/2} f\left(\boldsymbol{D}^{-N}\boldsymbol{k}\right) + O\left(|\det \boldsymbol{D}|^{-N/2}\|\boldsymbol{D}^{-1}\|_2^{NM}\right). \end{aligned} \tag{5.40}$$

Proof: The proof is based on the 2-D version of the Taylor expansion and is carried out as follows:

$$\begin{aligned} s_k^0 &= |\det \boldsymbol{D}|^{N/2} \int f(\boldsymbol{t})\Phi\left(\boldsymbol{D}^N\boldsymbol{t} - k\right) d\boldsymbol{t}, \\ &= |\det \boldsymbol{D}|^{N/2} \int f\left(\boldsymbol{t} + \boldsymbol{D}^{-N}\boldsymbol{k}\right)\Phi\left(\boldsymbol{D}^N\boldsymbol{t}\right) d\boldsymbol{t}. \end{aligned}$$

Since the partial derivatives of $f(\boldsymbol{t})$ of order less than or equal to $M-1$ are continuous over $[0,1]^2$, the 2-D version of the Taylor expansion of $f\left(\boldsymbol{t}+\boldsymbol{D}^{-N}\boldsymbol{k}\right)$ about $\boldsymbol{D}^{-N}\boldsymbol{k}$ gives us

$$\begin{aligned} s_k^0 &= |\det \boldsymbol{D}|^{N/2} \int \left[f\left(\boldsymbol{D}^{-N}\boldsymbol{k}\right) + \sum_{i=1}^{M-1} \frac{1}{i!} \sum_{j=0}^{i} \binom{i}{j} t^{(i-j,j)} \frac{\partial^i f\left(\boldsymbol{D}^{-N}\boldsymbol{k}\right)}{\partial t_1^{i-j}\partial t_2^j} \right] \Phi\left(\boldsymbol{D}^N\boldsymbol{t}\right) d\boldsymbol{t} \\ &\quad + \frac{|\det \boldsymbol{D}|^{N/2}}{M!} \int \sum_{j=0}^{M} \binom{M}{j} t^{(M-j,j)} \frac{\partial^M f\left(\boldsymbol{D}^{-N}\boldsymbol{\xi}(t)\right)}{\partial t_1^{M-j}\partial t_2^j} \Phi\left(\boldsymbol{D}^N\boldsymbol{t}\right) d\boldsymbol{t} \\ &= |\det \boldsymbol{D}|^{-N/2} \Bigg[\int f(\boldsymbol{D}^{-N}\boldsymbol{k})\Phi(\boldsymbol{t})\, d\boldsymbol{t} \\ &\quad + \sum_{i=1}^{M-1} \int \frac{1}{i!} \sum_{j=0}^{i} \binom{i}{j} \left(\boldsymbol{D}^{-N}\boldsymbol{t}\right)^{(i-j,j)} \frac{\partial^i f\left(\boldsymbol{D}^{-N}\boldsymbol{k}\right)}{\partial t_1^{i-j}\partial t_2^j} \Phi(\boldsymbol{t})\, d\boldsymbol{t} \Bigg] \\ &\quad + \frac{|\det \boldsymbol{D}|^{-N/2}}{M!} \int \sum_{j=0}^{M} \binom{M}{j} \left(\boldsymbol{D}^{-N}\boldsymbol{t}\right)^{(M-j,j)} \frac{\partial^i f\left(\boldsymbol{D}^{-N}\boldsymbol{\xi}(t)\right)}{\partial t_1^{M-j}\partial t_2^j} \Phi(\boldsymbol{t})\, d\boldsymbol{t}, \end{aligned}$$

where $(t_1,t_2)^{(i,j)} = t_1^i t_2^j$. Since, for $t_1, t_2 \in \mathbb{R}$, we have

$$\left|t_1^i\, t_2^j\right| \le \|(t_1,t_2)\|_2^{i+j}; \tag{5.41}$$

then, it is easy to see that

$$\left|(\boldsymbol{D}^{-N}\boldsymbol{t})^{(M-j,j)}\right| \le \|\boldsymbol{D}^{-N}\boldsymbol{t}\|_2^M \le \|\boldsymbol{D}^{-1}\|_2^{NM}\|\boldsymbol{t}\|_2^M \tag{5.42}$$

Since the first $M-1$ moments of $f(t)$ are zero, then for $i = 1, \cdots, M-1$,

$$|\det \boldsymbol{D}|^{-N/2} \int \sum_{j=0}^{i} \begin{pmatrix} i \\ j \end{pmatrix} \left(\boldsymbol{D}^{-N}\boldsymbol{t}\right)^{(i-j,j)} \frac{\partial^i f\left(\boldsymbol{D}^{-N}\boldsymbol{k}\right)}{\partial t_1^{i-j} \partial t_2^j} \Phi(\boldsymbol{t})\, d\boldsymbol{t} = 0. \tag{5.43}$$

Now, by (5.42), (5.43) and the fact that the partial derivatives of $f(t)$ of order M are bounded on $[0,1]^2$, one can easily prove that

$$\begin{aligned} &\left| s_{\boldsymbol{k}}^0 - |\det \boldsymbol{D}|^{-N/2} \int f(\boldsymbol{D}^{-N}\boldsymbol{k}) \Phi(\boldsymbol{t})\, d\boldsymbol{t} \right| \\ &= \left| s_{\boldsymbol{k}}^0 - |\det \boldsymbol{D}|^{-N/2} f(\boldsymbol{D}^{-N}\boldsymbol{k}) \right| \leq C |\det \boldsymbol{D}|^{-N/2} \|\boldsymbol{D}^{-1}\|_2^{NM}. \end{aligned}$$

Remark 15 The one-point quadrature formula given in [5] is a special case of the one given in the above proposition. In fact if $\boldsymbol{D} = 2$ and $\tau_M = 0$, then $s_{\boldsymbol{k}}^0$ given in the proposition becomes

$$s_{\boldsymbol{k}}^0 = 2^{-N/2} f(2^{-N}\boldsymbol{k}) + O\left(2^{-N(M+\frac{1}{2})}\right),$$

which is exactly the formula given in [5].

Remark 16 The one-point quadrature formula (5.40) is extremely important since it makes the computation of the coefficients of the finest approximation accurate and very fast; this is not the case with some other quadrature formulae. Hence, (5.40) accelerates the DBWT transform.

Remark 17 As for wavelets, the oscillation of the scaling function or equivalently the vanishing moment condition of $\Phi(\boldsymbol{t})$ is ensured by a simple requirement on the lowpass filter $\{H_n\}_n$ to be studied in more detail below.

5.2.2 Wavelet oscillation

In 1-D with dilation factor 2, it is known that if the wavelet $\psi(t)$ has $M-1$ vanishing moments and if $f(t)$ is M times differentiable, the wavelet coefficients satisfy the estimates

$$|d_k^j| = |< f, \psi_{-j,k} >| \leq C 2^{-j(M-(1/2))}. \tag{5.44}$$

Consequently, the larger M, the faster the decay of the wavelet coefficients. Hence, for a given threshold $\epsilon > 0$, there exists a positive integer J such that for all $j \geq J$, $|d_k^j| < \epsilon$. In such cases, d_k^j are automatically set to zero and need not be computed. In [5], 1-D orthonormal and compactly supported wavelets with a high number of vanishing moments have been successfuly used to compress large matrices (1024×1024) and reduce them to a sparse form. In our 2-D case with an arbitrary dilation matrix, the decay of the wavelet coefficients depends on the number of vanishing moments of the analysing wavelets as well as on the smoothness of the signal and the dilation matrix itself, as shown in the following proposition.

Proposition 5 *Assume that* $f \in C^{M-1}([0,1]^2)$ *and*

$$\frac{\partial^M f(t)}{\partial t_1^{M-j} \partial t_2^j}, \qquad j = 0, \ldots, M,$$

are bounded on $[0,1]^2$. *Moreover, assume that the wavelets* $\Psi^i(t)$, $i = 1, \ldots, d-1$, *have* M *vanishing moments:*

$$\int t_1^{m_1} t_2^{m_2} \Psi^i(t_1, t_2)\, dt_1\, dt_2 = 0, \quad 0 \leq m_1 + m_2 \leq M-1,\ m_1, m_2 \geq 0. \tag{5.45}$$

If the coefficients $d_{j,k}^i$ *are defined by the scalar products*

$$d_{j,k}^i = < f, \Psi_{-j,k}^i >, \tag{5.46}$$

then

$$|d_{j,k}^i| \leq C |\det \boldsymbol{D}|^{-N/2} \|\boldsymbol{D}^{-1}\|_2^{NM}. \tag{5.47}$$

Proof: The proof is entirely similar to the proof of the previous proposition. It suffices, for $i = 1, \ldots, d-1$, to replace $\Phi(t)$ by $\Psi^i(t)$, use the fact that $\int \Psi^i(t)\, dt = 0$ and follow the steps of the previous proof. □

Remark 18 Consider the dilation matrices

$$\boldsymbol{D}_1 = 2I_2, \qquad \boldsymbol{D}_2 = \begin{pmatrix} 1 & 1 \\ 1 & -1 \end{pmatrix},$$

and the corresponding decay estimates (5.47)

$$|d^i_{j,k}| \leq C2^{-j(M+(1/2))}, \qquad |d^i_{j,k}| \leq C2^{-j/2}\left(\sqrt{2}\right)^{-jM}.$$

These matrices correspond to tensor product wavelets and to the quincunx sampling lattice, respectively. From these estimates, it seems that the 2-D DBWT algorithms based on wavelets obtained by tensor product are more appropriate for compression purposes than those based on nonseparable 2-D wavelets associated with the dilation matrix $\boldsymbol{D}_2$. However, since in the former case, three wavelets have to be used in the DBWT algorithm and only one in the latter case, then the number of operations required by the former algorithm is larger than in the latter one, and consequently its execution is slower.

For an efficient implementation of DBWT's of Section 5.2, it is necessary that the biorthogonal scaling functions and wavelets satisfy the properties of Propositions 4 and 5.

5.2.3 Design of biorthogonal wavelets

In this section, we provide techniques for designing 1-D and 2-D biorthogonal wavelet bases which are adapted for fast DBWT. The 2-D biorthogonal wavelet bases will be symmetric, have nonseparable variables and be associated with the quincunx dilation matrix $\boldsymbol{D}_2$.

Design of 1-D biorthogonal wavelets

We now design symmetric lowpass and highpass biorthogonal wavelet filters such that the dual scaling functions and wavelets have a prescribed number of vanishing moments. As explained previously, it is desirable that the analysing scaling functions and wavelets have a reasonably high number of vanishing moments We proceed in two steps.

In the first step, we construct analysing scaling function, ϕ, and mother wavelet, ψ that satisfy

$$\int \phi(x)\,dx = 1, \qquad \int x^m \phi(x)\,dx = 0, \quad m = 1, \cdots, M-1, \tag{5.48}$$

$$\int x^m \psi(x)\,dx = 0, \qquad m = 0, \cdots, M-1, \tag{5.49}$$

respectively. This is equivalent to constructing a trigonometric polynomial $h_0(\xi)$ defined by

$$\widehat{\phi}(\xi) = h_0\left(\frac{\xi}{2}\right)\widehat{\phi}\left(\frac{\xi}{2}\right) := \sum_{n=-n_0}^{n_0} h_n\, e^{in\xi/2}\widehat{\phi}\left(\frac{\xi}{2}\right),$$

where $\{h_n\}_n$ is the analysing lowpass wavelet filter.

Conditions (5.48) and (5.49) are equivalent to the existence of two trigonometric polynomials $f_0(\xi)$ and $f_1(\xi)$ such that

$$h_0(\xi) = \left(\frac{1+e^{-i\xi}}{2}\right)^M f_0(\xi) = 1 + \left(1-e^{-i\xi}\right)^M f_1(\xi). \tag{5.50}$$

Note that M has to be an even integer if the wavelets are symmetric; hence we assume that $M = 2l$.

Now, it is clear that (5.50) is equivalent to the existence of two trigonometric polynomials $P_1(\xi)$ and $P_2(\xi)$ such that

$$m_0(\xi) = \left(\cos^2\frac{\xi}{2}\right)^l P_1(\xi) = 1 + \left(\sin^2\frac{\xi}{2}\right)^l P_2(\xi). \tag{5.51}$$

It is known [11] that $P_1(\xi)$ can be written in the form

$$P_1(\xi) = \sum_{k=0}^{l-1} \binom{l-1+k}{k} \left(\sin^2\frac{\xi}{2}\right)^k + \left(\sin^2\frac{\xi}{2}\right)^l P(\xi), \tag{5.52}$$

where $P(\xi)$ is a real trigonometric polynomial taken to be

$$P(\xi) = a_0 + a_1\cos\xi + a_2\cos 2\xi,$$

with appropriate constants α_0, α_1, α_2. This gives the lowpass analysing wavelet filter $\{h_n\}_n$.

The highpass analysing wavelet filter $\{g_n\}_n$ is simply given by

$$g_n = (-1)^{n+1} h_{1-n}.$$

The second step is the design of the synthetizing scaling functions and wavelets or equivalently the construction of lowpass and highpass synthetizing filters. This is achieved by constructing a symmetric trigonometric polynomial $\widetilde{m}_0(\xi)$ of the form

$$\tilde{h}_0(\xi) = \left[\frac{1}{2} + \frac{1}{4}\left(e^{i\xi} + e^{-i\xi}\right)\right]^{\tilde{l}} \left(\sum_{-N}^{N} \tilde{\beta}_n e^{in\xi}\right). \tag{5.53}$$

such that

$$h_0(\xi)\overline{\tilde{h}_0(\xi)} + h_0(\xi+\pi)\overline{\tilde{h}_0(\xi+\pi)} = 1, \qquad \forall \xi \in [0, 2\pi]. \tag{5.54}$$

By substituting (5.53) in (5.54), we are led to a system of linear equations whose solution is a candidate for the synthetizing lowpass filter $\{\tilde{h}_n\}_n$. For more detail, the reader is referred to the Chapter 2.

The above techniques have been used in the construction of biorthogonal wavelet filters $h_0(\xi)$, $\tilde{h}_0(\xi)$ whose coefficients are given in Table 5.1. The associated scaling functions and wavelets have seven and eight vanishing moments, respectively, and they satisfy the hypotheses of above Propositions 4 and 5. Consequently, they are adapted to fast DBWT.

Design of 2-D biorthogonal wavelets

In this section, we construct nonseparable 2-D biorthogonal wavelet basis for the fast DBWT described in Section 5.1. The dilation matrix is taken to be $\boldsymbol{D}_2$ and the 2-D dual scaling functions and wavelets satisfy the hypotheses of Propositions 4 and 5. It is shown in Chapter 4, that if $H_0(\xi_1, \xi_2)$ and $\widetilde{H}_0(\xi_1, \xi_2)$ are the frequency response of the dual lowpass wavelet filters, then

$$H_0(\xi_1, \xi_2)\overline{\widetilde{H}_0(\xi_1, \xi_2)} + H_0(\xi_1+\pi, \xi_2+\pi)\overline{\widetilde{H}_0(\xi_1+\pi, \xi_2+\pi)} = 1, \tag{5.55}$$

Table 5.1: The coefficients α_n, $-8 \leq n \leq 8$, of $h_0(\xi)$ and $\tilde{\alpha}_n$, $-15 \leq n \leq 15$, of $\tilde{h}_0(\xi)$.

n	α_n	$\tilde{\alpha}_n$
0	0.574 768 066 406	0.535 373 226 175 089
±1	0.299 072 265 625	0.300 409 410 336 021
±2	−0.059 814 453 125	−0.029 551 543 213 238
±3	−0.059 814 453 125	−0.063 046 795 337 744
±4	0.029 907 226 562	0.017 124 079 017 817
±5	0.011 962 890 625	0.015 339 181 773 527
±6	−0.008 544 921 875	−0.006 760 627 458 282
±7	−0.001 220 703 125	−0.003 394 649 001 350
±8	0.001 068 115 234	0.001 772 740 433 898
±9	0.000 000 000 000	0.000 876 300 836 220
±10	0.000 000 000 000	−0.000 302 264 035 129
±11	0.000 000 000 000	−0.000 207 855 620 659
±12	0.000 000 000 000	0.000 032 729 076 900
±13	0.000 000 000 000	0.000 025 918 059 808
±14	0.000 000 000 000	−0.000 001 726 909 510
±15	0.000 000 000 000	−0.000 001 511 045 821

for all $\xi_1, \xi_2 \in [0, 2\pi]$. As it is shown in Chapter 4, an efficient way of constructing dual trigomometric polynomials $H_0(\xi_1, \xi_2)$ and $\widetilde{H}_0(\xi_1, \xi_2)$ is to apply a McClellan transformation ([21] pp. 137-148) on zero-phase 1-D biorthogonal wavelet filters. It is shown in the previous Chapter that the number of vanishing moments of the wavelets, the biorthogonality and the exact reconstruction properties are invariant under a proper McClellan transformation. In our case, if we define the transformation function $F(\xi_1, \xi_2)$ by

$$F(\xi_1, \xi_2) = \frac{1}{2}\left(\cos\xi_1 + \cos\xi_2\right), \tag{5.56}$$

then the McClellan transformations of the 1-D zero-phase biorthogonal wavelet filters of the previous paragraph are defined by

$$H_0(\xi_1, \xi_2) = \sum_{-n_0}^{n_0} h_n T_n\Big(F(\xi_1, \xi_2)\Big), \tag{5.57}$$

$$\widetilde{H}_0(\xi_1, \xi_2) = \sum_{-N}^{N} \tilde{h}_n T_n\Big(F(\xi_1, \xi_2)\Big), \tag{5.58}$$

respectively. Here $T_n(x)$ is the nth-degree Chebyshev polynomial.

It remains to check that the number of vanishing moments of the analysing scaling function is invariant under this transformation. In fact, consider the frequency response of the analysing biorthogonal filter $m_0(\xi)$ defined by

$$h_0(\xi) = 1 + \left(\sin^2\frac{\xi}{2}\right)^l P\left(\cos^2\frac{\xi}{2}\right).$$

Then, it is clear that

$$\begin{aligned} h_0(\xi) &= 1 + \left[\frac{1}{2}(1-\cos\xi)\right]^l P\left[\frac{1}{2}(1+\cos\xi)\right], \\ &= 1 + \left[\frac{1}{2}(1-\cos\xi)\right]^l Q\left[\cos\xi\right]. \end{aligned}$$

Since, the given McClellan transformation transforms $\cos\xi$ into $F(\xi_1, \xi_2) = \frac{1}{2}\left(\cos\xi_1 + \cos\xi_2\right)$, then the frequency response of the 2-D analysing biorthogonal wavelet $m_0(\xi_1, \xi_2)$ is

Table 5.2: The coefficients $\tilde{\alpha}_{n,m}$, of $H_2(\omega_1, \omega_2)$ for $-8 \leq n, m \leq 8$.

$n\backslash m$	0	±1	±2	±3	±4
0	0.644345760345	0.172033309937	−0.012817382812	−0.005273818970	0.000066757202
±1	0.172033309937	−0.046663284302	−0.026235580444	0.008144378662	0.001802444458
±2	−0.012817382812	−0.026235580444	0.014586448669	0.004072189331	−0.002136230469
±3	−0.005273818970	0.008144378662	0.004072189331	−0.003004074097	−0.000333786011
±4	0.000066757202	0.001802444458	−0.002136230469	−0.000333786011	0.000292062759
±5	0.000173568726	−0.000667572021	−0.000200271606	0.000233650208	0.000000000000
±6	0.000000000000	−0.000066757202	0.000116825104	0.000000000000	0.000000000000
±7	−0.000009536743	0.000033378601	0.000000000000	0.000000000000	0.000000000000
±8	0.000004172325	0.000000000000	0.000000000000	0.000000000000	0.000000000000

$n\backslash m$	±5	±6	±7	±8
0	0.000173568726	0.000000000000	−0.000009536743	0.000004172325
±1	−0.000667572021	−0.000066757202	0.000033378601	0.000000000000
±2	−0.000200271606	0.000116825104	0.000000000000	0.000000000000
±3	0.000233650208	0.000000000000	0.000000000000	0.000000000000
±4	0.000000000000	0.000000000000	0.000000000000	0.000000000000
±5	0.000000000000	0.000000000000	0.000000000000	0.000000000000
±6	0.000000000000	0.000000000000	0.000000000000	0.000000000000
±7	0.000000000000	0.000000000000	0.000000000000	0.000000000000
±8	0.000000000000	0.000000000000	0.000000000000	0.000000000000

defined as follows:

$$\begin{aligned} H_0(\xi_1, \xi_2) &= 1 + \left[\frac{1}{2}\left(1 - \frac{1}{2}(\cos\xi_1 + \cos\xi_2)\right)\right]^l Q\left[\frac{1}{2}(\cos\xi_1 + \cos\xi_2)\right], \\ &= 1 + \left[\frac{1}{2}\left(\sin^2\frac{\xi_1}{2} + \sin^2\frac{\xi_2}{2}\right)\right]^l Q\left[\frac{1}{2}(\cos\xi_1 + \cos\xi_2)\right]. \end{aligned}$$

Hence, $m_0(\xi_1, \xi_2) - 1$ has a zero of multiplicity $2l$ at (π, π), or equivalently, the analysing scaling function satisfies (5.39) with $M = 2l - 1$.

Finally, note that once the 2-D lowpass biorthogonal wavelet filters $\{H_n\}_n$ and $\{\tilde{H}_n\}_n$ are designed, the design of their corresponding highpass filters $\{G_n\}_n$ and $\{\tilde{G}_n\}_n$ is straightforward and is given by

$$G_{n,m} = (-1)^n \widetilde{H}_{1-n,-m}, \qquad \tilde{G}_{n,m} = (-1)^n H_{1-n,-m}.$$

For more detail, see Chapter 4. We have used the 1-D biorthogonal wavelet filters given in Table 5.1 to construct 2-D biorthogonal wavelet filters H_{nm} and $\widetilde{H}_{nm}$ whose respective coefficients are given in Tables 5.2 and 5.3.

Table 5.3: The coefficients $\tilde{\alpha}_{n,m}$, of $\widetilde{H}_2(\omega_1, \omega_2)$ for $-15 \leq n, m \leq 15$.

$n\backslash m$	0	±1	±2	±3	±4	±5
0	0.571191132069	0.174037382007	−0.005537211429	−0.004429250024	−0.000529408164	−0.000113255948
±1	0.174037382007	−0.024977222085	−0.028688607737	0.004666236229	0.001998667605	−0.000351297989
±2	−0.005537211895	−0.028688607737	0.009284517728	0.005799842067	−0.001783791697	−0.000520566537
±3	−0.004429250024	0.004666236229	0.005799842067	−0.002712636720	−0.001161536551	0.000427917228
±4	−0.000529408164	0.001998667605	−0.001783791697	−0.001161536551	0.000571623736	0.000264629809
±5	−0.000113255948	−0.000351297989	−0.000520566537	0.000427917228	0.000264629809	−0.000082634491
±6	0.000103050013	−0.000037885122	0.000164246361	0.000147124039	−0.000066565917	−0.000052432562
±7	0.000029754186	0.000015880105	0.000034460965	−0.000033707332	−0.000034705077	0.000006571953
±8	−0.000007252931	−0.000004937674	−0.000009309677	−0.000014263392	0.000003922832	0.000004170757
±9	−0.000003407650	−0.000000573861	−0.000002841905	0.000001579358	0.000002163222	−0.000000211015
±10	0.000000129180	0.000000154034	0.000000379810	0.000000751988	−0.000000105508	−0.000000138479
±11	0.000000161462	0.000000032434	0.000000147865	−0.000000038366	−0.000000062945	0.000000000000
±12	−0.000000006766	0.000000004470	−0.000000009592	−0.000000020982	0.000000000000	0.000000000000
±13	−0.000000004445	−0.000000001476	−0.000000004842	0.000000000000	0.000000000000	0.000000000000
±14	−0.000000000105	−0.000000000692	0.000000000000	0.000000000000	0.000000000000	0.000000000000
±15	−0.000000000046	0.000000000000	0.000000000000	0.000000000000	0.000000000000	0.000000000000

$n\backslash m$	±6	±7	±8	±9	±10	±11
0	0.000103050013	0.000029754186	−0.000007252931	−0.000003407650	0.000000319180	0.000000161462
±1	−0.000037885122	0.000015880105	−0.000004937674	−0.000000573861	0.000000154034	0.000000032434
±2	0.000164246361	0.000034460965	−0.000009309677	−0.000002841905	0.000000379810	0.000000147865
±3	0.000147124039	−0.000033707332	−0.000014263392	0.000001579358	0.000000751988	−0.000000038366
±4	−0.000066565917	−0.000034705077	0.000003922832	0.000002163222	−0.000000105508	−0.000000062945
±5	−0.000052432562	0.000006571953	0.000004170757	−0.000000211015	−0.000000138479	0.000000000000
±6	0.000007772786	0.000005725865	−0.000000316523	−0.000000307979	0.000000000000	0.000000000000
±7	0.000005725865	−0.000000361740	−0.000000296740	0.000000000000	0.000000000000	0.000000000000
±8	−0.000000316523	−0.000000296740	0.000000000000	0.000000000000	0.000000000000	0.000000000000
±9	−0.000000230798	0.000000000000	0.000000000000	0.000000000000	0.000000000000	0.000000000000
±10	0.000000000000	0.000000000000	0.000000000000	0.000000000000	0.000000000000	0.000000000000
±11	0.000000000000	0.000000000000	0.000000000000	0.000000000000	0.000000000000	0.000000000000
±12	0.000000000000	0.000000000000	0.000000000000	0.000000000000	0.000000000000	0.000000000000
±13	0.000000000000	0.000000000000	0.000000000000	0.000000000000	0.000000000000	0.000000000000
±14	0.000000000000	0.000000000000	0.000000000000	0.000000000000	0.000000000000	0.000000000000
±15	0.000000000000	0.000000000000	0.000000000000	0.000000000000	0.000000000000	0.000000000000

$n\backslash m$	±12	±13	±14	±15
0	−0.000000006766	−0.000000004445	−0.000000000105	−0.000000000046
±1	0.000000004470	−0.000000001476	−0.000000000692	0.000000000000
±2	−0.000000009592	−0.000000004842	0.000000000000	0.000000000000
±3	−0.000000020982	0.000000000000	0.000000000000	0.000000000000
±4	0.000000000000	0.000000000000	0.000000000000	0.000000000000
±5	0.000000000000	0.000000000000	0.000000000000	0.000000000000
±6	0.000000000000	0.000000000000	0.000000000000	0.000000000000
±7	0.000000000000	0.000000000000	0.000000000000	0.000000000000
±8	0.000000000000	0.000000000000	0.000000000000	0.000000000000
±9	0.000000000000	0.000000000000	0.000000000000	0.000000000000
±10	0.000000000000	0.000000000000	0.000000000000	0.000000000000
±11	0.000000000000	0.000000000000	0.000000000000	0.000000000000
±12	0.000000000000	0.000000000000	0.000000000000	0.000000000000
±13	0.000000000000	0.000000000000	0.000000000000	0.000000000000
±14	0.000000000000	0.000000000000	0.000000000000	0.000000000000
±15	0.000000000000	0.000000000000	0.000000000000	0.000000000000

The graphs of the corresponding scaling functions $\Phi(x_1, x_2)$, $\tilde{\Phi}(x_1, x_2)$ and wavelets $\Psi(x_1, x_2)$, $\tilde{\Psi}(x_1, x_2)$ whose respective graphs are given in Figs. 5.1 to 5.4.

5.3 Numerical Results

A C program was written to implement the 1-D and 2-D biorthogonal wavelet transform algorithm of Section 5.1 with the wavelet filters given in Section 5.2. The numerical experiments have been performed on a Sun Microsoft SPARCstation 10, model 30, running under operating system SunOS 5.3 with Solaris 2.3 and SPARCompiler C 3.0. It is known (see [11], [5]) that, in general, if the signal has support $[0,1]$ or $[0,1]^2$ then the wavelet transform introduces a discontinuity at the edges. To overcome this problem, we extend the original signal to a periodic signal whose restriction on $[0,1]$ (in the 1-D case) or $[0,1]^2$ (in the 2-D case) coincides with the original signal. Note that periodizing the signal is equivalent to replacing the original biorthogonal wavelet bases with their periodized versions (see [12]). The algorithms of Section 5.1 was applied to four different signals. The choice of the signals is for academic purposes only, and corresponds to examples on which the proposed algorithms can be applied.

The first two signals are 1-D signals given by

$$f_1(x) = \sin x, \qquad f_2(x) = \sin 2x + \cos x,$$

respectively. The signals are analysed and synthetized by using different values of N. The number of iterations is $N_0 = 2$. For each value of N, we give the l^2-error norm of the DBWT defined by

$$l^2\text{-norm} = \frac{1}{2^{N/2}} \left(\sum_i \left[f(x_i) - \tilde{f}(x_i) \right]^2 \right)^{1/2},$$

where $\tilde{f}(x_i)$ is the value of the reconstructed signal at the discretization point x_i. We also give the l^∞-error norm defined by

$$l^\infty\text{-norm} = \max_i \left| f(x_i) - \tilde{f}(x_i) \right|.$$

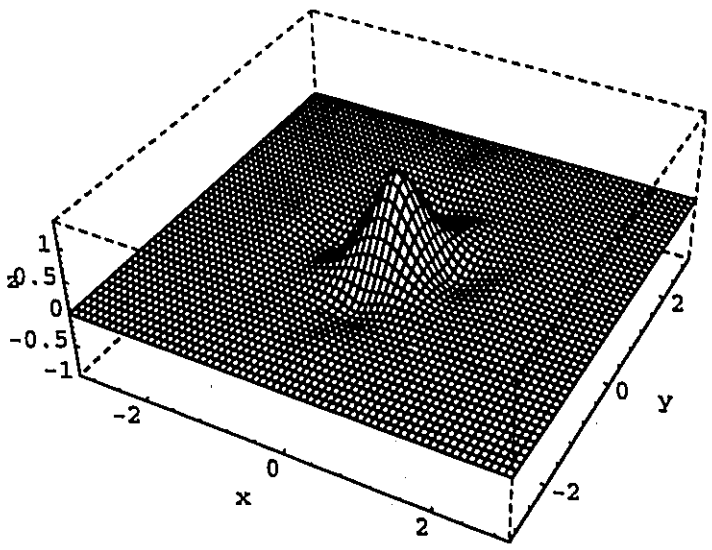

Figure 5.1: Graph of the scaling functions $\Phi(x_1, x_2)$.

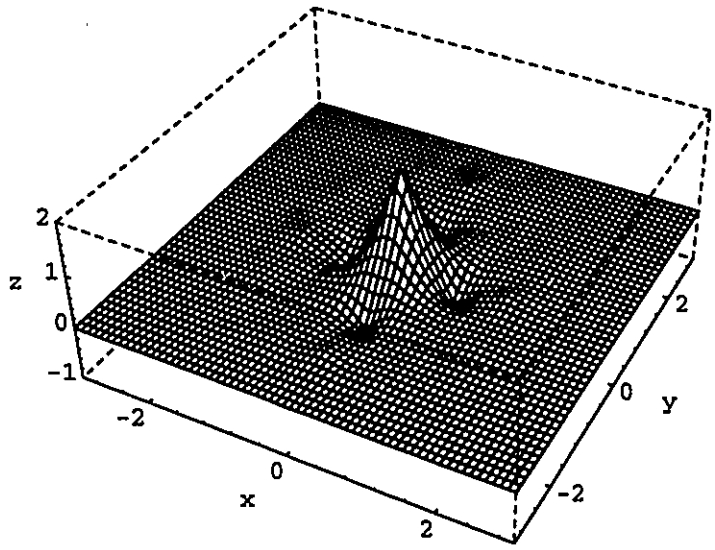

Figure 5.2: Graph of the scaling functions $\tilde{\Phi}(x_1, x_2)$.

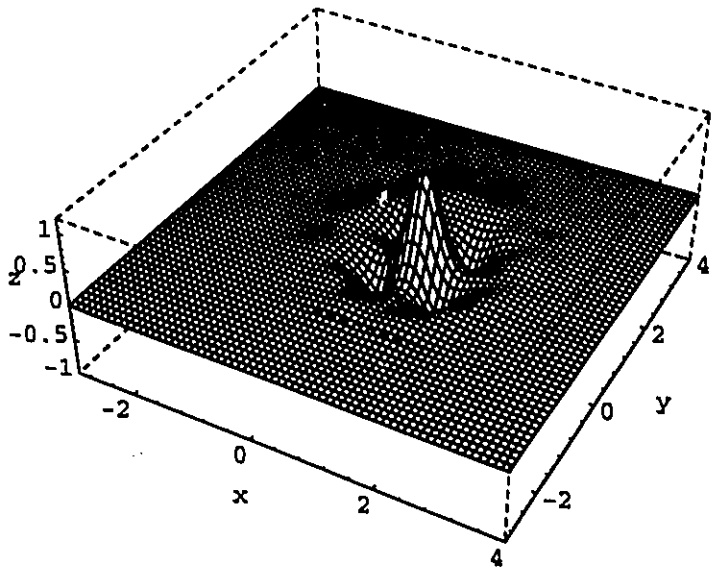

Figure 5.3: Graph of the wavelet $\Psi(x_1, x_2)$.

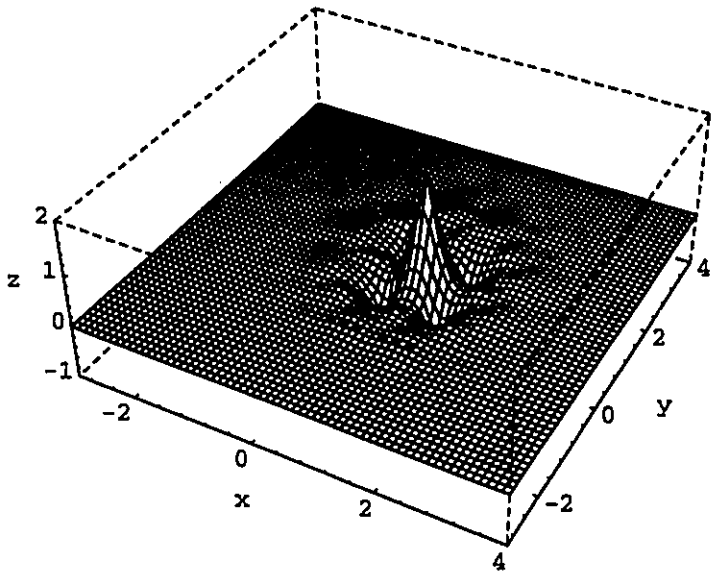

Figure 5.4: Graph of the wavelet $\tilde{\Psi}(x_1, x_2)$.

Table 5.4: Numerical results corresponding to the signals $f_1(x)$ and $f_2(x)$.

	Results for $f_1(x)$		Results for $f_2(x)$	
N	l^∞-norm	l^2-norm	l^∞-norm	l^2-norm
5	7.95E-05	1.70E-09	1.83E-03	6.50E-07
6	5.53E-04	2.65E-07	1.83E-03	5.74E-06
7	7.52E-04	9.27E-07	1.83E-03	1.22E-05
8	8.38E-04	1.84E-06	1.83E-03	2.00E-05
9	8.75E-04	3.05E-06	1.83E-03	3.00E-05
10	8.94E-04	4.64E-06	1.83E-03	4.36E-05
11	9.02E-04	6.79E-06	1.83E-03	6.23E-05
12	9.10E-04	9.78E-06	1.83E-03	8.87E-05
13	9.10E-04	1.39E-05	1.83E-03	1.26E-04
14	9.10E-04	1.98E-05	1.83E-03	1.78E-04
15	9.10E-04	2.81E-05	1.83E-03	2.52E-04

The numerical results for both signals are given in Table 5.4.

Finally, the 2-D biorthogonal wavelet transform algorithm of Subsection 5.1.3 is applied to two 2-D signals given respectively by

$$F_1(x,y) = \sin(x+y), \qquad F_2(x,y) = \sin(x+y) + \cos(2x-y).$$

Different values of N have been used and the wavelet coefficients whose absolute value was smaller than $\epsilon = 10^{-6}$ have been automatically set to zero. In this case, the l^2-error norm and l^∞-error norm are defined by

$$l^2\text{-norm} = \frac{1}{2^N}\left(\sum_{i,j}\left[f(x_i,x_j) - \tilde{f}(x_i,x_j)\right]^2\right)^{1/2},$$

$$l^\infty\text{-norm} = \max_{i,j}\left|f(x_i,x_j) - \tilde{f}(x_i,x_j)\right|,$$

respectively. Finally, we give the compression ratio C_r of the signal which is the number of the different wavelet coefficients with absolute values smaller than a threshold $\epsilon = 10^{-6}$ divided by the number of the different wavelet coefficients. The numerical results corresponding to these two signals are given in Table 5.5.

Table 5.5: Numerical results corresponding to the signals $F_1(x,y)$ and $F_2(x,y)$.

	Results for $F_1(x,y)$			Results for $F_2(x,y)$		
N	l^2-norm	l^∞-norm	C_r	l^2-norm	l^∞-norm	C_r
6	0.00003288	0.00014889	0.56	0.00003904	0.00036776	0.54
8	0.00001292	0.00082159	0.59	0.00001698	0.00128519	0.58
10	0.00000457	0.00105518	0.63	0.00000648	0.00165331	0.62
12	0.00000159	0.00114155	0.65	0.00000236	0.00180065	0.65

Chapter 6

Fast Wavelet Transforms for Signals with Sharp Transitions

Although extensive work has been done on the fast wavelet transform algorithm (see [58], [11]), few papers have dealt with the techniques related to the implemention process. This process becomes less obvious in case where we have to deal with non smooth signals or signals having sharp transition points. The fast discrete biorthogonal wavelet transform algorithm DBWT given in [41],[5] becomes inefficient in these cases. This is due to the fact that the DBWT is based on a one-point quadrature formula that requires the smoothness of the signals as well as reasonable small magnitude of its derivatives. Nonetheless, we show how a minor modification is needed in order to overcome the limitations of the proposed DBWT. Hence, this work can be considered as an extension of a previous work done in [41]. The modification is done on the given signal rather on the wavelet filters used in the process. It can be described as a dilation of the signal by a factor three and then an insertion of two auxiliary points between two successive sampling points. The value of each auxiliary point is computed using a smooth piecewise polynomial constructed from the neighbouring sampling points. We shall refer to this modification as a smoothing process. In fact, we have changed the original signal by a smooth one with resonable bounded derivatives that is suitable to the DBWT. The immediate concern about this method is that the amount of information needed is now multiplied by three,

which means an increased amount of storage space and execution time. However, by another simple modification of the algorithm and the use of the symmetry property of the biorthogonal wavelet filters, it is possible to considerably reduce the storage space and execution time requirements. The signals considered in this Chapter are assumed to be real and compactly supported.

This chapter is organized as follows. In section 6.1, we give a brief review of the fast 1-D wavelet transform algorithm. In section 6.2, we describe in more details the proposed method. Also, we give a way by which it is possible to considerably improve the efficiency of the modified algorithm. Section 6.3, is devoted to some numerical results and concluding remarks.

6.1 Fast Wavelet Transforms

From now on, only 1-D fast wavelet transform algorithms based on the use of biorthogonal wavelet filters will be considered. However, the whole analysis is valid for the orthonormal case. To understand why the DBWT algorithm given in [41] does not work in the case of non smooth signals, signals having sufficiently large derivatives and signals with sharp transitions, it is necessary to give a brief review of the DBWT of Chapter 5. Hence, assume that we have in hand two real and compactly supported functions denoted by $\phi(t)$, $\tilde{\phi}(t)$ and $\psi(t)$, $\tilde{\psi}(t)$, respectively. It is assumed that these functions generate two families of biorthogonal scaling and wavelets given by $(\phi_{jk}(t), \psi_{jk}(t))_{j,k\in Z}$ and $\left(\tilde{\phi}_{jk}(t), \tilde{\psi}_{jk}(t)\right)_{j,k\in Z}$, where again, the notation $g_{jk}(t)$ means

$$g_{jk}(t) = 2^{-j/2} g(2^{-j}t - k). \tag{6.1}$$

Without loss of generality, we may assume that the signal $f(t)$ has support $[0, 1]$. Let $(h_n)_n$, $(\tilde{h}_m)_m$ and $(g_m)_m$, $(\tilde{g}_n)_n$, $-n_0 \leq n \leq n_0$, $\quad -n_1 \leq m \leq n_1$ denote the different lowpass and highpass wavelet filters, respectively. The first step of the direct DBWT is to identify the periodized version of signal $f(t)$ denoted also by $f(t)$ with its projection on some subspace $\tilde{V}_{-n}$ of the biorthogonal version of the multiresolution

analysis in [47]. This gives us the approximation

$$f(t) \approx \sum_{k=0}^{2^n-1} < f, \phi_{-nk} > \tilde{\phi}_{-nk}(t), \tag{6.2}$$

where $N = 2^n$ is the number of sampling points and where for two $L^2(\mathbb{R})$ functions $g_1(t)$, $g_2(t)$, the notation $< f, g >$ means

$$< g_1, g_2 >= \int g_1(t)\overline{g_2(t)}dt. \tag{6.3}$$

If for $n \geq j \geq j_0$, j_0 being the maximum number of iterations, we let T_j, D_j denote the projection operators on the subspaces $\tilde{V}_{j-n} \subset \tilde{V}_{-n}$ and its complement in $\tilde{V}_{j-1-n}$ denoted by $\tilde{W}_{j-n}$, then we have

$$T_j f(t) = \sum_{k=0}^{2^{n-j}} S_k^j \tilde{\phi}_{j-n,k}(t), \tag{6.4}$$

$$D_j f(t) = \sum_{k=0}^{2^{n-j}} d_k^j \tilde{\psi}_{j-n,k}(t), \tag{6.5}$$

where

$$S_k^j =< f, \phi_{j-n,k} >, \qquad d_k^j =< f, \psi_{j-n,k} > .$$

An interesting property of the wavelet transform is that the coefficients S_k^j and d_k^j are easily computed from S_n^{j-1}, $n \in \mathbb{Z}$ as follows:

$$S_k^j = \sum_n h_{n-2k} S_n^{j-1}, \quad d_k^j = \sum_m g_{m-2k} S_m^{j-1},$$

where h_n, $n_0 \leq n \leq n_0$ are the coefficients of the lowpass wavelet filter and $g_m = (-1)^{m+1}\tilde{h}_{1-m}$ are those of the highpass wavelet filter. Conversely, the finer approximation of the signal is recovered by a repeated application of the following formulae

$$\tilde{S}_k^{j-1} = \sum_m \tilde{h}_{k-2m} S_m^j + \sum_n \tilde{g}_{k-2n} d_n^j, \quad k = 0, \ldots, 2^{n-j+1}. \tag{6.6}$$

and

$$f(t) \approx \sum_{k=0}^{2^n-1} \tilde{S}_k^0 \tilde{\phi}_{-nk}(t) = \tilde{f}(t). \tag{6.7}$$

It is clear now how important is the way by which we compute the finest coefficients S_k^0 of the signal $f(t)$. Since many methods can be considered for this task, we believe that it is important to briefly review these schemes and at the same time indicate their limitations when dealing with the signals considered by this Chapter. A first and obvious method is to use a classical integration scheme from numerical analysis such as the composite trapezoidale rule. Such schemes require many function evaluations and generate a non accurate approximation when the signal is not smooth or has large derivatives. Consequently, it is not advised to consider these schemes in our case. The second method (see [15]) is based on Fourier transform, in fact under the assumption that the signal is given in sampled form i.e only the values $f(l)$, $l = 0, \ldots, 2^n - 1$, are known. Then under the assumption that $f(t) \in V_0$, it is easy to see that

$$S_k^0 = < f, \phi_{0k} > = \sum_n a_{k-n} f(n), \tag{6.8}$$

where

$$a_m = \frac{1}{2\pi} \int_0^{2\pi} e^{im\xi} \left[\sum_l \phi(l) e^{-il\xi} \right]^{-1} d\xi. \tag{6.9}$$

This method has the advantage of being independent of the signal's smoothness. However its main drawback is the heavy computational load needed to calculate the finest coefficients. A third method (see [5]) is based on a wavelet based quadrature formula of the type

$$S_k^0 = 2^{-n/2} \sum_{l=0}^{M-1} c_l f\left(l + 2^{-n} k\right) + O\left(2^{-n(M+1/2)}\right). \tag{6.10}$$

For more details, the reader is referred to [5]. This method is very fast but requires smooth enough signals. The fourth method is the fastest way of computing the wavelet coefficients and it is based on a one-point quadrature formula. It has been first given in [5] and then generalized to the 2-D case in (see [41]). As the previous wavelet based quadrature formula, this method works only for smooth signals whose derivatives are bounded by small constants. This quadrature formula is given by the following proposition.

Proposition 6 *Assume that* $f(t) \in C^M(0,1)$. *Moreover assume that the scaling function* $\phi(t)$ *satisfies*

$$\int t^m \phi(t) dt = 0, \quad 1 \le m \le M-1. \tag{6.11}$$

Then

$$\begin{aligned} S_k^0 &= 2^{n/2} \int f(t) \Phi(2^n t - k) dt, \\ &= 2^{-n/2} f\left(2^{-n} k\right) + O\left(2^{-n(M+1/2)}\right). \end{aligned} \tag{6.12}$$

Proof: The proof is based on a Taylor expansion of the signal $f(t)$. Since

$$\begin{aligned} S_k^0 &= 2^{n/2} \int f(t) \phi\left(2^n t - k\right) dt, \\ &= 2^{n/2} \int f\left(t + 2^{-n} k\right) \phi\left(2^n t\right) dt. \end{aligned}$$

A Taylor expansion of $f\left(t + 2^{-n}k\right)$ around $2^{-n/2}$ gives us

$$f\left(t + 2^{-n}k\right) = f\left(2^{-n}k\right) + \sum_{i=1}^{M-1} \frac{f^{(i)}\left(2^{-n}k\right)}{i!} t^i + \frac{f^{(M)}\left(\xi_k(t)\right)}{M!} t^M. \tag{6.13}$$

By multiplying (6.13) by $\phi\left(2^n t\right)$, integrating everything and using property (6.11), it is easy to see that

$$\left| S_k^0 - 2^{-n/2} f\left(2^{-n}k\right) \right| \le C 2^{-n(M+1/2)}, \tag{6.14}$$

where C is a constant satisfying

$$\left| f^{(M)}(t) \right| \le C, \qquad \forall t \in [0,1]. \quad \square$$

The error bound (6.14) is meaningful only for smooth signals whose derivatives are bounded by small constants. The quadrature formula (6.14) becomes inefficient if the signal has large derivatives. As an example, we consider the chirp signal given by

$$f(t) = \sin(t^3), \quad 1 \le t \le 1024. \tag{6.15}$$

The direct DBWT algorithm has failed to generate an approximation to the signal. This is essentially due to the non accurate approximation of the coefficients S_k^0 by (6.14). In fact, if $\tilde{S}_k^0 = S_k^0 + \delta_k$ is an approximation to S_k^0, then it can be shown that

$$\tilde{f}(l) - f(l) = \sum_k \delta_k \tilde{\phi}(l-k), \quad l = 0, \ldots, 2^n - 1, \tag{6.16}$$

is the reconstruction error of the signal whose values are given at the integers $0, \ldots, 2^n - 1$. Note that in our case the scaling function $\tilde{\phi}(t)$ is well localized around zero. Consequently, the coefficients S_k^0, k around l, contribute most to the reconstruction error (6.16). A solution to this problem is given in the following section.

6.2 A Modified DBWT

6.2.1 Description of the method

As we have mentioned earlier, the modification is done on the signal rather than on the wavelet filters. It can be described as follows. Without loss of generality, we may assume that the signal is given in sampled form, in the sense that only $f(l)$, $l = 0, \ldots, 2^n - 1$, are known. Also, assume that the scaling function $\phi(t)$ has $M - 1$ vanishing moments as described in Proposition 1. Now let us consider a piecewise continuous polynomial $P_m(t)$ of minimal degree m and satisfying

$$P_m(3k) = f(k), \quad P_m(3k+3) = f(k+1), \quad k = 0, \ldots, 2^n - 2. \tag{6.17}$$

$$P_m^{(i)}(3k) = P_m^{(i)}(3k+3) = 0, \quad \forall i = 1, \ldots, i_0. \tag{6.18}$$

Condition (6.17) ensures that the $P_m(t)$ fits the signal at the sampled points. After all, the purpose of this method is a good reconstruction of the signal at the sampling points. Condition (6.18) ensures that $P_m(t)$ has i_0 continuous derivatives. It is easy to see that, under these conditions, the degree of $P_m(t)$ is at least $n = 2i_0 + 1$. As an example, we have constructed two polynomials, $P_3(t)$ and $P_5(t)$, that satisfy (6.17)

and (6.18). Their respective restrictions on the interval $[3k, 3k+3]$ are given by

$$\begin{aligned} P_3(t) &= \Big[f(k+1)-f(k)\Big]\Big[\frac{2}{27}t^3+\frac{1}{9}(3+2k)t-\frac{2}{3}k(1+\frac{1}{3}k)t^2 \\ &\quad +\frac{1}{3}k^2(1+\frac{2}{9}k)\Big]+f(k), \\ P_5(t) &= \frac{\Big[f(k+1)-f(k)\Big]}{81}\Big[2t^5-5(2k+3)t^4+(20k^2+60k+30)t^3-(20k^3+ \\ &\quad 90k^2+90k)t^2+(10k^2+60k^3+90k^2)t-(2k^5+15k^4+30k^3)\Big]+f(k). \end{aligned}$$

Particularly interesting values of $P_3(t)$ and $P_5(t)$ are given by

$$\begin{aligned} P_3(3k+1) &= \frac{20}{27}f(k)+\frac{7}{27}f(k+1), \\ P_3(3k+2) &= \frac{7}{27}f(k)+\frac{20}{27}f(k+1), \end{aligned} \tag{6.19}$$

and

$$\begin{aligned} P_5(3k+1) &= \frac{64}{81}f(k)+\frac{17}{81}f(k+1), \\ P_5(3k+2) &= \frac{17}{81}f(k)+\frac{64}{81}f(k+1). \end{aligned} \tag{6.20}$$

Note that only the above values will be used by the modified algorithm. It is of interest to mention that the above polynomials have reasonably small derivatives. As an example,

$$\max_{k\le t\le k+1}\left|P_5^{(2)}(t)\right| = \frac{10}{27}\sqrt{3}\,|f(k+1)-f(k)|, \tag{6.21}$$

and

$$\max_{k\le t\le k+1}\left|P_3^{(1)}(t)\right| = \frac{1}{2}|f(k+1)-f(k)|. \tag{6.22}$$

In the special case where $f(t)$ is given by (6.15), then

$$\max_t\left|P_5^{(2)}(t)\right| \le \frac{20}{27}\sqrt{3}, \quad \max_t\left|P_3^{(1)}(t)\right| \le 1.$$

This is a considerable improvement since

$$\max_{1\le t\le 1024}|f^{(1)}(t)| = 1048580, \quad \max_{1\le t\le 1024}|f^{(2)}(t)| = 9.8956\times 10^{12}.$$

Now, the modification we intend to apply becomes clear. Instead of considering the original signal $f(t)$, we consider the smooth piecewise polynomial $P_m(t)$ that satisfies (6.17) and (6.18). This polynomial is in general well adapted for the DBWT based on the extremely fast one-point quadrature formula of Proposition 1. Let $F(t) = P_m(2^n t)$ and $\tilde{F}(t)$ be the reconstruction of $F(t)$. The following proposition gives us a bound of the reconstruction error.

Proposition 7 *Under the assumption that the biorthogonal scaling functions and wavelets $\phi(t)$, $\tilde{\phi}(t)$ and $\psi(t)$, $\tilde{\psi}(t)$ are compactly supported and that $\phi(t)$ satisfies (6.11), we have*

$$|F(x) - \tilde{F}(x)| \leq C2^{-n/2}, \tag{6.23}$$

where C depends only on the piecewise polynomial $P_m(t)$.

Proof: We first prove that the scaling function $\tilde{\phi}(t)$ satisfies the property

$$\sum_l \tilde{\phi}(x-l) = 1, \quad \forall x \in \mathbb{R}.$$

We assume that there exists $N_0 < N_1$ such that the dual scaling function and wavelets have their supports in $[N_0, N_1]$. If for $x \in \mathbb{R}$, we let

$$g(t) = \begin{cases} 1 & \text{if } x + N_0 - N_1 \leq t \leq x + N_1, \\ 0 & \text{otherwise,} \end{cases}$$

then $g(t)$ is an $L^2(\mathbb{R})$ function. Since we have at hand a biorthogonal wavelet basis of $L^2(\mathbb{R})$, then $g(x)$ has the expansion

$$g(x) = \sum_{l \in \mathbb{Z}} (g, \phi_{0l}) \tilde{\phi}_{0l}(x) + \sum_{j \in \mathbb{Z}, j<0} \sum_{l \in \mathbb{Z}} (g, \psi_{jl}) \tilde{\psi}_{jl}(x). \tag{6.24}$$

Using the facts that for $j < 0$, $\tilde{\phi}_0(t)$, $\tilde{\psi}_{jk}(t)$ have support in $[N_0, N_1]$ and the facts that

$$\int \phi(t)dt = 1, \quad \int \psi_{jk}(t)dt = 0, \tag{6.25}$$

then one easily sees that

$$(g, \phi_{0l}) = 1, \quad (g, \psi_{jl}) = 0. \tag{6.26}$$

Substituting (6.26) in (6.24), one can easily conclude that $\sum_l \tilde{\phi}(x-l) = 1$. Since x is arbitrary, the equality holds for any real number. Now, to prove the desired error bound, we let $S_k^0 = (F, \phi_{-nk})$, and remark that

$$\begin{aligned} S_k^0 &= 2^{n/2} \int F(t)\phi\left(2^n t - k\right) dt = 2^{n/2} \int F\left(2^{-n}t + 2^{-n}k\right) \phi(t) dt. \\ &= 2^{-n/2} \int \left[F\left(2^{-n}k\right) + \sum_{i=1}^{i_0-1} (2^{-n}t)^i \frac{F^{(i)}\left(2^{-n}k\right)}{i!} + \right. \\ &\quad \left. (2^{-n}t)^{i_0} \frac{F^{(i_0)}\left(\xi_k(t)\right)}{i_0!} \right] \phi(t) dt. \end{aligned}$$

Since $F^{(i_0)}(t) = 2^{i_0 n} P_n^{(i_0)}(t)$, then, by using the facts that $\left|P_n^{(i_0)}(t)\right| \leq C$ and

$$\int \phi(t)dt = 1, \quad \int t^m \phi(t)dt = 0, \quad 1 \leq m \leq i_0 - 1, \tag{6.27}$$

We obtain the error bound

$$\left|S_k^0 - 2^{-n/2} F(2^{-n}k)\right| = |\delta_k| \leq C 2^{-n/2}. \tag{6.28}$$

As mentioned earlier, it is easy to see that under the above notation, the reconstruction error satisfies the following bound

$$\left|F(x) - \tilde{F}(x)\right| \leq \left|\sum_k \delta_k \tilde{\phi}(x-k)\right|. \tag{6.29}$$

Using $\sum_k \tilde{\phi}(x-k) = 1$ in (6.29) leads to

$$\left|F(x) - \tilde{F}(x)\right| \leq \max_k |\delta_k| \leq C 2^{-n/2}. \tag{6.30}$$

Remark 19 *Since $F(t) = P_m(2^n t)$, then the reconstruction formula for the original signal $f(t)$ at the sampled points is given by*

$$f(l) \approx \tilde{F}(3 \times 2^{-n} l).$$

The above approximation is adequate for processing large input signals where typically $n \geq 10$.

Remark 20 *Our first concern about this method is its requirement of an input equal to three times the original data and the longer processing time. A possible solution to this problem is given by the following algorithm that reduces the number of data to be processed and also takes advantage of the structure of biorthogonal wavelet filters.*

6.2.2 The improved algorithm

This paragraph is devoted to improvements that can be applied to the above method and to appropriate implementations. First, note that the biorthogonal wavelet filters $(h_n)_n, -n_0 \leq n \leq n_0$ and $(\tilde{h}_n)_n, -n_1 \leq n \leq n_1$ to be used are symmetric. Their corresponding analysing scaling function satisfies the conditions of Proposition 1. The design technique of such filters is described in more details in [41]. Since the discrete wavelet transform is essentially based on the convolution of the filters with a decimated version of the signal, then a considerable reduction of execution time is done by the following factorization process given by Algorithm 1.

Algorithm 1.

Given the coefficients $S_k^0, k = 0, \ldots, 2^n - 1$, a symmetric filter $(h_m)_m, n_0 \leq m \leq n_0$, this algorithm computes the coefficients S_k^j, $k = 0, \ldots, 2^{n-j}$.

Step 1 for $k = 0, \ldots, n_0$

$S_k^j = 0$;

for $l = 0, \ldots, 2k + n_0$

$S_k^j = S_k^j + h_{l-2k} S_l^{j-1}$;

Step 2 for $k = n_0 + 1, \ldots, 2^{n-j} - n_0$

$S_k^j = 0$;

for $l = 2k - n_0, \ldots, 2k - 1$

$S_k^j = S_k^j + h_{l-2k} \left(S_l^{j-1} + S_{4k-l}^{j-1} \right)$;

$S_k^j = S_k^j + h_0 S_k^{j-1}$;

Step 3 for $k = 2^{n-j} - n_0 + 1, \ldots, 2^{n-j}$

$S_k^j = 0;$

for $l = 2k - n_0, \ldots, 2k + n_0$

$S_k^j = S_k^j + h_{l-2k} S_l^{j-1};$

Note that Step 2 of this algorithm requires $n_0 + 1$ multiplications (mults) and $2n_0 + 1$ additions (addts) per each computed coefficient S_k^j. A straightforward convolution as it is done in step 1 and step 3 would requires $2n_0 + 1$ mults and $2n_0$ addts. Since, in general, n_0 is very small compared to 2^{n-j}, then the majority of operations are done in step 2. Also, since the multiplications are the most time consuming operations, Algorithm 1 can considerably speed up the DBWT. Yet, it is possible to further reduce the execution time by simply adapting the extremely fast Winograd algorithm [32] for the computation of the convolutions in Algorithm 1.

To reduce the storage space requirement, we consider only one extra array A of size $N = 2^n$. The array A is used to temporarily store the transformed data. The operation is described in more detail in the following algorithm.

Algorithm 2. (The improved algorithm)

This algorithm reconstruct an input signal $f(i), i = 0\ldots, 2^n - 1$. It is appropriate for signals that have many sharp transitions.

Input: the sampled data $f(i)$, $i = 0, \ldots, 2^n - 1$, the symmetric biorthogonal wavelet filters $(h_m)_m, n_0 \leq m \leq n_0$, and $(\tilde{h}_m)_m, n_1 \leq m \leq n_1$, the constant $\alpha = 20/27$ or $64/81$ and j_0 the maximum number of iterations (MNI).

Output: an approximation $\tilde{f}(i)$ to $f(i)$, $i = 0, \ldots, 2^n - 1$.

Step 1 for $j = 0, 1, 2$

for $i = j, \ldots, 2^n - 4$

$A[i] = f(i);$

$A[i+1] = \alpha f(i) + (1 - \alpha) f(i+3);$

$A[i+2] = \alpha f(i+3) + (1 - \alpha) f(i);$

$A[i+3] = f(i+3);$

$i = i + 3;$

Step 2 Apply DBWT to $A[i], i = 0, \ldots, 2^n - 1$, with j_0 as MNI and where Algorithm 1 is used to compute the different wavelet coefficients.

Step 3 for $i = j, \ldots, 2^n - 4$

$\tilde{f}(i) = 2^{n/2}\tilde{S}^0_i$;

$\tilde{f}(i+3) = 2^{n/2}\tilde{S}^0_{i+3}$;

$i = i + 6$;

$j = j + 1$;

stop.

Remark 21 *The reconstruction formula of the above algorithm is more simply given by* $\tilde{f}(i) = 2^{n/2}\tilde{S}^0_i$ *rather than by (6.7). In fact due to the design property of the biorthogonal wavelet filters, the two formulae lead to approximately the same accuracy.*

Finally, note that the computational complexity of the algorithm is of order $O(N)$ where $N = 2^n$ is the input data size. In fact, if j_0 iterations are to be performed, then Step 1 of the algorithm requires 12×2^n mults and 6×2^n addts. The number of multiplications and additions required by Step 2 are respectively

$$3\left[(2^n - 2^{n-j_0})(n_0 + n_1 + 2) - j_0((n_0 + n_1)(3 + n_0 + n_1))\right],$$

and

$$3\left[(2^n - 2^{n-j_0})(2n_0 + 2n_1 + 2) - 11j_0((n_0 + n_1)(1 + n_0 + n_1) + 14/11)\right].$$

In conclusion, the total number of multiplications and additions remains acceptable. However, in practice, it is more usual to deal with signals having smooth transitions on some regions and sharp transitions on others. For this type of signals, both methods, the direct and the improved version of the DBWT are inefficient. While the first method is unable to handle the sharp transitons and consequently provides a poor approximation at these points, the second method does provide a good reconstruction but at the cost of unnecessary extra computations. A better algorithm must be able to handle the sharp transitions of the signal with a smaller amount of computations.

In a sense, this algorithm is a combination of the direct DBWT of Section 2 and the modified DBWT of Section 3. The combination is done as follows. We first use a numerical scheme to predict the points where the sharp transitions occur. Once the prediction of the sharp transitions is done, a smoothing process is to be applied to the signal. The smoothing operation follows the rule: If the current point t_k is considered as a sharp transition point, then use a piecewise smooth polynomial to insert two extra points between the sampling points t_{k-1} and t_k. If the signal shows a smooth transiton at t_k, then keep it and look for the next sampling point. Note that the prediction is done by inspecting the magnitude of the relative change of the signal. To be more precise, suppose that $k = 0\ldots, 2^n - 1$ are the sampling points, then for each k, evaluate the quantities

$$\delta(k) = \frac{|f(k) - f(k-1)|}{|f(k)| + \epsilon}, \qquad \delta(k+1) = \frac{|f(k+1) - f(k)|}{|f(k)| + \epsilon}.$$

Here ϵ is a small positive real number used to avoid division by zero. If for some fixed $\delta > 0$, $\delta(k) \geq \delta$ or $\delta(k+1) \geq \delta$, then the signal has a sharp transition at k. The combined algorithm can now be described as follows

Algorithm 3. (The combined algorithm)

Given an input signal $f(i)$, $i = 0, \ldots, 2^n - 1$, this algorithm predicts its sharp transitions where a smoothing process is to be applied. The modified signal is then analysed and synthetized by a direct DBWT.

Input: the sampled data $f(i)$, $i = 0, \ldots, 2^n - 1$, the symmetric biorthogonal wavelet filters $(h_m)_m$ and $(\tilde{h}_m)_m$, the constant $\alpha = 20/27$ or $64/81$, j_0 the maximum number of iterations (MNI) and the positive numbers ϵ, δ.

Output: an approximation $\tilde{f}(i)$ to $f(i)$, $i = 0, \ldots, 2^n - 1$.

Step 1 /* prediction and smoothing of the sharp transitions*/

$A[0] = f(0)$; $L[0] = 0$; $L[1] = 1$;

for $i = 1, \ldots, 2^n - 1$

$a = \frac{|f(i)-f(i-1)|}{|f(i)|+\epsilon}$; $b = \frac{|f(i+1)-f(i)|}{|f(i)|+\epsilon}$;

if $a \geq \delta$ or $b \geq \delta$, then

$A[L[i]-1] = f(i-1);$

$A[L[i]] = \alpha f(i-1) + (1-\alpha) f(i);$

$A[L[i]+1] = \alpha f(i) + (1-\alpha) f(i-1);$

$A[L[i]+2] = f(i+1);$

$L[i] = L[i]+2;\ L[i+1] = L[i]+1;$

else

$A[l[i]] = f(i);\ L[i+1] = L[i]+1;$

step2 /* analyze and synthetize the modified signal*/

apply the DBWT to $A[i],\ i = 0, \cdots, L[2^n - 1]$ with j_0 iterations.

The wavelet coefficients are computed via algorithm 1.

step3 /* output the reconstructed signal */

for $i = 1, \ldots, 2^n - 1$

$\tilde{f}(i) = 2^{n/2} \tilde{S}^0_{L[i]};$

stop.

It is easy to see that if N_t is the number of sharp transition points and $\beta = 2^{-n} N_t$, then the number of mults and addts required by the combined algorithm are respectively equal to

$$(1+2\beta)\left[(2^n - 2^{n-j_0})(n_0+n_1+2) - j_0((n_0+n_1)(3+n_0+n_1))\right] + 12\beta 2^n,$$

and

$$(1+2\beta)\left[(2^n - 2^{n-j_0})(2n_0+2n_1+2) - 11 j_0((n_0+n_1)(1+n_0+n_1)+14/11)\right] + 6\beta 2^n.$$

Note that if the signal shows a sharp transition at each sampling point, then $\beta = 1$. In this case, the combined algorithm has the same complexity as the improved one. In the special case where $\beta = 0$, i.e there is no sharp transition, the number of operations is minimum; this corresponds to the direct DBWT case.

Finally, the following numerical tests illustrate the efficiency of the proposed algorithms.

Table 6.1: The filter coefficients h_n, $-6 \leq n \leq 6$, and $\tilde{h}_n$, $-9 \leq n \leq 9$.

n	h_n	$\tilde{h}_n$
0	0.6640 6250 0000 0000	0.4946 1256 9264 1019
±1	0.2968 7500 0000 0000	0.2860 6519 3892 3029
±2	-0.1289 0625 0000 0000	0.0059 5350 4348 3512
±3	-0.0546 8750 0000 0000	-0.0352 5217 8186 1487
±4	0.0585 9375 0000 0000	-0.0046 6659 8094 5766
±5	0.0078 1250 0000 0000	-0.0029 4534 6235 5809
±6	-0.0117 1875 0000 0000	0.0013 9943 6828 1193
±7	0.0000 0000 0000 0000	0.0021 2127 2100 3442
±8	0.0000 0000 0000 0000	0.0000 7372 2860 5508
±9	0.0000 0000 0000 0000	0.0000 1105 8429 0826

6.3 Numerical results

A C code has been written to implement Algorithm 2 and Algorithm 3. The numerical experiments have been performed on a Sun SPARC 10. Many signals of the type described in this paper are considered and the numerical results are consistent with the theoretical work. The design technique given in [41] is used to construct appropriate symmetric biorthogonal wavelet filters whose coefficients are given in Table 6.1. The analyzing scaling function satisfies the conditions of Proposition 1 with three vanishing moments. The signals are analysed and synthetized by using different numbers of sampling points $N = 2^n$, where the samples are taken at the positive integers. For each value of N, we give the reconstruction error in the l^∞-norm and defined by

$$l^\infty\text{-norm} = \max_i |f(t_i) - \tilde{f}(t_i)|.$$

Also, we provide the l^1-norm defined by

$$l^1\text{-norm} = 2^{-n} \sum_{0}^{2^n-1} |f(t_i) - \tilde{f}(t_i)|.$$

We also give the time T_s in seconds needed to analyse, synthetize and reconstruct the signal. The number of iterations j_0 is kept to one during all these experiments.

The first of the two signals to be considered here is given by

$$f_1(t) = \sin\left(\frac{t}{100}\right) + g(t), \quad t = 1, \ldots, 2^n,$$

where

$$g(t) = \begin{cases} \sin(t^3) & \text{if } 300 \leq t \leq 320, \quad 600 \leq t \leq 620, \\ 0 & \text{otherwise.} \end{cases}$$

$f_1(t)$ has very smooth transitions except at the few points where $g(t)$ is not zero (see Fig 6.1(a)). In this case, the combined algorithm is much faster than the improved algorithm and it is equivalent to the direct DBWT. The second signal $f_2(t)$ is given by

$$f_2(t) = \sin(10^{-6}t^3) + \cos(0.01\,t^2), \quad t = 1, \ldots, 2^n.$$

For t large enough, $f_2(t)$ has sharp transitions at the sampling points (see Fig 6.2(a)). In this case, the combined algorithm is equivalent to the improved one, (see Table 6.3). The numerical results obtained by applying Algorithm 2 and Algorithm 3 are given in Table 6.2 and Table 6.3, respectively.

Fig 6.1 and Fig 6.2 show the graphs of the signals $f_1(t)$ and $f_2(t)$ as well as their reconstructed version $\tilde{f}_1(t)$, $\tilde{f}_2(t)$ and the graphs of the reconstruction errors made by applying Algorithm 3 with $n = 10$. Finally, we should mention that among the algorithms presented in this paper, Algorithm 3 is the most appropriate and a general purpose one. The generalization of the proposed methods to the 2-D case can be done in a straightforward way.

Table 6.2: The numerical results for the signals $f_1(t)$ obtained by Algorithm 2 and Algorithm 3.

	Results of Algorithm 2			Results of Algorithm 3		
N	l^∞-norm	l^1-norm	T_s	l^∞-norm	l^1-norm	T_s
512	0.030753	0.000362	0.1	0.036347	0.004842	0.1
1024	0.044665	0.000378	0.2	0.051207	0.004752	0.1
2048	0.044665	0.000193	0.4	0.051207	0.004310	0.2
4096	0.044665	0.000101	0.8	0.051207	0.004012	0.3
8192	0.044665	0.000054	1.6	0.051207	0.003872	0.7
16384	0.044665	0.000031	3.2	0.051702	0.003803	1.4
32768	0.044665	0.000020	6.4	0.051207	0.003771	2.8

Table 6.3: The numerical results for the signals $f_2(t)$ obtained by Algorithm 2 and Algorithm 3.

	Results of Algorithm 2			Results of algorithm 3.		
N	l^∞-norm	l^1-norm	T_s	l^∞-norm	l^1-norm	T_s
512	0.093727	0.007985	0.1	0.106280	0.023449	0.1
1024	0.097711	0.008378	0.2	0.113554	0.027264	0.2
2048	0.099413	0.008879	0.5	0.113554	0.029931	0.4
4096	0.099413	0.009085	0.9	0.116147	0.030105	0.8
8192	0.103925	0.009220	1.8	0.124508	0.030393	1.7
16384	0.105351	0.009303	3.7	0.124508	0.030748	3.6
32768	0.118646	0.009293	7.5	0.131691	0.030757	7.5

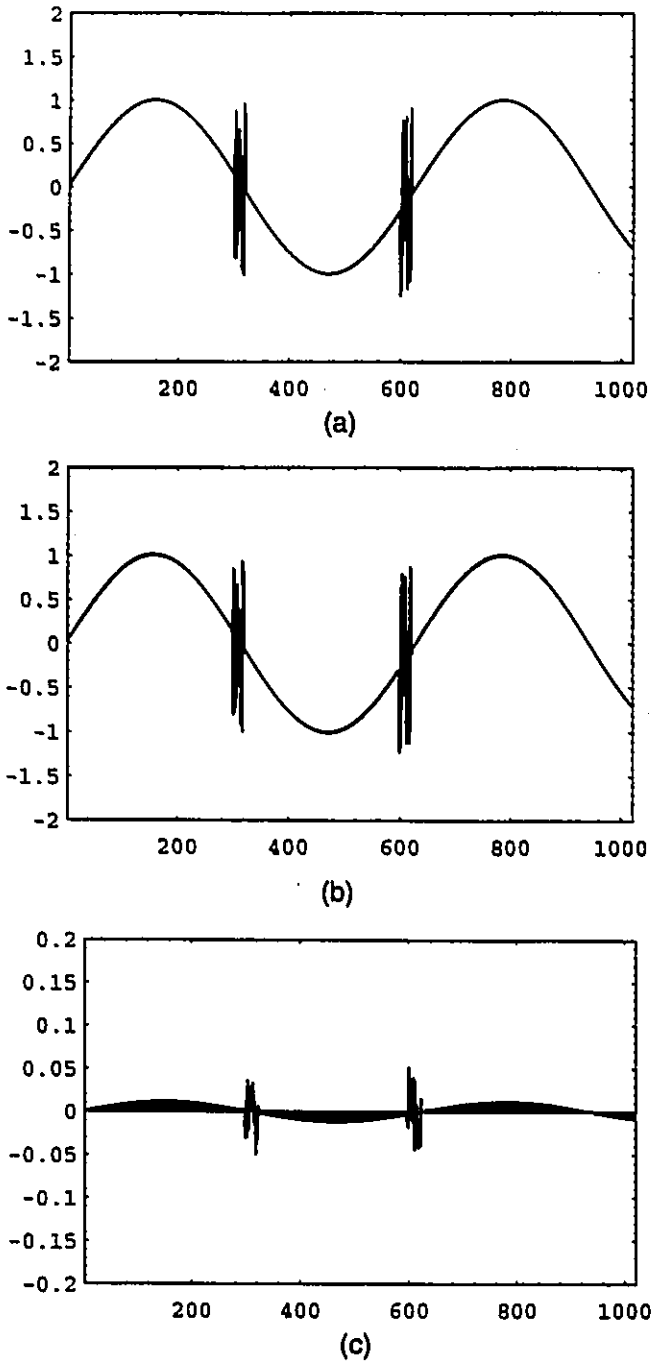

Figure 6.1: Graphs of (a) $f_1(t)$, (b) $\tilde{f}_1(t)$ and (c) $f_1(t) - \tilde{f}_1(t)$.

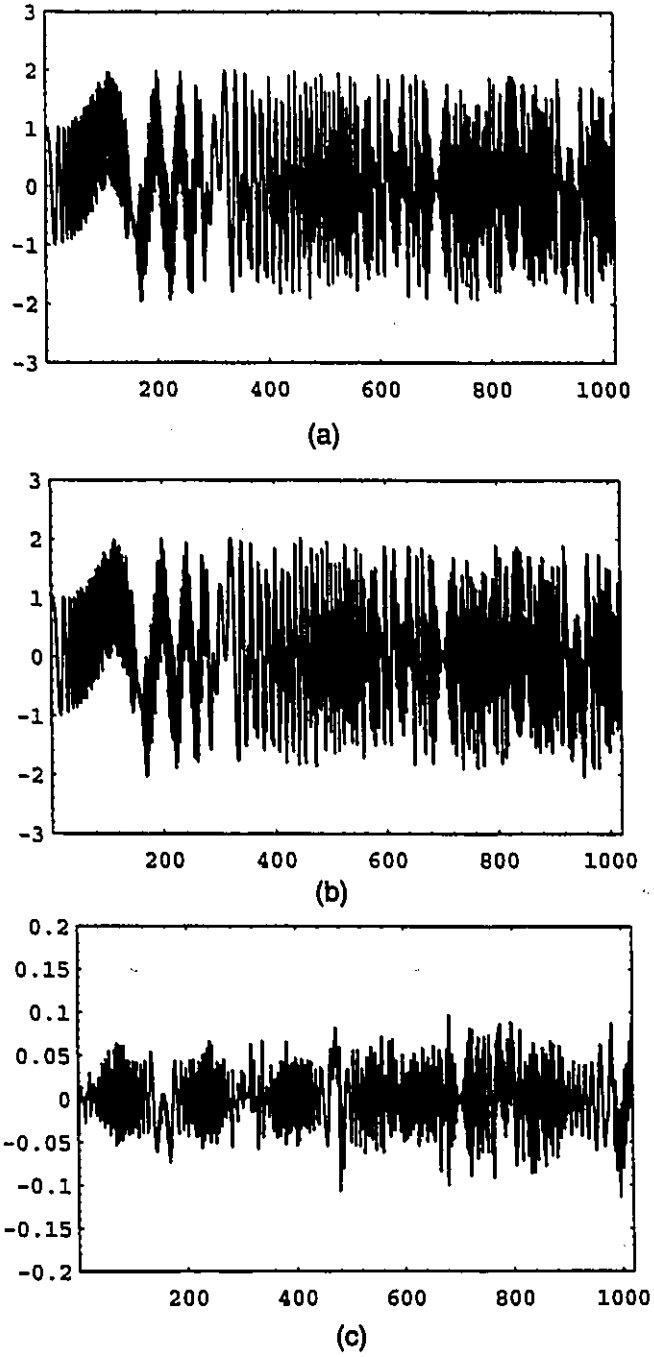

Figure 6.2: Graphs of (a) $f_2(t)$, (b) $\tilde{f}_2(t)$ and (c) $f_2(t) - \tilde{f}_2(t)$.

Chapter 7

Conclusion

This thesis has provided some practical numerical techniques for the construction and regularity estimate of one-dimensional biorthogonal wavelet bases. Although the emphasis was on the construction of symmetric wavelets, the proposed techniques can be used to design more general 1-D biorthogonal wavelets, whose corresponding lowpass filters are given in parametric forms. This 1-D wavelet filter design is a general purpose design in the sense that it does not take specific applications into acount. Nevertheless, minor changes to the proposed design would provide appropriate wavelet filters for many applications.

Two important 1-D wavelet design problems have not been considered in this thesis. The first problem is the construction of 1-D biorthogonal wavelets whose support is a prescribed interval. It is expected that this type of wavelets is well adapted for the numerical solution of boundary value problems by means of wavelets. The second problem is the design of 1-D biorthogonal wavelet packets. It is expected that in certain applications, biorthogonal wavelet packets will give better results than ordinary wavelets. Certainly, a detailed investigation of the above problems is an interesting research topic.

Despite the numerous advantages in using nonseparable multidimensional wavelet

basis, little research work have been published in the design of multidimensional wavelets. Consequently, we became aware of the necessity for further investigation of the design issue. Two contributions to the subject have been made in this thesis. The first contribution is the use of the McClellan transformation as an efficient tool for the construction of nonseparable bidimensional biorthogonal wavelet bases. The second contribution is the generalization of some results related to the theory and design of wavelets. These generalizations have yielded better understanding of a more practical multidimensional wavelet design.

I believe that many chalenging problems related to the design of multidimensional wavelets are still without answers. Among these problems are the design of regular orthonormal wavelet bases and a good practical way for estimating the regularity of multidimensional wavelets. Certainly, any contribution to the subject will have a great impact in many applications.

It is well known that the use of a good wavelet transform algorithm is crucial for an efficient implementation of the wavelet theory. In this thesis, we have given a definition of a good wavelet transform algorithm. Furthermore, we have followed our definition in the construction of 1-D and 2-D biorthogonal wavelets that are adapted for fast wavelet transform algorithms. A special attention is given to the case where the signals have sharp transitions points. In this case, we have applied a smoothing process to obtain an accurate reconstruction of the signal. The implementation of the proposed algorithms for some digital signal processing applications will be my future research interests.

Finally, it is my belief that despite the very important contributions that have been done to the subject during the past ten years, there are still many challenging questions without answers.

Bibliography

[1] B. K. Alpert, *Wavelets and other bases for fast numerical linear algebra*, Wavelets: A Tutorial in Theory and Applications, (C. K. Chui, ed.), Academic Press, San Diego CA, 1992, pp. 181–216.

[2] M. Antonini, M. Barlaud, and P. Mathieu, *Image coding using lattice vector quantization of wavelet coefficients*, Proc. IEEE Int. Conf. ASSP, Toronto, Canada, (1991), 2273–2276.

[3] M. Antonini, M. Barlaud, P. Mathieu, and I. Daubechies, *Image coding using wavelet transform*, IEEE Trans. Image Proc., **1**, no. 2, (1992), 205–220.

[4] G. Beylkin, *On the representation of operators in bases of compactly supported wavelets*, SIAM J. Numer. Anal., **6**, no. 6, (1992), 1716–1740.

[5] G. Beylkin, R. Coifman, and V. Rokhlin, *Fast wavelet transforms and numerical algorithms*, Comm. Pure Appl. Math., **44** no. 2, (1991), 141–183.

[6] H. Caglar and A. N. Akansu, *A generalized parametric PR-QMF design technique based on Bernstein polynomial approximation*, IEEE Trans. Signal Proc., **41**, no. 7, (1993), 2314–2321.

[7] C. K. Chui, *An Introduction to Wavelets*, Academic Press, San Diego CA, 1992.

[8] A. Cohen, *Biorthogonal wavelets*, Wavelets: A Tutorial in Theory and Applications, (C. K. Chui, ed.), Academic Press, San Diego CA, 1992, pp. 123–152.

[9] A. Cohen and I. Daubechies, *A stability criterion for biorthogonal wavelet bases and their related subband coding scheme*, Duke Math. J., **68**, no. 2, (1992), 313–335.

[10] A. Cohen and I. Daubechies, *Non-separable bidimensional wavelet bases*, Revista Matemática Iberoamericana, **9**, no. 1, (1993), 51–137.

[11] A. Cohen, I. Daubechies, and J.-C. Feauveau, *Biorthogonal bases of compactly supported wavelets*, Comm. Pure Appl. Math., **45**, no. 5, (1992), 485–560.

[12] A. Cohen, I. Daubechies, and P. Vial, *Wavelets on the interval and fast wavelet transforms*, preprint.

[13] R. R. Coifman, Y. Meyer, and V. Wickerhauser, *Size properties of wavelet packets*, Wavelets and their Applications, (M. B. Ruskai et al., eds.), Jones and Bartlet Boston, MA, 1992, pp. 453–470.

[14] I. Daubechies, *Orthonormal bases of compactly supported wavelets*, Comm. Pure Appl. Math., **41**, no. 7, (1988), 909–996.

[15] I. Daubechies, *Ten Lectures on Wavelets*, Society for Industrial and Applied Mathematics, Philadelphia PA, 1992.

[16] I. Daubechies, *Wavelet transforms and orthonormal wavelet bases*, Different Perspectives on Wavelets, (I. Daubechies, ed.), American Mathematical Society, 1993, pp. 1–33.

[17] I. Daubechies and J. C. Lagarias, *Two scale difference equations I, Existence and global regularity of solutions*, SIAM. J. Math. Anal., **22**, no. 5, (1991), 1388–1410.

[18] I. Daubechies and J. C. Lagarias, *Two scale difference equations II, Local regularity, infinite products of matrices and fractals*, SIAM. J. Math. Anal., **23**, no. 4, (1992), 1031–1079.

[19] G. David and J. L. Journé, *A boundedness criterion for generalized Calderón-Zygmund operators*, Annals of Math., **120**, (1984), 371–397.

[20] R.A. Devore, B. Jawerth, and B. J. Lucier, *Image compression through wavelet transform coding*, IEEE Trans. Inf. Th., **38**, no. 2, (1992), 719–746.

[21] D. E. Dudgeon and R. M. Mersereau, *Multidimensional digital signal processing*, Prentice-Hall, Englewood Cliffs NJ, 1984.

[22] T. Eirola, *Sobolev characterization of solutions of dilation equations*, SIAM. J. Math. Anal., **23**, no. 4, (1992), 1015–1030.

[23] B. Engquist, S. Osher, and S. Zhong, *Fast wavelet based algorithms for linear evolution equations*, Technical Report no. 92-14, ICASE, Hampton, Virginia, 1992.

[24] J. C. Feauveau, *Nonorthogonal multiresolution analysis using wavelets*, Wavelets: A Tutorial in Theory and Applications, (C. K. Chui ed.), Academic Press, San Diego CA, 1992, pp. 153–178.

[25] J. Froment and S. Mallat, *Second generation compact image coding with wavelets*, Wavelets: A Tutorial in Theory and Applications, (C. K. Chui ed.), Academic Press, San Diego CA, 1992, pp. 655–678.

[26] G. H. Golub and C. F. Van Loan, *Matrix Computations*, 2nd ed., The Johns Hopkins University Press, Baltimore MD, London, 1989.

[27] R. A. Gopinath and C. S. Burrus, *Wavelets transforms and filter banks*, Wavelets: A Tutorial in Theory and Applications, (C. K. Chui ed.), Academic Press, San Diego CA, 1992, pp. 603–654.

[28] K. Gröchenig, *Analyse multi-échelle et bases d'ondelettes*, C.R. Acad. Sci. Paris, **305** Série I, 1987, pp. 13–15.

[29] K. Gröchenig and W. R. Madych, *Multiresolution analysis, Haar bases and self-similar tilings of R^n*, IEEE Trans. Inf. Th., **38**, no. 2, (1992), 556–568.

[30] A. Grossman and J. Morlet, *Decomposition of Hardy functions into square integrable wavelets of constant shape*, SIAM J. Math. Anal., **15**, (1984), 723–736.

[31] A. Haar, *Zur Theorie der orthogonalen Funktionensysteme*, Math. Ann. **69**, (1910), 331–371.

[32] R. A. Hadded and T. W. Parsons, *Digital Signal Processing Theory, Applications and Hardware*, Computer Science Press, New York, Oxford, 1991.

[33] C. Herley and M. Vetterli, *Wavelets and recursive filter banks*, IEEE Trans. Signal Proc., **41**, no. 8, (1993), 2536–2556.

[34] O. Hermann, *On the approximation problem in nonrecursive digital filter design*, IEEE Trans. Circuit Theory, **CT-18**, no. 1, (1971), 411–413.

[35] S. Jaffard, *Wavelet methods for fast resolution of elliptic problems*, SIAM. J. Numer. Anal., **29**, no. 4, (1992), 965–986.

[36] S. Jaffard and Ph. Laurençot, *Orthonormal wavelets, analysis of operators, and applications to numerical analysis*, Wavelets: A Tutorial in Theory and Applications, (C. K. Chui, ed.), Academic Press, San Diego CA, 1992, pp. 543–601.

[37] A. Karoui and R. Vaillancourt, *Families of biorthogonal wavelets*, Comp. Math. Appl., **28**, no. 4, (1994), 25–39.

[38] A. Karoui and R. Vaillancourt, *Design of parametric biorthogonal wavelet bases*, submitted for publication.

[39] A. Karoui and R. Vaillancourt, *On the construction of nonseparable bidimensional wavelet bases*, to appear in Comp. Math. Applic., 1995.

[40] A. Karoui and R. Vaillancourt, *Nonseparable biorthogonal wavelet bases of* $L^2(R^n)$, submitted for publication.

[41] A. Karoui and R. Vaillancourt, *Biorthogonal wavelet bases for fast one- and two-dimensional wavelet transforms*, submitted for publication.

[42] J. Kovačević and M. Vetterli, *Nonseparable multidimensional perfect reconstruction filter banks and wavelet bases for* R^n, IEEE Trans. Inf. Th., **38**, no. 2, (1992), 533–555.

[43] R. Kronland-Martinet, J. Morlet, and A. Grossmann, *Analysis of sound patterns through wavelet transforms*, Internat. J. Pattern Recognition and Artificial Intelligence, **1**, no. 2, (1987), 273–301.

[44] G. A. Lampropoulos and M. M. Fahmy, *A new technique for the design of two-dimensional FIR and IIR filters*, IEEE Trans. Acoustics, Speech, and Signal Processing, **ASSP-33**. no. 1, (1985), 268–279.

[45] P. G. Lemarié, *Ondelettes à localisation exponentielle*, J. Math. Pures et Appl., **67**, no. 3, (1988), 227–236.

[46] S. Mallat, *Multiresolution approximations and wavelet orthonormal bases of* $L^2(R)$, Trans. Amer. Math. Soc., **315**, (1989), 69–88.

[47] S. Mallat, *A theory for multiresolution signal decomposition: The wavelet representation*, IEEE Trans. on Pattern Analysis and Machine Intelligence, **PAMI-11**, no. 7, (1989), 674–693.

[48] J. H. McClellan and D. S. K. Chan, *A 2-D FIR filter structure derived from the Chebyshev recursion*, IEEE Trans. Circuits and Systems, **CAS-24**, no. 7, (1976), 372–378.

[49] W. F. G. Mecklenbräuker and R. M. Mersereau, *McClellan transformations for two-dimensional digital filtering: II - Implementation*, IEEE Trans. Circuits and Systems, **CAS-23**, no. 7, (1976), 414–422.

[50] R. M. Mersereau, F. G. Mecklenbräuker, and T. F. Quatieri, Jr., *McClellan transformation for two-dimensional digital filtering: I - Design*, IEEE Trans. Circuits and Systems, **CAS-23**, no. 7, (1976), 405–414.

[51] Y. Meyer, *Wavelets and Operators*, transl. from the French by D. H. Salinger, Cambridge Studies in Advanced Mathematics, **37**, Cambridge University Press, Cambridge, UK, 1992.

[52] Y. Meyer, *Ondelettes et opérateurs II, Opérateurs de Calderón–Zygmund*, Hermann, Paris 1990.

[53] Y. Meyer, *Principe d'incertitude, bases hilbertiennes et algèbres d'opérateurs*, Séminaire Bourbaki 1985/86, Exposé 662, Astérisque, Soc. Math. de France, Paris, (1987), pp. 209–223.

[54] S. D. Riemenschneider and Z. Shen, *Box splines, cardinal series and wavelets*, Approximation Theory and Functional Analysis, (C. K. Chui, ed.), Academic Press, New York, 1991, pp. 133–149.

[55] F. Riesz and B. Sz.-Nagy, *Functional Anaysis*, transl. from the 2nd French edition by L. F. Boron, Ungar, New York, 1955.

[56] O. Rioul, *Simple regularity criteria for subdivision schemes*, SIAM. J. Math. Anal., **23**, no. 6, (1992), 1544–1576.

[57] O. Rioul, *A discrete-time multiresolution theory*, IEEE Trans. Signal Proc., **41**, no. 8, (1993), 2591–2606.

[58] O. Rioul and P. Duhamel, *Fast algorithms for discrete and continuous wavelet transforms*, IEEE Trans. Inf. Th., **38**, no. 2, (1992), 569–586.

[59] E. P. Simoncelli and E. H. Adelson, *Non-separable extensions of quadrature mirror filters to multiple dimensions*, Proc. IEEE, **78**, no. 4, (1990), 652–664.

[60] G. Strang and V. Strela, *Short wavelets and matrix dilation equations*, preprint.

[61] M. J. T. Smith and T. P. Barnwell III, *Exact reconstruction technique for tree-structured subband coders*, IEEE Trans. on Acoustics, Speech and Signal Processing, **ASSP-34**, no. 3, (1986), 434–441.

[62] J. O. Strömberg, *A modified Franklin system and higher-order spline systems on R^n as unconditional bases for Hardy spaces*, Conference in Harmonic Analysis in Honor of Antoni Zygmund, **II**, (W. Beckner et al., eds.), Wadsworth Math. Series, Wadsworth, Belmont CA, 1982, pp. 475–493.

[63] Ph. Tchamitchian, *Biorthogonalité et théorie des opérateurs*, Revista Matemática Iberoamericana, **3**, no. 2, (1987), 163–189.

[64] M. Unser and A. Aldroubi, *Polynomial splines and wavelets—A signal processing perspective*, Wavelets: A Tutorial in Theory and Applications, (C. K. Chui, ed.), Academic Press, San Diego CA, 1992, pp. 91–122.

[65] P. P. Vaidyanathan, *Theory and design of M-channel maximally decimated quadrature mirror filters with arbitrary M, having the perfect reconstruction property*, IEEE Trans. on Acoustic, Speech and Signal Processing, **ASSP-35**, no. 4, (1987), 476–492.

[66] M. Vetterli, *Filters banks allowing perfect reconstruction*, Signal Processing, **10**, no. 3, (1986), 219–244.

[67] M. Vetterli and C. Herley, *Wavelets and filter banks: Theory and design*, IEEE Trans. Signal Proc., **40**, no. 9, (1992), 2207–2232.

[68] E. Viscito and J. P. Allebach, *The analysis and design of multidimensional FIR perfect reconstruction filter banks for arbitrary sampling lattices*, IEEE Trans. Circuits and Systems, **CAS-38**, no. 1, (1991), 29–41.

[69] M. V. Wickerhauser, *Acoustic signal compression with wavelet packets*, Wavelets: A Tutorial in Theory and Applications, (C. K. Chui, ed.), Academic Press, San Diego CA, 1992, pp. 679–700.

[70] J. C. Xu, and W. C. Shann, *Galerkin-wavelet methods for two-point boundary value problems*, Numer. Math, **63**, (1992), 123–144.